

JSCSEN 76(10)1339–1454(2011)



International Year of
CHEMISTRY
2011

Journal of the Serbian Chemical Society

ersion
lectronic

VOLUME 76

No 10

BELGRADE 2011

Available on line at



www.shd.org.rs/JSCS/

The full search of JSCS
is available through

DOAJ DIRECTORY OF
OPEN ACCESS
JOURNALS
www.doaj.org



CONTENTS

Organic Chemistry

- A. Dandia, R. Singh and A. Laxkar: A facile catalyst and solvent-free synthesis of spirothia heterocycles on grinding 1339
- A. Khorshidi and K. Tabatabaeian: An ultrasound-promoted green approach for the synthesis of 3-(indol-3-yl)-3-hydroxyindolin-2-ones catalyzed by Fe(III) 1347

Biochemistry and Biotechnology

- I. Fatima, M. A. Munawar, A. Tasneem, S. Jahan, M. A. Khan and S. Ahmed: Antithyroid activity of some 6-(alkylsulfanyl)-9H-purines 1355
- X. Liu, X. Wang and L. Ding: Mechanisms of the interaction between Pr(DNR)₃ and herring-sperm DNA 1365
- A.-U.-Rehman, S. Gulzar, M. A. Abbasi, T. Shahzadi, T. Riaz, S. Z. Siddiqui and M. Ajaib: *In vitro* assessment of the protection from oxidative stress by various fractions of *Artemisia incisa* Pamp. 1379

Inorganic Chemistry

- S. Malik, S. Ghosh and L. Mitu: Complexes of some 3d-metals with a Schiff base derived from 5-acetamido-1,3,4-thiadiazole-2-sulphonamide and their biological activity..... 1387

Theoretical Chemistry

- X. Lu, J. Han, Z. Lian and Y. Li: *Ab initio* study of the mechanism of the formation of a bis-heterocyclic compound containing Si and Ge by reaction of germylene silylene (H₂Ge=Si:) and ethene 1395

Physical Chemistry

- S. P. Petrović, Z. M. Vuković, T. B. Novaković, Z. P. Nedić and Lj. S. Rožić: Fractal analysis of bentonite modified with heteropoly acid using nitrogen sorption and mercury intrusion porosimetry 1403

Materials

- A. Milutinović-Nikolić, J. Dostanić, P. Banković, N. Jović-Jovičić, S. Lukić, B. Rosić and D. Jovanović: A new type of bentonite-based non-woven composite..... 1411

Environmental

- I. Andjelković, D. D. Manojlović, D. Djordjević, B. Dojčinović, G. Roglić and Lj. Ignjatović: Arsenic removal from aqueous solutions by sorption onto zirconium- and titanium-modified sorbents 1427
- B. M. Jovanović, V. L. Vukašinović-Pešić, Đ. N. Veljović and Lj. V. Rajaković: Arsenic removal from water using low-cost adsorbents – a comparative study 1437
- Errata..... 1453

Published by the Serbian Chemical Society
Karnegijeva 4/III, 11000 Belgrade, Serbia
Printed by the Faculty of Technology and Metallurgy
Karnegijeva 4, P.O. Box 35-03, 11120 Belgrade, Serbia



J. Serb. Chem. Soc. 76 (10) 1339–1346 (2011)
JSCS–4208

A facile catalyst and solvent-free synthesis of spiro thia heterocycles on grinding

ANSHU DANDIA*, RUBY SINGH and ASHOK LAXKAR

Department of Chemistry, University of Rajasthan, Jaipur-302004, India

(Received 21 September 2010, revised 31 May 2011)

Abstract: An efficient and mild method for the synthesis of spiro 1,3-oxathiolan/oxathianes in the solid state reaction at room temperature has been described. This method is a good option to obtain the title compounds in quantitative yields in a simple and inexpensive way. Applying this methodology, different thia heterocycles were synthesized.

Keywords: spiro 1,3-oxathiolane/oxathianes; solid-state synthesis; room temperature.

INTRODUCTION

Development of organic solid state reaction has emerged as a frontier area of research in synthetic organic chemistry.¹ These reactions are especially appealing because they have certain advantages such as high efficiency, selectivity,² easy separation, purification, mild reaction conditions³ and environmental acceptability.⁴ This approach has been widely used in a variety of organic reactions.⁵

Experience has shown that compounds with biological activity are often derived from heterocyclic structures. Indeed, one of the richest sources of diversity for the medicinal chemist are small heterocyclic rings, which, in addition to often exhibiting biological activity, may serve as rigid scaffolds for further display of functionalities. 1,3-Oxathiolane/1,3-oxathianes are one such class of heterocycles which have attracted much attention as they have been reported to possess a wide range of biological activities, including antiviral,⁶ anticonvulsant,⁷ antiulcer⁸ and antifungal activity.⁹ In addition, they also showed anti-HIV and anti-HBV activity,¹⁰ and oxathiolanes act both as agonists^{11–13} and antagonists on muscarinic receptors.¹² Cevimeline (*cis*-2-methylspiro[1,3-oxathiolane-5,3'-quinuclidine] hydrochloride) is a selective M₁ receptor agonist. It induces atropine-sensitive contractions of isolated guinea pig ilea and trachea preparations (*EC*₅₀ values are

* Corresponding author. E-mail: dranshudandia@yahoo.co.in
doi: 10.2298/JSC100921117D



3.5 and 3 μM , respectively) and reverses AF64A-induced cognitive impairments *in vivo*.¹⁴

A literature survey showed that many different protocols have been developed for the synthesis of various 1,3-oxathiolane derivatives. However, the general applicability of the reported methods are limited as the reactions require prolonged heating using dry toluene and the catalysts *p*-toluenesulfonic acid (*p*-TSA),¹⁵ the dimethyltin diiodide–HMPTA complex,¹⁶ LiBr,¹⁷ *etc.* Furthermore, purification of the product requires tedious workup with further use of large amount of volatile organic solvents. In order to circumvent these difficulties and to develop a facile green chemical approach, our attention was focused on the development of an alternative method for the synthesis of spiro 1,3-oxathiolane/oxathianes.

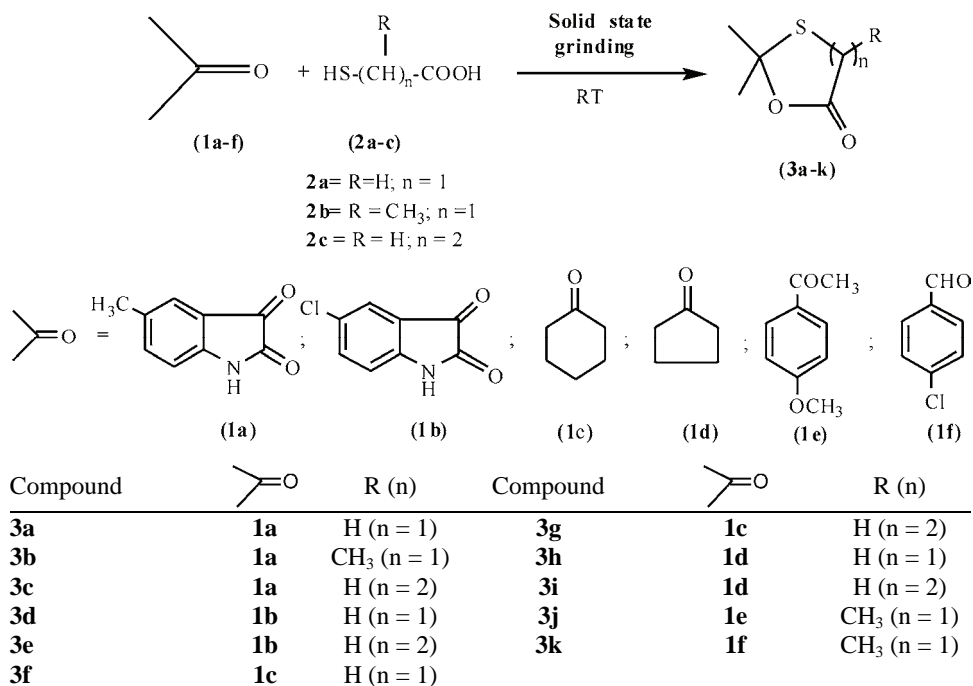
On the other hand, spiro-oxindole derivatives occupy a special place in organic and medicinal chemistry because these compounds are well-known as microtubule assembly inhibitors (spirotryprostatin A and B),¹⁸ muscarinic M1, serotonin receptor modulators (pteropodine and isopteropodine)¹⁹ and nonpeptidyl growth-hormone secretagogues (MK-0677).²⁰ Horsfiline and elacomine are more straightforward derivatives of the naturally occurring oxindole alkaloids with cell cycle inhibition activity.²¹

The unique structural array and the highly pronounced pharmacological activity displayed by the class of spirooxindole compounds have made them attractive synthetic targets.^{19b,22} In continuation of earlier interest on the synthesis of spiro thia heterocycles,²³ herein an easy, practical and efficient procedure for the synthesis of spiro 1,3-oxathiolanes containing different alicyclic/heterocyclic moieties, *e.g.*, indole, cyclohexane, cyclopentane, by the solid state reaction at room temperature in 2–3 min after grinding the two reactants in an agate mortar is reported for the first time (Scheme 1). The method can also be extended to reaction of aromatic aldehydes/ketones giving 2-(substituted aryl)-4-methyl-1,3-oxathiolane derivatives.

RESULTS AND DISCUSSION

As an initial endeavor, 5-methylisatin **1a** and mercapto acid **2a** were heated under reflux in dry toluene. After 4 h, only 60 % of the expected product **3a** was obtained after workup and recrystallization from ethanol. In an attempt to improve the yields of the reaction and acknowledging the benefits of grinding,²⁴ the same reaction was performed under solvent-free conditions at room temperature by grinding both reaction components in a mortar at room temperature (Scheme 1). It was observed that the mixture, which was initially in a partial liquid state, solidified during the grinding process to a light colored solid mass and thin layer chromatography, at this moment, indicated complete conversion to the desired product and TLC studies showed 100 % conversion of the reactants to the pro-

duct in quantitative yield in 2–3 min at room temperature. The pure product spiro derivative **3a** (monitored by TLC) was obtained after thorough washing with water and recrystallization with ethanol.



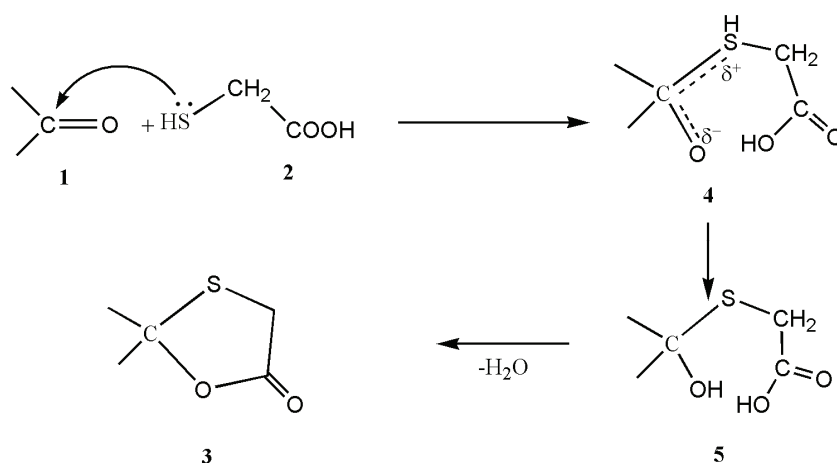
Scheme 1. The synthesis of the title compounds.

This cyclocondensation reaction is two-step reaction. The first step involves nucleophilic attack of thiol group on carbon oxygen double bond of carbonyl group giving the intermediates **4** and **5** (hydroxyalkylthio acid) which on elimination of water molecule gives product **3** (Scheme 2).

To optimize the method, the cyclocondensation reaction was examined using different quantities of mercapto acid and it was found that the yield of isolated product increased as the molar ratio of mercapto acid increased and the optimum molar ratio of carbonyl compound to mercapto acid for complete formation of the spiro product was determined to be 1:1.5.

The structures of the products **3a–k** were established by spectral and elemental analyses. The IR spectra of compounds **3a–e** showed a characteristic absorption band at 1715–1690 cm⁻¹ due to the two carbonyl groups and the remaining compounds showed only one C=O absorption band at 1710–1702 cm⁻¹. The *spiro* compound **3b** where R=CH₃ contains two chiral centers and hence exists in two diastereomeric forms, which was confirmed by the appearance of two sets of signals in its ¹H-NMR spectrum giving two sets of doublet (*J* = 4.44 Hz) due to

CH–CH₃ at δ 1.67/1.98 ppm and a quartet ($J = 4.44$ Hz) due to CH–CH₃ at δ 4.39/4.79 ppm and a broad singlet at δ 8.24/8.58 ppm (NH) in a 3:1 molar ratio, corresponding to the two diastereomeric forms **3b** and **3b'**. However, the complex multiplets of the aromatic protons of the two diastereomers could not be resolved.



Scheme 2. The suggested mechanism for the formation of the title compounds.

The structural elucidations of the products were based on their spectral (IR, ¹H- and ¹³C-NMR and mass) data as given below.

5-Methylspiro[indoline-3,2'-[1,3]oxathiolane]-2,5'-dione (3a). M.p. 190 °C; Anal. Calcd. for C₁₁H₉NO₃S: C, 56.16; N, 5.95; S, 13.63 %. Found: C, 56.35; N, 5.97; S, 13.67 %. IR (KBr, cm⁻¹) 3280–3340 (NH str.), 1714 (C=O), 1690 (C=O), 1570, 1495, 1180. ¹H-NMR (300 MHz, CDCl₃, δ / ppm): 2.35 (3H, *s*, CH₃), 3.85–4.48 (2H, *dd*, $J = 13.8$ Hz, CH₂), 6.98–7.52 (3H, *m*, Ar–H), 9.08 (1H, *bs*, NH exchanges with D₂O). ¹³C-NMR (74.46 MHz, CDCl₃, δ / ppm): 21.2 (CH₃), 34.8 (CH₂), 85.2 (spiro carbon) 120.8, 127.7, 128.3, 130.7, 133.8, 139.1 (aromatic carbons), 168.3 (C=O), 171.2 (C=O). MS (m/z): 236 (M+H)⁺.

4',5-Dimethylspiro[indoline-3,2'-[1,3]oxathiolane]-2,5'-dione (3b). M.p. 100 °C; Anal. Calcd. for C₁₂H₁₁NO₃S: C, 57.82; N, 5.62; S, 12.86 %. Found: C, 58.01; N, 5.64; S, 12.90 %. IR (KBr, cm⁻¹) 3285–3330 (NH str.), 1715 (C=O), 1695 (C=O), 1580, 1490, 1175. ¹H-NMR (300 MHz, CDCl₃, δ / ppm): 2.38 (3H, *s*, CH₃), diastereomeric ratio (3:1) 1.67/1.98 (3H, *d*, $J = 4.44$ Hz, CH–CH₃) 4.39/4.79 (1H, *q*, $J = 4.44$ Hz, CH–CH₃), 6.98–7.54 (3H, *m*, Ar–H), 8.24/8.58 (1H, *bs*, NH exchanges with D₂O). ¹³C-NMR (74.46 MHz, CDCl₃, δ / ppm): 16.52 (CH–CH₃), 22.6 (CH₃), 44.19 (CH–CH₃), 82.24 (spiro carbon) 121.2, 124.6, 128.3, 130.2, 134.4, 138.2 (aromatic carbons), 168.22 (C=O), 172.90 (C=O). MS (m/z): 250 (M+H)⁺.

5-Methylspiro[indoline-3,2'-[1,3]oxathiane]-2,6'-dione (3c). M.p. 110 °C; Anal. Calcd. for C₁₂H₁₁NO₃S: C, 57.82; N, 5.62; S, 12.86 %. Found: C, 57.63; N, 5.60; S, 12.82 %. IR (KBr, cm⁻¹) 3290–3328 (NH str.), 1712 (C=O), 1692 (C=O) 1585, 1498, 1170. ¹H-NMR (300 MHz, CDCl₃, δ / ppm): 2.36 (3H, s, CH₃), 2.66 (2H, t, CH₂), 2.85 (2H, t, CH₂), 6.92–7.58 (3H, m, Ar-H), 9.02 (1H, bs, NH exchanges with D₂O). ¹³C-NMR (74.46 MHz, CDCl₃, δ / ppm): 20.8 (CH₃), 32.4 (CH₂), 38.2 (CH₂), 86.3 (spiro carbon), 121.2, 124.8, 128.3, 132.3, 136.4, 140.2 (aromatic carbons), 166.8 (C=O), 174.2 (C=O). MS (*m/z*): 250 (M+H)⁺.

5-Chlorospiro[indoline-3,2'-[1,3]oxathiolane]-2,5'-dione (3d). M.p. 135 °C; Anal. Calcd. for C₁₀H₆ClNO₃S: C, 46.98; N, 5.48; S, 12.54 %. Found: C, 47.14; N, 5.46; S, 12.58 %. IR (KBr, cm⁻¹) 3290–3320 (NH str.), 1708 (C=O), 1692 (C=O), 1580, 1490, 1180, 740. ¹H-NMR (300 MHz, CDCl₃, δ / ppm): 3.82–4.46 (2H, dd, *J* = 13.9 Hz, CH₂), 6.98–7.50 (3H, m, Ar-H), 8.88 (1H, bs, NH exchanges with D₂O). ¹³C-NMR (74.46 MHz, CDCl₃, δ / ppm): 35.2 (CH₂), 89.6 (spiro carbon), 120.1, 124.3, 128.4, 130.2, 136.2, 140.4 (aromatic carbons), 169.4 (C=O), 174.3 (C=O). MS (*m/z*): 256 (M+H)⁺.

5-Chlorospiro[indoline-3,2'-[1,3]oxathiane]-2,6'-dione (3e). M.p. 180 °C; Anal. Calcd. for C₁₁H₈ClNO₃S: C, 48.99; N, 5.19; S, 11.89 %. Found: C, 48.83; N, 5.17; S, 11.85 %. IR (KBr, cm⁻¹) 3292–3318 (NH str.), 1715 (C=O), 1695 (C=O), 1575, 1480, 1178, 745. ¹H-NMR (300 MHz, CDCl₃, δ / ppm): 2.62 (2H, t, CH₂), 2.83 (2H, t, CH₂), 6.98–7.52 (3H, m, Ar-H), 9.06 (1H, bs, NH exchanges with D₂O). ¹³C-NMR (74.46 MHz, CDCl₃, δ / ppm): 30.1 (CH₂), 37.5 (CH₂), 86.5 (spiro carbon), 122.8, 128.4, 129.3, 130.4, 136.8, 140.4 (aromatic carbons), 167.3 (C=O), 173.3 (C=O). MS (*m/z*): 270 (M+H)⁺.

1-Oxa-4-thiaspiro[4.5]decan-2-one (3f). M.p. 125 °C; Anal. Calcd. for C₈H₁₂O₂S: C, 55.78; S, 18.62 %. Found: C, 55.60; S, 18.68 %. IR (KBr, cm⁻¹) 2880–2930 (CH str.), 1705 (C=O). ¹H-NMR (300 MHz, CDCl₃, δ / ppm): 1.27–1.35 (2H, t, CH₂), 1.52–1.65 (2H, m, CH₂), 2.06–2.30 (2H, t, CH₂), 1.86–1.98 (4H, m, CH₂), 3.85–4.48 (2H, dd, CH₂). ¹³C-NMR (74.46 MHz, CDCl₃, δ / ppm): 17.8, 26.7, 36.5 (cyclohexane ring carbons), 36.7 (CH₂), 84.2 (spiro carbon), 172.2 (C=O). MS (*m/z*): 173 (M+H)⁺.

1-Oxa-5-thiaspiro[5.5]undecan-2-one (3g). M.p. 130 °C; Anal. Calcd. for C₉H₁₄O₂S: C, 58.03; S, 17.21 %. Found: C, 58.22; S, 17.26 %. IR (KBr, cm⁻¹) 2870–2945 (CH str.), 1708 (C=O). ¹H-NMR (300 MHz, CDCl₃, δ / ppm): 1.29–1.38 (2H, t, CH₂), 1.50–1.66 (2H, m, CH₂), 2.04–2.31 (2H, t, CH₂), 1.85–1.96 (4H, m, CH₂), 2.65 (2H, t, CH₂), 2.88 (2H, t, CH₂); ¹³C-NMR (74.46 MHz, CDCl₃, δ / ppm): 17.5, 26.8, 36.4 (cyclohexane ring carbons), 28.7 (CH₂), 38.2 (CH₂), 84.8 (spiro carbon), 172.8 (C=O). MS (*m/z*): 173 (M+H)⁺.

1-oxa-4-thiaspiro[4.4]nonan-2-one (3h). M.p. 150 °C; Anal. Calcd. for C₇H₁₀O₂S: C, 53.14; S, 20.27. Found: C, 53.32; S, 20.21. IR (KBr, cm⁻¹): 2885–

–2940 (CH str.), 1702 (C=O). $^1\text{H-NMR}$ (300 MHz, CDCl_3 , δ / ppm): 1.28–1.36 (*t*, 2H, CH_2), 1.55–1.62 (*m*, 4H, CH_2), 2.08–2.13 (*t*, 2H, CH_2), 3.85–4.43 (*dd*, 2H, CH_2). $^{13}\text{C-NMR}$ (74.46 MHz, CDCl_3 , δ / ppm): 17.2, 37.3 (cyclopentane ring carbons), 38.2 (CH_2), 89.5 (spiro carbon), 171.3 (C=O). MS (*m/z*): 159 ($\text{M}+\text{H}$) $^+$.

6-Oxa-10-thiaspiro[4.5]decan-7-one (3i). M.p. 120 °C; Anal. Calcd. for $\text{C}_8\text{H}_{12}\text{O}_2\text{S}$: C, 55.78; S, 18.62 %. Found: C, 55.96; S, 18.56 %. IR (KBr, cm^{-1}) 2865–2930 (CH str.), 1710 (C=O). $^1\text{H-NMR}$ (300 MHz, CDCl_3 , δ / ppm): 1.27–1.38 (2H, *t*, CH_2), 1.57–1.63 (4H, *m*, CH_2), 2.08–2.17 (2H, *t*, CH_2), 2.66 (2H, *t*, CH_2), 2.89 (2H, *t*, CH_2). $^{13}\text{C-NMR}$ (74.46 MHz, CDCl_3 , δ / ppm): 17.5, 36.8 (cyclopentane ring carbons), 28.5 (CH_2), 38.8 (CH_2), 84.6 (spiro carbon), 172.8 (C=O). MS (*m/z*): 173 ($\text{M}+\text{H}$) $^+$.

2-(4-Methoxyphenyl)-2,4-dimethyl-1,3-oxathiolan-5-one (3j). M.p. 140 °C; Anal. Calcd. for $\text{C}_{12}\text{H}_{14}\text{O}_3\text{S}$: C, 60.48; S, 13.46 %. Found: C, 60.68; S, 13.42 %. IR (KBr, cm^{-1}) 2875–2932 (CH str.), 1704 (C=O). $^1\text{H-NMR}$ (300 MHz, CDCl_3 , δ / ppm): 1.39 (3H, *d*, CH_3), 1.86 (3H, *s*, CH_3), 3.72 (3H, *s*, CH_3), 3.88 (1H, *q*, CH), 6.98–7.52 (4H, *m*, CH). $^{13}\text{C-NMR}$ (74.46 MHz, CDCl_3 , δ / ppm): 17.6 (CH_3), 20.2 (CH_3), 56.4 (CH_3), 90.2 (CH), 92.6 (spiro carbon), 122.8, 124.2, 128.4, 138.4, 142.2, 158.6 (aromatic carbons), 158.4 (C–O), 192.4 (C=O). MS (*m/z*): 239 ($\text{M}+\text{H}$) $^+$.

2-(4-Chlorophenyl)-4-methyl-1,3-oxathiolan-5-one (3k). M.p. 145 °C; Anal. Calcd. for $\text{C}_{10}\text{H}_9\text{ClO}_2\text{S}$: C, 52.52; S, 14.02 %. Found: C, 52.35; S, 14.06 %. IR (KBr, cm^{-1}) 2862–2938 (CH str.), 1708 (C=O). $^1\text{H-NMR}$ (300 MHz, CDCl_3 , δ / ppm): 1.42 (3H, *d*, CH_3), 3.86 (1H, *q*, CH), 5.44 (1H, *s*, CH), 6.96–7.28 (4H, *m*, CH). $^{13}\text{C-NMR}$ (74.46 MHz, CDCl_3 , δ / ppm): 17.4 (CH_3), 92.8 (CH), 88.4 (spiro carbon), 118.8, 122.4, 124.2, 128.4, 132.4, 138.8 (aromatic carbons), 194.6 (C=O). MS (*m/z*): 229 ($\text{M}+\text{H}$) $^+$.

EXPERIMENTAL

Melting points were determined in open glass capillaries and are uncorrected. The IR spectra (KBr) were recorded on a Shimadzu FT IR-8400S spectrophotometer and the ^1H - and ^{13}C -NMR spectra were recorded on Bruker DRX-300 in CDCl_3 at 300.15 and 75.47 MHz, respectively. TMS was used as the internal reference. The mass spectra of representative compounds were recorded on XEVO QTOF and Thermo LCQ Advantage Max Ion Trap spectrometers. Elemental microanalyses were performed on a Carlo-Erba 1108 CHN analyzer. The purity of all compounds was checked by TLC using silica Gel “G” coated glass plates and benzene: ethyl acetate (8:2) as the eluent.

General procedure for the synthesis of spiro compounds 3a–k

A mixture of the appropriate carbonyl compound **1** (1 mmol) and mercapto acids **2** (1.5 mmol) was thoroughly ground in an agate mortar. The grinding was continued until completion of the reaction (2–3 min), as monitored by TLC. On completion of the reaction, the mixture became a solid mass which was treated with water. The resultant product was filtered

and washed with water, recrystallized from methanol and dried under vacuum to yield the pure products.

CONCLUSIONS

An efficient, environmentally friendly, economically viable and cleaner methodology for the preparation of *spiro* [1,3-oxathiolane/oxathianes] under solid-state conditions at room temperature was developed. The reaction is fairly general, facile and is devoid of any side products. Due to the simplicity of the conditions, high yields and purity of the products, the above mentioned methodology should find utility in organic synthesis. In addition, this method is safer; it avoids the use of toxic or hazardous solvents. Furthermore, it was found that this solid state reaction is much faster and more efficient than the solution phase reaction, probably because the solid state reaction is a very high concentration reaction.

Acknowledgements. Financial assistance from the Council for Scientific and Industrial Research (01/2248/08/EMR-II, No. 13(8424-A)2010-Pool), New Delhi, India, is gratefully acknowledged. We are also thankful to the Regional Sophisticated Instrumentation Centre Chandigarh, and the Central Drug Research Institute, Lucknow, India, for the elemental and spectral analyses.

ИЗВОД

ЕФИКАСНА СИНТЕЗА СПИРО ТИЈА ХЕТЕРОЦИКЛА У ЧВРСТОЈ ФАЗИ

ANSHU DANDIA, RUBY SINGH и ASHOK LAXKAR

Department of Chemistry, University of Rajasthan, Jaipur-302004, India

Описана је синтеза спиро 1,3-оксатиолан/оксатиан у чврстој фази под благим реакционим условима, на собној температури. Поступак представља добар приступ за синтезу наведених једињења у квантитативном приносу на ефикасан начин по приступачној цени. Применом описаног поступка синтетисана су различита тија хетероциклична једињења.

(Примљено 21. септембра 2010, ревидирано 31. маја 2011)

REFERENCES

1. a) J. P. Li, Y. L. Wang, H. Wang, Q. F. Luo, X. Y. Wang, *Synth. Commun.* **5** (2001) 781; b) S. Mallakpour, A. R. Hajipour, H. A. Taghizadeh, *Molecules* **8** (2003) 359; c) G. R. Desiraju, B. S. Goud, *Reactivity of solids: Past, Present, and Future*, Blackwell Science, London, 1994, p. 223; d) N. B. Singh, R. J. Singh, N. P. Singh, *Tetrahedron* **50** (1994) 6441; e) G. R. Desiraju, *Solid State Ionics* **101** (1997) 839
2. G. R. Desiraju, *Organic Solid State Chemistry*, Elsevier Science, Amsterdam, 1987, p. 197
3. M. O. Rasmussen, O. Axelsson, D. Tanner, *Synth. Commun.* **27** (1997) 4027
4. Y. M. Wang, Z. Wen, X. M. Chen, D. M. Du, T. Matsuura, J. B. Meng, *J. Heterocycl. Chem.* **35** (1998) 313
5. a) K. Satish, S. Poonam, K. K. Kapoor, S. H. Maninder, *Tetrahedron* **64** (2008) 536; b) D. A. Goff, R. N. Zuckermann, *J. Org. Chem.* **60** (1995) 5744; c) D. M. Du, S. M. Meng, Y. M. Wang, J. B. Meng, X. Z. Zhou, Y. Zhu, *Chin. J. Struct. Chem.* **4** (1995) 277; d) L.

- X. Li, D. M. Du, Y. M. Wang, J. B. Meng, *Sci. China Ser. B* **2** (1997) 205; e) J. Morey, J. M. Saa, *Tetrahedron* **49** (1993) 105
6. B. N. Nguyen, N. Lee, L. Chan, B. Zacharie, *Bioorg. Med. Chem. Lett.* **10** (2003) 2223
 7. M. Rajopadhye, F. D. Popp, *J. Med. Chem.* **31** (1988) 1001
 8. J. C. Aloup, J. Bouchaudon, D. Farge, J. Deregnacourt, M. H. Hardy, *J. Med. Chem.* **1** (1987) 24
 9. H. Miyauchi, T. Tanio, N. Ohashi, *Bioorg. Med. Chem. Lett.* **20** (1996) 2377
 10. J. Nokami, K. Ryokume, J. Inada, *Tetrahedron Lett.* **34** (1995) 6099
 11. A. Fisher, R. Brandeis, Z. Pittel, I. Karton, M. Sapir, S. Dachir, A. Levy, E. Heldman *Neurosci. Lett.* **102** (1989) 325
 12. S. Dei, C. Bellucci, M. Buccioni, M. Ferraroni, L. Guandalini, D. Manetti, G. Marucci, R. Matucci, M. Nesi, M. N. Romanelli, S. Scapecchi, E. Teodori, *Bioorg. Med. Chem.* **16** (2008) 5490
 13. P. Angeli, L. Brasili, M. Giannella, F. Gualtieri, M. T. Picchio, E. Teodori, *Naunyn-Schmiedeberg's Arch. Pharmacol.* **337** (1988) 241
 14. a) F. Wanibuchi, T. Konishi, M. Harada, M. Terai, K. Hidaka, T. Tamura, S. Tsukamoto, S. Usuda, *Eur. J. Pharmacol.* **187** (1990) 479; b) A. Fisher, R. Brandeis, I. Karton, Z. Pittel, D. Gurwitz, R. Haring, M. Sapir, A. Levy, E. Heldman, *J. Pharmacol. Exp. Ther.* **257** (1991) 392
 15. J. L. Kraus, G. Attardo, *Synthesis* (1991) 1046
 16. I. Shibata, A. Baba, H. Iwaski, H. Matsuda, *J. Org. Chem.* **51** (1986) 2177
 17. K. Sharma, K. Saleem, A. Salim, *Indian J. Chem., B* **41** (2002) 2676
 18. a) M. M. Khafagy, A. H. F. A. El-Wahas, F. A. Eid, A. M. El-Agrody, *Farmaco* **57** (2002) 715; b) P. R. Sebahar, R. M. Williams, *J. Am. Chem. Soc.* **122** (2000) 5666
 19. T. H. Kang, K. Matsumoto, Y. Murakami, H. Takayama, M. Kitajima, N. Aimi, H. Watanabe, *Eur. J. Pharmacol.* **444** (2002) 39
 20. a) P. E. Maligres, I. Houppis, K. Rossen, A. Molina, J. Sager, V. Upadhyay, K. M. Wells, R. A. Reamer, J. E. Lynch, D. Askin, R. P. Volante, P. J. Reider, *Tetrahedron* **53** (1997) 10983; b) B. L. Palucki, S. D. Feighner, S. S. Pong, K. K. McKee, D. L. Hrenuik, C. Tan, A. D. Howard, L. H. Y. Vanderploeg, A. A. Patchett, R. P. Nargund, *Bioorg. Med. Chem. Lett.* **11** (2001) 1955
 21. S. T. Hilton, T. C. T. Ho, G. Pljevaljcic, K. Jones, *Org. Lett.* **2** (2000) 2639
 22. a) C. Fischer, C. Meyers, E. M. Carreira, *Helv. Chim. Acta* **83** (2000) 1175; b) P. B. Alper, C. Meyers, A. Lerchner, D. R. Siegel, E. M. Carreira, *Angew. Chem., Int. Ed.* **38** (1999) 3186; c) R. G. Redkin, L. A. Shemchuk, V. P. Chernykh, O. V. Shishkin, S. V. Shishkina, *Tetrahedron* **63** (2007) 1144; d) R. S. Kumar, S. Perumal, *Tetrahedron Lett.* **48** (2007) 7164
 23. a) A. Dandia, M. Sati, A. Loupy, *Green Chem.* **4** (2002) 599; b) A. Dandia, R. Singh, S. Khaturia, *Bioorg. Med. Chem.* **14** (2006) 1303; c) A. Dandia, R. Singh, S. Khaturia, C. Mérienne, G. Morgant, A. Loupy, *Bioorg. Med. Chem.* **14** (2006) 2409
 24. a) Z. J. Ren, W. G. Cao, W. Q. Tong, *Synth. Commun.* **32** (2002) 3475; b) Z. J. Ren, W. G. Cao, W. Y. Ding, W. Shi, *Synth. Commun.* **34** (2004) 4395; c) K. Tanaka, S. Kishigami, F. Toda, *J. Org. Chem.* **56** (1991) 4333.



J. Serb. Chem. Soc. 76 (10) 1347–1353 (2011)
JSCS–4209

An ultrasound-promoted green approach for the synthesis of 3-(indol-3-yl)-3-hydroxyindolin-2-ones catalyzed by Fe(III)

ALIREZA KHORSHIDI* and KHALIL TABATABAEIAN

Department of Chemistry, Faculty of Sciences, University of Guilan,
P. O. Box 41335-1914, Iran

(Received 20 April, revised 15 June 2011)

Abstract: Ferric chloride hexahydrate was used as a recyclable homogeneous catalyst in aqueous media for the synthesis of 3-(indol-3-yl)-3-hydroxyindolin-2-ones under sonication. It was found that the employed conditions afford the products smoothly in good to excellent yields.

Keywords: ultrasonic irradiation; homogeneous; catalysis; ferric chloride hexahydrate.

INTRODUCTION

Indole-containing structures have widespread occurrence in many pharmacologically and biologically active compounds and the investigation of the chemistry of indoles has been, and continues to be, one of the most active areas of heterocyclic chemistry.^{1–4} Isatins are also familiar for their biological activities. Oxindoles are well known amongst different isatin derivatives and are useful as antibacterial, anti-inflammatory and laxatives.^{5,6} Such heterocyclic compounds were recently isolated from plants and marine animals, for example, the marine alkaloid convolutamydine A from the marine bryozoan *Amathia convoluta*.⁷ Recently, efficient routes to the synthesis of oxindole derivatives were reported.^{8,9} The synthesis of 3-(indol-3-yl)-3-hydroxyindolin-2-ones, however, would be a synthetically useful transformation since Friedel–Crafts reaction of indoles and isatins usually results in 3,3-di-3-indolyindolin-2-ones.^{10–13} A literature survey showed that the reported methods on the synthesis of 3-(indol-3-yl)-3-hydroxyindolin-2-ones have several drawbacks, such as long reaction times, low yields, use of toxic solvents and need for specific reagents.^{14–17} Thus, a mild and environmentally benign practical methodology under neutral conditions with a recyclable catalyst is actively sought after. Organic reactions in aqueous media have attracted increasing interest due to environmental and economical issues.¹⁸

*Corresponding author. E-mail: rucatalyst@yahoo.com
doi: 10.2298/JSC110420120K

Considerable organic solvent waste in the purification step, however, is still a major concern.

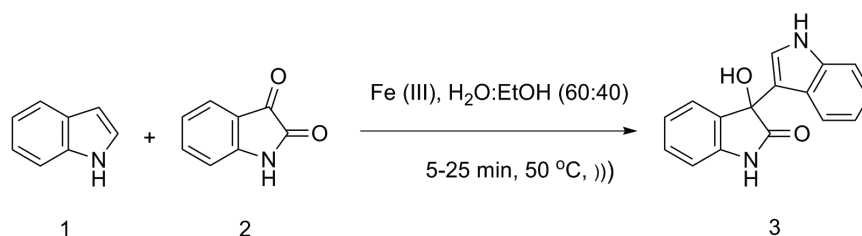
In recent years, iron(III) chloride has emerged as a powerful Lewis acid catalyst and has catalyzed many useful organic transformations under mild reaction conditions.^{19,20} Moreover, iron salts are inexpensive, easy to handle and are environmentally friendly.

Ultrasound irradiation, on the other hand, has emerged as an efficient technique for reagent activation in organic synthesis. Using cavitation as an energy source to promote molecular interactions resulted in shorter reaction times. The rarefaction-compression cycle in the cavitation process, which involves the separation of molecules of the liquid and then the collapse of the bubbles, provides violent impulsions that generate short-lived regions with high temperature and pressure. Such localized hot spots can be thought of as micro reactors in which the sound energy is transformed into a useful chemical form.²¹⁻²³

In this contribution, the synthesis of 3-indolyl-3-hydroxyoxindoles from isatins and indoles utilizing Fe(III) as a recyclable homogeneous catalyst under ultrasound irradiation is described.

RESULTS AND DISCUSSION

The optimized details of the ultrasound-promoted reaction of indoles with isatins to give the corresponding products (**3**) are summarized in Scheme 1.



Scheme 1. Ultrasound-promoted, Fe(III) catalyzed 3-indolylation of isatins.

In order to optimize the reaction conditions, indole and isatin were selected as model substrates and the progress of the reaction was monitored by gas liquid chromatography (GLC). To examine the influence of the catalyst concentration, the reaction was performed with different catalyst concentrations. The decrease in the corresponding indole peak area was selected as a measure of the reaction coordinate. In addition, the ethanol peak was used as an internal standard. The results are summarized in Table I.

Based on these data, 2.5 mol % Fe(III) per mole of indole was selected as the optimized catalyst concentration. Solvent screening experiments showed that the yields were solvent dependent (Table II).

TABLE I. Fe(III)-catalyzed reaction of indole and isatin using different catalyst concentrations (the reaction was carried out according to the general experimental procedure)

Entry	Reaction time, min	Indole consumption, %	Fe catalyst content, mol %
1	1	20	1
2	3	45	1
3	5	65	1
4	10	80	1
5	1	30	2.5
6	3	65	2.5
7	5	95	2.5
8	1	33	5
9	3	78	5
10	5	95	5

Since ultrasound is known to generate extremely fine emulsions to enhance mass transfer,²⁴ a mixture of H₂O:ethanol (60:40) was used as the best solvent. The large excess of water may have a dual role. First, it helps in the precipitation of the products and results in an easy work-up procedure and catalyst recycling (see experimental), which minimizes organic solvent waste. Second, it may prevent dehydration of the product and subsequent attack of a second indole nucleophile to form 3,3-di-3-indolyindolin-2-one.

TABLE II. Effect of solvents on the yield of 3-(indol-3-yl)-3-hydroxyindolin-2-one (the reaction was carried out according to the general experimental procedure)

Entry	Solvent	Reaction time, min	Isolated yield, %
1	1,2-Dichloroethane	60	50
2	Acetonitrile	45	55
3	Methanol	5	78
4	Ethanol	5	77
5	H ₂ O: Ethanol (60:40)	5	95

The effect of the intensity of the ultrasound irradiation on the reaction time is summarized in Table III. As it is shown, increase in the rated power of the ultrasonic horn from 20 to 100 % (92 to 460 W cm⁻², respectively) resulted in a decrease in the reaction time. This could be due to maximization of cavitation and effective distribution of the reactants throughout the reaction mixture. In the absence of ultrasound irradiation, however, the yields were unsatisfactory.

With the optimized conditions to hand (Scheme 1), various substrates were used, indicating the generality and scope of the reaction. Typical results are shown in Table IV. In all cases, the products were insoluble in the reaction media and simple filtration followed by rinsing with cold reaction solvent provided spectroscopically pure products.

One interesting example is the reaction of 3-methylindole with isatin (Table IV, entry c), which provided the product **3c**, while other reported methods failed

for this reaction. 3-Alkylation of 7-azaindole, which is susceptible to *N*-alkylation,²⁵ is also noteworthy (entry **e**). FeCl₃·6H₂O was found to be an efficient catalyst in terms of handling, temperature, yields and reaction times.

TABLE III. The effect of ultrasound irradiation intensity on the reaction time (the reaction was carried out according to the general experimental procedure)

Max. power density, W cm ⁻²	92	184	276	368	460
Reaction time, min	25	20	15	10	5

TABLE IV. Ultrasound-promoted synthesis of 3-(indol-3-yl)-3-hydroxyindolin-2-ones catalyzed by Fe(III)

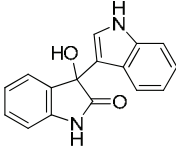
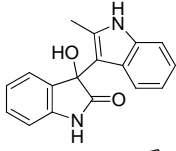
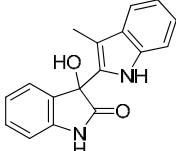
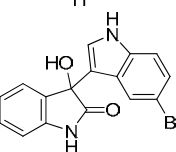
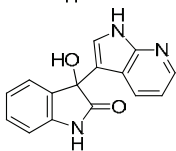
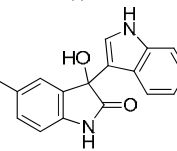
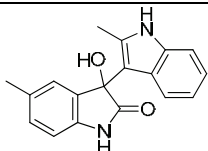
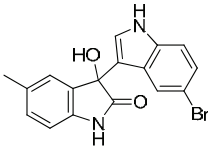
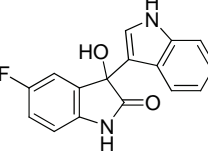
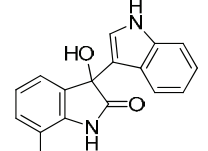
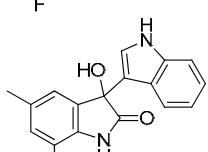
Entry ^a	Indole	Isatin	Product	Reaction time min	Yield ^b %
3a	Indole	Isatin		5	95 ^c
3b	2-Methylindole			5	97 ^c
3c	3-Methylindole			15	85
3d	5-Bromoindole			10	88 ^c
3e	7-Azaindole			10	90 ^c
3f	Indole	5-Methylisatin		10	93 ^c

TABLE IV. Continued

Entry ^a	Indole	Isatin	Product	Reaction time min	Yield ^b %
3g	2-Methylindole	5-Methylisatin		5	95 ^c
3h	5-Bromoindole	5-Methylisatin		10	88 ^c
3i	Indole	5-Fluoroisatin		5	92 ^c
3j	Indole	7-Fluoroisatin		10	87 ^c
3k	Indole	5,7-Dimethylisatin		15	70 ^c

^aAll products were characterized by ¹H-NMR, ¹³C-NMR and IR data; ^bisolated yields; ^cidentified by comparison with authentic samples¹⁴

One of the main aims of the study was to investigate the reuse and recycling of FeCl₃·6H₂O. After filtration of the cold reaction mixture to separate the product (**3a**), the filtrate was charged with the same substrates and was reused for four cycles, which afforded yields similar to those obtained in the first run, although increases in reaction time were observed (Table V).

TABLE V. The reuse of FeCl₃·6H₂O in successive runs (the reaction was carried out according to the general experimental procedure)

Run No.	Isolated yield, %	Reaction time, min
1	95	5
2	89	20
3	85	60
4	77	120

EXPERIMENTAL

General

The IR spectra were recorded on a Shimadzu FTIR-8400S spectrometer. The ^1H -NMR spectra were obtained on a Bruker DRX-500 Avance spectrometer and ^{13}C -NMR spectra were obtained on a Bruker DRX-125 Avance spectrometer. Chemical shifts of the ^1H - and ^{13}C -NMR spectra were expressed in ppm downfield from tetramethylsilane. Melting points were measured on a Büchi Melting Point B-540 instrument and are uncorrected. Elemental analyses were made by a Carlo-Erba EA1110 CNNO-S analyzer and the results agreed with the calculated values. The ultrasonic device used was a UP 400 S instrument, emitting 24 kHz ultrasound at tunable intensity levels (up to a maximum of 460 W cm^{-2}). Analytical GLC evaluations of product mixtures were performed on a Varian CP-3800 chromatograph (using a split/splitless injector, CP Sil 8CB column, FID assembly).

Materials

All materials were purchased from Merck and used without further purification.

General procedure for the ultrasound-promoted synthesis of 3-(indol-3-yl)-3-hydroxyindolin-2-ones catalyzed by Fe(III)

Indole (1 mmol), isatin (1 mmol) and $\text{FeCl}_3 \cdot 6\text{H}_2\text{O}$ (2.5 mol %) were added to 20 mL of a 60:40 mixture of H_2O :ethanol and the reaction mixture was irradiated at $50\text{ }^\circ\text{C}$ for the appropriate time (Table IV). After completion of the reaction (as indicated by GLC), the mixture was cooled in an ice bath and then filtered to separate the precipitated product, which was further purified by rinsing with cold reaction solvent. The filtrate was charged with the same substrates and was reused for successive cycles. The products were identified by comparison with authentic samples.

CONCLUSIONS

In conclusion, an operationally simple and efficient synthesis of 3-indolyl-3-hydroxyoxindoles is reported. Highlights of the present work are:

- i) Simultaneous application of sonic waves and Fe(III) resulted in greater efficiency in terms of reaction time and yield.
- ii) All products were solely monoindolylated isatins and were not contaminated by 3,3-di-3-indolyindolin-2-ones.
- iii) The reusability of the catalyst and environmentally friendly conditions are also noticeable.

Acknowledgements. Partial support of this study by the Research Council of University of Guilan, Iran, is gratefully acknowledged. A. Khorshidi is also thankful to Mrs. P. Rahimi for her generous support.

ИЗВОД

СИНТЕЗА 3-(ИНДОЛ-3-ИЛ)-3-ХИДРОКСИИНДОЛИН-2-ОНА КАТАЛИЗОВАНА Fe(III) И УНАПРЕЂЕНА ПОД ДЕЈСТВОМ УЛТРАЗВУКА

ALIREZA KHORSHIDI и KHALIL TABATABAEIAN

Department of Chemistry, Faculty of Sciences, University of Guilan, P. O. Box 41335-1914, Iran

Фери-хлоридхексахидрат је употребљен као хомогени катализатор у воденој средини за синтезу 3-(индол-3-ил)-3-хидроксииндолин-2-она под условима озрачивања ултразвуком.

Утврђено је да под примењеним условима, производи настају у добром до одличном приносу.

(Примљено 20. априла, ревидирано 15. јуна 2011)

REFERENCES

1. H.-C. Zhang, H. Ye, A. F. Moretto, K. K. Brumfield, B. E. Maryanoff, *Org. Lett.* **2** (2000) 89
2. R. J. Sundberg, *The chemistry of indoles*, Academic Press, New York, USA, 1996
3. T. L. Gilchrist, *Heterocyclic Chemistry*, Academic Press, London, UK, 1997
4. G. R. Humphrey, J. T. Kuethe, *Chem. Rev.* **106** (2006) 2875
5. F. D. Popp, *J. Heterocycl. Chem.* **21** (1984) 1367
6. F. Garrido, J. Ibanez, E. Gonalons, A. Giraldez, *Eur. J. Med. Chem.* **10** (1975) 143
7. Y. Kamano, H. P. Zhang, Y. Ichihara, H. Kizu, K. Komiyama, H. Itokawa, G. R. Pettit, *Tetrahedron Lett.* **36** (1995) 2783
8. A. Khorshidi, K. Tabatabaeian, *Orient. J. Chem.* **26** (2010) 837
9. K. Tabatabaeian, M. Mamaghani, N. O. Mahmoodi, A. Khorshidi, *Can. J. Chem.* **87** (2009) 1213
10. J. Bergman, N. Eklund, *Tetrahedron* **36** (1980) 1445
11. J. Azizian, A. A. Mohammadi, N. Karimi, M. R. Mohammadzadeh, *Cat. Commun.* **7** (2006) 752
12. J. Azizian, A. A. Mohammadi, A. R. Karimi, M. R. Mohammadzadeh, *J. Chem. Res. Synop.* **6** (2004) 424
13. J. S. Yadav, B. V. Subbareddy, U. G. Kamakolanu, *Synthesis* **24** (2006) 4121
14. V. P. Kumar, V. P. Reddy, R. Sridhar, B. Srinivas, M. Narender, K. R. Rao, *J. Org. Chem.* **73** (2008) 1646
15. J. Deng, S. Zhang, P. Ding, H. Jiang, W. Wang, J. Li, *Adv. Synth. Catal.* **352** (2010) 833
16. H. M. Meshram, D. A. Kumar, P. R. Goud, B. C. Reddy, *Synth. Commun.* **40** (2010) 39
17. K. Rad-Moghadam, M. Sharifi-Kiasaraie, H. Taheri-Amlashi, *Tetrahedron* **66** (2010) 2316
18. C. J. Li, *Chem. Rev.* **105** (2005) 3095
19. C. Bolm, J. Legros, J. L. Paih, L. Zani, *Chem. Rev.* **104** (2004) 6217
20. D. D. Diaz, P. O. Miranda, J. I. Padron, V. S. Martin, *Curr. Org. Chem.* **10** (2006) 457.
21. R. M. Srivastava, R. A. W. N. Filho, C. A. Silva, A. Bortoluzzi, *Ultrason. Sonochem.* **16** (2009) 737
22. A. Duarte, W. Cunico, C. M. P. Pereira, A. F. C. Flores, R. A. Freitag, G. M. Siqueira, *Ultrason. Sonochem.* **17** (2010) 281
23. H. A. Stefani, C. M. P. Pereira, R. B. Almeida, R. C. Braga, K. P. Guzenb, R. Cella, *Tetrahedron Lett.* **46** (2005) 6833
24. R. Cella, H. A. Stefani, *Tetrahedron* **65** (2009) 2619
25. K. Tabatabaeian, M. Mamaghani, N. O. Mahmoodi, A. Khorshidi, *Tetrahedron Lett.* **49** (2008) 1450.



J. Serb. Chem. Soc. 76 (10) 1355–1364 (2011)
JSCS–4210

Antithyroid activity of some 6-(alkylsulfanyl)-9H-purines

ISMAT FATIMA¹, MUNAWAR A. MUNAWAR^{1*}, AFFIA TASNEEM²,
SARWAT JAHAN³, MISBAHUL A. KHAN¹ and SHAKEEL AHMED³

¹Institute of Chemistry, University of the Punjab-Lahore, ²CENUM, Mayo Hospital -Lahore
and ³Department of Animal Sciences, Quid-i-Azam University Islamabad, Pakistan

(Received 13 December 2010, revised 4 February 2011)

Abstract: Some alkyl and aryl derivatives of 9H-purine-6-thiol were synthesized and evaluated *in vitro* and *in vivo* for potential antithyroid effects. Spectrophotometric studies demonstrated 1:1 charge transfer complexation between iodine and these compounds with quite high values of the formation constants. The blood assays of rats treated with these compounds revealed significant antithyroid activity for almost all the compounds, which was further supported by a histological study of the thyroid tissues of the animals. These compounds are expected to provide less toxic alternative of the existing medicines as the sulfanyl group, which is known to be a cause of toxicity of many drugs, is blocked by alkyl/aryl substituents.

Keywords: 9H-purine-6-thiol; derivatives; iodine; antithyroid.

INTRODUCTION

Hyperthyroidism is a major dysfunction of the thyroid gland in which the gland produces more hormones than is normally required by the body for its normal metabolic functions as well as mental and physical growth. Thyroid disorder disturbs not only other glands of endocrine system, but also other organs since they act on nearly every cell in the body.¹ The available treatments for hyperactive thyroid are: thyroidectomy (surgical removal of a part of or the whole gland), radioactive iodine therapy and antithyroid drugs. The former two modes provide permanent treatment but have serious drawbacks. The side effects of radioiodine are the development of tumors, leukemia, thyroid cancer and birth defects in women but the reported incidences are low.² On the other hand, surgery may lead to tracheal compression due to bleeding, infection, bilateral vocal fold paralysis and superior laryngeal nerve damage. Perpetual hypothyroidism is common for both these treatments.^{3,4} Moreover, certain hyperthyroid conditions

* Corresponding author. E-mail: mamunawar.chem@pu.edu.pk
doi: 10.2298/JSC101209041I

are not permanent and do not need surgery or radioiodine therapy. The use of antithyroid drug becomes the only choice under such conditions but there is a scarcity of drugs in this particular area. Propylthiouracil, methimazole (MMI) and carbimazole are the only widely used synthetic antithyroid agents (SATs).⁵ These drugs have many serious side-effects, such as agranulocytosis, liver damage, aplastic anemia and vasculitis, while minor side-effects, such as itching, rash, hives, pain and swelling in joints, fever, change in taste, nausea and vomiting have been observed in fifteen percent of the patients treated with these drugs.⁶⁻⁸ The presence of free SH group in these drugs is reported to be the cause of the toxic side effects, as with many other compounds containing the sulfonamide group.⁹ For this reason, an earnest need was felt to search for new, less toxic and more effective SATs. Many compounds were evaluated and some were reported to possess recognizable antithyroid activity.^{5,10} SATs are supposed to act either through inhibition of the thyroperoxidase enzyme or by making stable charge transfer (CT) complexes with iodine in which iodine acts as a σ -acceptor and the synthetic compound as an n -donor.¹¹ Although, many drugs, such as levamisole, tetramethylthiourea, tetrahydrozoline and phenothiazines, have no effect on peroxidase yet exhibit strong antithyroid activity *in vivo* due to complexation with iodine.¹² Studies of CT complexation of various drugs having a thiazole or imidazole ring with iodine using UV/visible spectroscopy revealed a positive correlation between the formation constant (K_c) and *in vivo* antithyroid activity. Compounds having $K_c \geq 100 \text{ L mol}^{-1}$ were found to exhibit recognizable antithyroid activity.¹³ MMI acts predominantly through CT complexation with a K_c value of 23193 L mol^{-1} .¹⁴ Heterocyclic compounds, including purines, form CT complexes with iodine.¹⁵⁻¹⁷ Similarly, the medicinal value of certain purines and purine derivatives, including 6-mercaptopurine (6MP, 9H-purine-6-thiol); against HIV-1, cancer, bacteria and miscellaneous microbes was also reported.¹⁸⁻²¹ In light of the above, it was proposed to derivatize 6MP and to evaluate the antithyroid potential of the formed compounds. These compounds were expected to form stable CT complexes with iodine, like other heterocyclic compounds, which is a clue to antithyroid activity. Moreover, the suspected toxic effects due to free -SH group were ruled out by blocking this site with alkyl substituents. This also led to 1:1 complexation as the only site for an n - σ complex was available at the N-9 position.

EXPERIMENTAL

Materials, instruments and methods

Iodine (suprapur, bisublimed) was obtained from Merck and kept in dark in a dessicator containing P_2O_5 . Dimethyl sulfoxide (DMSO) of spectroscopic grade was obtained from Merck. It was dried over calcium hydride, distilled under reduced pressure and stored over type 4Å molecular sieves. 9H-Purine-6-thiol monohydrate (6MP) was obtained from Sigma-Aldrich and was used without further purification. 1-Methyl-1H-imidazole-2-thiol (MMI, methima-

zole) of analytical grade was purchased from Sigma-Aldrich and used without further purification for the *in vivo* study. Free T3 and T4 kits of Immunotech (France) and rat-TSH ELISA kit from Cusabio Biotech Co. Ltd. were used.

The spectra were recorded on a double beam UVD-3500 spectrophotometer (Labomed Inc.) and the slides of thyroid tissues were studied under an Olympus BX51 microscope fitted with an Olympus DP12 digital camera. The melting points were determined on a Gallenkamp melting point apparatus and are uncorrected. The $^1\text{H-NMR}$ and $^{13}\text{C-NMR}$ were determined in $\text{DMSO-}d_6$ using TMS as the internal standard on a Bruker Avance 300 (300 MHz for ^1H - and 75 MHz for $^{13}\text{C-NMR}$). The mass spectra were recorded on a Bruker Esquire 300+ ion trap with ESI ionization. Microanalysis for carbon, hydrogen and nitrogen was realized on a Perkin Elmer 2400-CHN analyzer.

Synthesis of 9H-purine-6-thiol derivatives

9H-Purine-6-thiol monohydrate (0.170 g, 1 mmol) in aqueous sodium hydroxide (2 M, 10 mL) was stirred at room temperature with the respective alkyl halides (1 mmol). The clear solution was stirred until the insoluble alkyl halides disappeared. After completion of the reaction, the pH of the solution was adjusted to 5.0 by the addition of glacial acetic acid and the white precipitates were filtered and recrystallized. All the compounds (Fig. 1) were synthesized using literature methods,^{22–25} except for (9) which was not found in the literature.

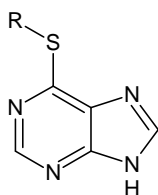


Fig. 1. General structure of the 9H-purine-6-thiol derivatives (R: **1**, CH_3 ; **2**, C_2H_5 ; **3**, C_3H_7 ; **4**, C_4H_9 ; **5**, C_5H_{11} ; **6**, C_6H_{13} ; **7**, C_7H_{15} ; **8**, C_8H_{17} ; **9**, C_9H_{19} ; **10**, $\text{C}_{10}\text{H}_{21}$; **11**, PhCH_2).

Assessment of antithyroid activity

In vitro. The *in vitro* activity was assessed by studying spectrophotometrically the complexation of the compounds with iodine. Solutions of iodine and the compounds were prepared just before the start of the experiment by diluting accurately prepared stock solutions in DMSO. The iodine concentration was kept constant (2×10^{-5} M), while those of the compounds were varied between 1×10^{-4} M and 1×10^{-3} M. The reactions were performed directly in the spectrophotometric cell by mixing 1.5 mL of the compound solutions and iodine solution and the spectra were recorded immediately. New absorption bands appeared which demonstrated the formation of CT complexes between iodine and the compound(s). The stoichiometry of the complex was ascertained by the method of continuous variations.²⁶

In vivo. The *in vivo* study was performed on young male Wistar rats of 175 ± 25 g weight. The animals were divided into fifteen groups, *i.e.*, the control, the vehicle control (solvent treated), the MMI treated and twelve groups for the compounds under study (6MP and **1–11**). MMI was used as a positive control, so that the efficacy of the potential compounds could also be compared with the most popular existing drug. Five animals were allocated to each group and were fed chick feed with water *ad libitum*. Solutions of the compounds and MMI in DMSO were administered *via i.p.* injection to the respective groups at a dose rate of 20 mg kg^{-1} per animal daily in the morning for 15 days. The control and vehicle control categories received an equivalent dose of normal saline and the solvent, respectively, for the same duration. On the 16th day, the animals were weighed and carried to the dissection room for blood

sampling and dissection. Due time was allowed before blood sampling to avoid hormonal changes because of any stress caused by transportation. Blood samples were collected from all the animals by puncturing the abdominal aorta under light diethyl ether anesthesia. Standard animal protocols were adopted for the experimentation.²⁷ Free T3 and T4 levels were determined using radioimmunoassay technique, while that of TSH by the ELISA method. The animals were subsequently sacrificed on the same day under deep diethyl ether anesthesia and the thyroid was removed, washed and weighed. Sections of the gland were fixed in 4 % paraformaldehyde (PFA) solution for 4–6 h and stained with hematoxylin and eosin to prepare slides for histological studies.

RESULTS AND DISCUSSION

All the compounds (Fig. 1) were synthesized using literature methods except **9**, which is not known to be reported. Previously, confirmation of the structures of the known compounds was established using melting point and elemental analysis only. Complete spectral information, including mass spectrometry, ¹H-NMR, ¹³C-NMR and CHN, were determined in the present study for detailed structure elucidation. The results are given in the Supplementary material.

All compounds absorbed in the UV region between 280 and 330 nm. The compounds **1–11** exhibited 1:1 complexation with iodine. 6MP also showed complexation but not of 1:1 stoichiometry. The compounds were soluble only in DMSO, therefore, its use as a solvent was inevitable, apart from its interaction with I₂, like many other aromatic and alkyl halide solvents.²⁸ A solution of iodine in DMSO gave sharp peaks at 295 and 365 nm, which are characteristic of the I₃⁻.²⁹ Occasionally other peaks around 250–255 nm were also observed. The interaction of DMSO with iodine is a slow process resulting in a weak complex.^{30,31} It was observed that in the presence of strong *n*-donors, its interaction with I₂ becomes very restrained. The CT band generally appears at 265–270 nm. The reaction mixture exhibited negligible absorption for the compound at concentrations below 2×10⁻⁴ M. On increasing the concentration of compounds (≥ 3×10⁻⁴ M), two peaks appeared usually at 300 and 270 nm, the latter being characteristic of complex formation.

The formation constants and molar extinction coefficients of the complexes were determined using the Lang method.³² This method derives a mathematical expression to calculate *K_c* for 1:1 stoichiometric complexes:

$$K_c = [C]/([I_0]-[C])([P_0]-[C]) \quad (1)$$

where, [I₀] and [P₀] are the initial concentrations of iodine and the compound(s), respectively, whilst [C] is the concentration of the complex. Now, according to Beer–Lambert Law:

$$[C] = \epsilon_c d_c$$

where *d_c* and *ε_c* are the absorbance and extinction coefficient of the complex, respectively. The value of *d_c* was calculated by subtracting the absorbance due to

free iodine present in the mixture from the observed absorbance of the reaction mixture. The solution of pure compound of same concentration is kept in the reference cell of the spectrophotometer. Now Eq. (1) can be re-written in the form:

$$Y = (1/\varepsilon_c) \cdot X + 1/(K_c \varepsilon_c) \quad (2)$$

where $Y = [I_0][P_0]/d_c$ and $X = [I_0] + [P_0] - d_c/\varepsilon_c$

Equation (2) is an equation of a straight line with slope $1/\varepsilon_c$ and Y -intercept $1/(K_c \varepsilon_c)$. First, the equation was solved using an assumed value of ε_c . This gave not only a value for K_c , but also a new value of ε_c was obtained. This new value differed from the old assumed value of ε_c . Now, the new value of ε_c was used to solve the equation and so forth until both ε_c and K_c converged to discrete values (Table I). This is a lengthy process and was performed by developing a computer-based iterative algorithm, which not only calculated the ε_c and K_c values, but also the values of X and Y . A linear regression curve gave the best fit for the XY scatter ($R^2 > 0.99$), thus confirming 1:1 complexation between iodine and the compounds **1–11**.

TABLE I. Spectrophotometric properties of the CT complexes of the studied compounds with I_2

Compound	CTB^a / nm	$K_c / 10^4$ L mol ⁻¹	$\varepsilon_c^b / 10^5$ L mol ⁻¹ cm ⁻¹
1	265	1.031	0.552
2	270	0.250	1.52
3	315	0.458	1.301
4	265–70	0.562	1.129
5	315	0.642	1.205
6	265–70	0.279	1.121
7	265–70	0.479	0.876
8	265–270	0.256	1.255
9	265–70	0.536	1.0452
10	265–70	0.962	0.635
11	265–70	2.335	0.794

^aCharge transfer band; ^bmolar extinction coefficient

The antithyroid effects of potential compounds can be ascertained *in vivo* by a decrease in the thyroid hormones, which is further confirmed by a corresponding increase in the pituitary hormone (TSH) levels. Similarly, regular exposure to SATs is known to increase the thyroid weight and change the thyroid histology.³³ In the present study, due consideration was given to all these aspects.

The radioimmunoassay results showed a decrease of free T_3 and T_4 levels in the serum of the treated groups, as compared to the control and vehicle control animals. In addition, a relative increase was observed in the TSH levels for the treated groups (Table II), which is a clear sign of the antithyroid potential of the studied compounds.

The hormonal variations were quite explicit, yet the data was analyzed statistically using the Dunnett test to further validate the results. This is a popular and useful hypothesis testing method used for comparing the treatments with a control when the sample size is the same in the control and the treatments. The Dunnett D value is:

$$D = d_{\alpha}(k, \nu)(2S_w^2/n)^{1/2}$$

where, $d_{\alpha}(k, \nu)$ is the critical Dunnett value at a given significance level (α), the number of non-control treatments (k) and the degree of freedom (ν); n is the sample size and S_w^2 is the combined estimate of the common variance.³⁴

TABLE II. Hormonal variations observed after 15 day dose administration ($n = 5$, dose rate = 20 mg kg^{-1})

Animal group	Mean hormone levels		
	$FT_3 / \text{pmol L}^{-1}$	$FT_4 / \text{pmol L}^{-1}$	$TSH / \mu \text{ i.u. mL}^{-1}$
Control	$8.41^{\text{a}} \pm 0.64^{\text{b}}$	35.86 ± 2.14	1.64 ± 0.32
Vehicle control	8.15 ± 0.81	34.09 ± 1.67	1.70 ± 0.23
	Treatment ^c		
6MP	5.86 ± 0.33	24.49 ± 2.48	2.99 ± 0.27
1	5.01 ± 0.65	24.32 ± 2.31	2.93 ± 0.45
2	6.78 ± 0.90	26.66 ± 2.82	2.40 ± 0.58
3	6.01 ± 0.97	25.92 ± 2.23	2.59 ± 0.71
4	5.82 ± 0.92	26.67 ± 2.34	2.62 ± 0.34
5	5.88 ± 0.71	25.16 ± 3.26	2.68 ± 0.39
6	6.69 ± 0.81	26.96 ± 2.58	2.40 ± 0.56
7	5.90 ± 0.93	26.77 ± 2.39	2.56 ± 0.38
8	6.79 ± 0.85	27.50 ± 2.40	2.38 ± 0.56
9	5.89 ± 1.17	26.99 ± 2.14	2.40 ± 0.26
10	5.37 ± 0.97	25.00 ± 2.08	2.88 ± 0.25
11	3.33 ± 1.05	16.08 ± 2.00	3.38 ± 0.30
MMI	3.36 ± 0.96	17.28 ± 1.98	3.53 ± 0.39

^aMean values of assay results run in duplicate; ^bstandard deviation; ^c $p \leq 0.05$ (with respect to the vehicle control)

The research hypotheses were:

H_a : $\mu_i < \mu_c$; will be true if $(y_i - y_c) \leq -D$ (for comparison of the FT_3 and FT_4 levels) and H_b : $\mu_i > \mu_c$; will be true if $(y_i - y_c) \geq D$ (for comparison of the TSH levels). Here, i and c stand for the treatment sample and the control, while μ and y for the population and sample means, respectively.

The hormone levels for all the treatments were compared with the controls using this method at $\alpha = 0.05$. The test results confirmed the efficacy of the compounds in lowering the serum free T_3 and T_4 levels with a corresponding simultaneous increase in the TSH levels. This clearly demonstrates the antithyroid potential of these compounds. However, **11** was proved to be the most potent among the whole series. It exhibited antithyroid potential almost equivalent to MMI.

Comparison between the K_c values and the pertaining hormonal variations revealed a positive correlation between K_c and the *in vivo* antithyroid activity. The relationship was observed to be fairly linear for moderate values of K_c . All the compounds demonstrated *in vivo* antithyroid effects; the higher activity of **11** can be attributed to resonance, which resulted in a more stable equilibrium, evident from the high K_c value of the **11**:I₂ complex.

SATs are known to increase in the weight of the thyroid gland. Since thyroid weight also depends on the size of the animal, a useful index called “thyroid body index” (*TBI*) was introduced to account for the effect of body weight on the thyroid weight. *TBI* can be defined as the weight of clean thyroid tissues (mg) per 100 g of body weight. These indices for treated animals were found to be higher than those of the controls (Table III). Moreover; the *TBI* values, like those of K_c , were also found proportional to the change in hormone levels. This depicts that the *TBI* can also be used as an empirical parameter for the assessment of anti-thyroid activity. Sections from thyroids of the treated animals showed marked difference in the shape of the glandular cells and quantity of intracellular fluid (colloid). Follicular cell hyperplasia and hypertrophy of various degrees were also observed in the treated animals (Table III).

Table III. Histological observations of the thyroid tissues from different animal groups (±: slight; +: mild; ++: moderate; +++: severe)

Animal group/description	Follicular cell hypertrophy/hyperplasia	Colloid depletion	<i>TBI</i> ×100 / mg g ⁻¹
Control	Nil	Nil	5.21
Vehicle control	±	+	6.01
6MP	++	++	10.35
1	+++	+++	11.23
2	+	++	7.41
3	++	++	7.83
4	++	++	9.26
5	+	++	8.61
6	+	++	7.37
7	++	++	8.79
8	+	++	7.03
9	++	++	7.58
10	++	+++	11.26
11	+++	+++	14.27
MMI	+++	+++	16.11

The thyroid of the control and vehicle control animals showed a cuboidal follicular epithelium with ample quantities of colloid. On the other hand, severe colloid depletion with a semi-cylindrical to cylindrical-shaped epithelium was observed for the treated animals (Fig. 2). Very slight atrophy was noted in the follicular cells, which demonstrates the smaller toxicity of these compounds.

Obesity in the treated animals was also seen in the second week of treatment, without any sign of intoxication because eating and drinking habits remained normal. No animal died during the study period.

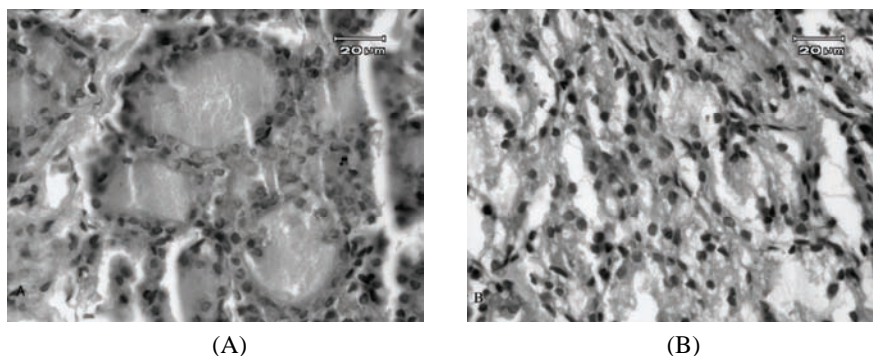


Fig. 2. Microscopic view of thyroid sections: A) control with epithelium full of colloid and normal nuclei of follicular cells, B) 11-treated animal, severe colloid depletion is visible with follicular cell hypertrophy and hyperplasia.

CONCLUSIONS

The studied derivatives of 9*H*-purine-6-thiol form 1:1 charge transfer complexes with iodine and were found to possess highly significant antithyroid activity *in vivo*, which was in good correlation with the K_c values. 6-(Benzylsulfonyl)-9*H*-purine showed the maximum antithyroid effects, comparable to that of methimazole and may have less side effects due to the blockage of the free SH group. Further research on these compounds could lead to the discovery of new drugs.

SUPPLEMENTARY MATERIAL

Analytical and spectral data of synthesized compounds are available electronically from <http://www.shd.org.rs/JSCS/>, or from the corresponding author on request.

Acknowledgements. The authors are obliged to the Higher Education Commission of Pakistan for providing the financial assistance to realize the research. The cooperation of Mr. Syed Abbas Sultan, Muhammad Ashraf Mughal and Muhammad Rehan Adil of AEMC-Lahore (Pakistan) during the study is also acknowledged by the authors.

ИЗВОД

АНТИТИРОИДНА АКТИВНОСТ 6-(АЛКИЛСУЛФАНИЛ)-9*H*-ПУРИНА

ISMAT FATIMA¹, MUNAWAR A. MUNAWAR¹, AFFIA TASNEEM², SARWAT JAHAN³,
MISBAHUL A. KHAN¹ и SHAKEEL AHMED³

¹Institute of Chemistry, University of the Punjab-Lahore, ²CENUM, Mayo Hospital – Lahore u

³Department of Animal Sciences, Quid-i-Azam University Islamabad, Pakistan

Синтетисани су алкил и арил деривати 9*H*-пурин-6-тиола и испитивана је њихова *in vitro* и *in vivo* антитироидна активност. Спектрофотометријска анализа је показала да се ства-

рају комплекси између јода и ових једињења у односу 1:1, уз високу константу асоцијације. Анализа крви пацова третираних овим једињењима је показала да сва једињења имају значајну антитироидну активност, што је даље потврђено хистолошким налазима тироидног ткива. Могућа предност ових једињења у односу на постојеће антитироидне лекове је у смањеној токсичности, пошто је сулфанил група, иначе позната као узрочник токсичности многих лекова, блокирана алкил/арил супституентима.

(Примљено 13. децембра 2010, ревидирано 4. фебруара 2011)

REFERENCES

1. D. S. Cooper, *Lancet* **62** (2003) 459
2. B. Solomon, D. Glinoe, R. Lagasse, L. Wartofsky, *J. Clin. Endocrinol. Metab.* **70** (1990) 1518
3. O. Alsanea, O. H. Clark, *Endocrinol. Metab. Clin. North Am.* **29** (2000) 321
4. E. I. Tamagna, G. A. Levine, J. M. Hershman, *J. Nucl. Med.* **20** (1979) 387
5. C. Laurence, M. J. El Ghomari, J. Y. Le Questel, M. Berthelot, R. Mokhlisse, *J. Chem. Soc., Perkin Trans. 2* (1998) 1545
6. D. S. Cooper, *N. Engl. J. Med.* **352** (2005) 905
7. J. R. Reid, S. F. Wheeler, *Am. Fam. Physician* **72** (2005) 623
8. U. Bandyopadhyay, K. Biswas, R. K. Banerjee, *Toxicol. Lett.* **128** (2002) 117
9. J. F. Lagorce, F. Comby, A. Rousseau, J. Buxeraud, C. Raby, *Chem. Pharm. Bull.* **41** (1993) 1258
10. R. A. Abou-Shaaban, H. A. Al-Khamees, H. S. Abou-Auda, A. P. Simonelli, *Saudi Pharm. J.* **3** (1995) 156
11. C. Raby, J. F. Lagorce, A. C. Jambut-Absil, J. Buxeraud, G. Catanzano, *Endocrinol.* **126** (1990) 1683
12. A. C. Jambut-Absil, J. Buxeraud, J. Calude, C. Raby, *Arzneim. Forsch. Drug Res.* **37** (1987) 772
13. F. Comby, J. F. Lagorce, J. Buxeraud, C. Raby, *J. Pharm. Pharmacol.* **46** (1994) 50
14. J. Buxeraud, A. C. Jambut-Absil, C. Raby, *J. Pharm. Sci.* **73** (1984) 1687
15. P. Machmer, J. Duchesne, *Nature* **206** (1965) 618
16. R. Beukers, A. Szent-Gyorgyi, *Rec. Trav. Chim. Pays-Bas.* **81** (1962) 256
17. D. V. Helm, S. D. Christian, L. Lian, *J. Am. Chem. Soc.* **95** (1973) 2409
18. S.T. Malton, A. Ornoy, A. Fisherman, L. Drucker, M. Lishner, *Human Reprod.* **20** (2005) 1397
19. L. L. Gunderson, N. M. Jon, B. Spilsberg, *J. Med. Chem.* **45** (2002) 1383
20. M. Tuncbilek, Z. Ates-Alagoz, N. Altanlar, A. Karayel, S. Ozbey, *Bioorg. Med. Chem.* **17** (2009) 693
21. I. Fatima, M. A. Munawar, M. A. Khan, A. Tasneem, Asmatullah, M. Khalil, *J. Braz. Chem. Soc.* **21** (2010) 1699
22. G. B. Elion, E. Burgi, G. H. Hitchings, *J. Am. Chem. Soc.* **74** (1952) 411
23. T. P. Johnson, B. L. Holum, J. A. Montgomery, *J. Am. Chem. Soc.* **80** (1958) 6265
24. C. G. Skinner, R. G. Ham, D. C. Fitzgerald, R. E. Eakin, W. Shive, *J. Org. Chem.* **21** (1956) 1330
25. S. A. Laufer, D. M. Domeyer, T. R. Scior, W. Albrecht, E. J. H. Domonik, *J. Med. Chem.* **48** (2005) 710
26. G. H. Duffey, *Physical Chemistry*, McGraw Hill Book Co., New York, USA, 1962, p. 493

27. The Council of European Communities, *Council Directive 86/609/EEC*, 1986
28. a) P. Klæboe, *Acta Chem. Scand.* **18** (1964) 27; b) B. Pullman, A. Pullman, *Biochemistry* **44** (1958) 1197
29. R. P. Lang, *J. Am. Chem. Soc.* **84** (1962) 1185
30. S. K. Si, A. A. Gewirth, *Phys. Chem. Chem. Phys.* **3** (2002) 3325
31. N. Alizadeh, M. A. Zanjanchi, H. Sharghi, R. Khalifeh, M. Shamsipur, *J. Iran. Chem. Soc.* **5** (2008) 610
32. R. P. Lang, *J. Phys. Chem.* **72** (1968) 2129
33. R. N. Hill, T. M. Crisp, P. M. Hurley, S. L. Rosenthal, D. V. Singh, *Environ Health Perspect.* **106** (1998) 447
34. R. L. Ott, M. Longnecker, *An Introduction to Statistical Methods and Data Analysis*, Cengage Learning Brooks/Cole Publishing Co., Belmont, CA, USA, 2008, p. 451.



SUPPLEMENTARY MATERIAL TO
Antithyroid activity of some 6-(alkylsulfanyl)-9H-purines

ISMAT FATIMA¹, MUNAWAR A. MUNAWAR^{1*}, AFFIA TASNEEM²,
SARWAT JAHAN³, MISBAHUL A. KHAN¹ and SHAKEEL AHMED³

¹Institute of Chemistry, University of the Punjab-Lahore, ²CENUM, Mayo Hospital -Lahore
and ³Department of Animal Sciences, Quid-i-Azam University Islamabad, Pakistan

J. Serb. Chem. Soc. 76 (10) (2011) 1355–1364

ANALYTICAL AND SPECTRAL DATA OF THE PREPARED COMPOUNDS

6-(Methylsulfanyl)-9H-purine (1). Yield: 92 %; m.p. 223 °C (lit.** 218–220 °C²²). Anal. Calcd. for C₆H₆N₄S: C, 43.36; H, 3.64; N, 33.71 %. Found: C, 43.33, H, 3.59, N, 33.69 %. ¹H-NMR (400 MHz, DMSO-*d*₆, δ / ppm): 13.48 (1H, *s*, NH imidazole), 8.68 (1H, *s*, CH imidazole), 8.42 (1H, *s*, CH pyrimidine), 2.64 (3H, *s*, CH₃). ¹³C-NMR (100 MHz, DMSO-*d*₆, δ / ppm): 153.92 (C), 153.41 (C), 151.47 (CH), 143.11 (CH), 129.36 (C), 11.15 (CH₃). EI-MS (*m/z*, (relative abundance, %)): 167.0 (M+1) (15.33), 166.0 (M⁺) (100.0). UV-Vis (DMSO-*d*₆) (λ_{max} / nm, (ε / L mol⁻¹ cm⁻¹)): 280 (39290).

6-(Ethylsulfanyl)-9H-purine (2). Yield: 89 %; m.p. 196 °C (lit. 196 °C²³). Anal. Calcd. for C₇H₈N₄S: C, 46.65; H, 4.47; N, 31.09 %. Found: C, 46.63; H, 4.43; N, 31.02 %. ¹H-NMR (300 MHz, DMSO-*d*₆, δ / ppm): 13.45 (1H, *s*, NH imidazole), 8.67 (1H, *s*, CH imidazole), 8.41 (1H, *s*, CH pyrimidine), 3.27 (2H, *q*, *J* = 7.20 Hz, CH₂), 1.35 (3H, *t*, *J* = 7.20 Hz, CH₃). ¹³C-NMR (75 MHz, DMSO-*d*₆, δ / ppm): 157.95 (C), 151.45 (C), 150.51 (CH), 143.25 (CH), 129.38 (C), 22.41 (CH₂), 14.94 (CH₃). EI-MS (*m/z*, (relative abundance, %)): 181 (M+1), (9.99), 180.0 (M⁺) (96.64), 164.9 (51.34), 151.9 (47.51), 147.0 (BP), (100). UV-Vis (DMSO-*d*₆) (λ_{max} / nm, (ε / L mol⁻¹ cm⁻¹)): 300 (21670).

6-(Propylsulfanyl)-9H-purine (3). Yield: 94 %; m.p. 182 °C (lit. 179 °C²³). Anal. Calcd. for C₈H₁₀N₄S: C, 49.46; H, 5.19; N, 28.84 %. Found: C, 48.95, H, 5.18, N, 28.79 %. ¹H-NMR (400 MHz, DMSO-*d*₆, δ / ppm): 13.24 (1H, *s*, NH imidazole), 8.65 (1H, *s*, CH imidazole), 8.40 (1H, *s*, CH pyrimidine), 3.31 (2H, *t*, *J* = 7.20 Hz, SCH₂), 1.71 (2H, *sext.*, *J* = 7.20 Hz, CH₂), 0.99 (3H, *t*, CH₃, *J* = 7.20 Hz). ¹³C-NMR (100.6 MHz, DMSO-*d*₆, δ / ppm): 158.01 (C), 151.34 (C), 150.41 (CH), 143.44 (CH), 129.33 (C), 29.69 (CH₂), 22.61 (CH₂), 13.20

* Corresponding author. E-mail: mamunawar.chem@pu.edu.pk

** Reference numbers hold for the list given in the paper.

(CH₃). EI-MS (*m/z*, (relative abundance, %)): 194.0 (M⁺) (86.5), 179.0 (76.7), 166.0 (89.9), 165.0 (52.8), 161.0 (48.0), 153.0 (21.5), 152.0 (BP) (100). UV-Vis (DMSO-*d*₆) (λ_{\max} / nm, (ϵ / L mol⁻¹ cm⁻¹)): 330 (20910).

6-(Butylsulfanyl)-9H-purine (4). Yield: 95 %; m.p. 152 °C (lit. 152 °C²³). Anal. Calcd. for C₉H₁₂N₄S: C, 51.9; H, 5.81; N, 26.90 %. Found: C, 52.1, H, 5.79, N, 26.93 %. ¹H-NMR (300 MHz, DMSO-*d*₆, δ / ppm): 13.47 (1H, *s*, NH imidazole), 8.66 (1H, *s*, CH imidazole), 8.41 (1H, *s*, CH pyrimidine), 3.33 (2H, *t*, *J* = 7.20 Hz, SCH₂), 1.67 (2H, *quin.*, *J* = 7.20 Hz, SCH₂CH₂), 1.43 (2H, *sext.*, *J* = 7.20 Hz, CH₂CH₃), 0.90 (3H, *t*, *J* = 7.20 Hz, CH₃). ¹³C-NMR (75 MHz, DMSO-*d*₆, δ / ppm): 158.03 (C), 151.44 (C), 150.34 (CH), 143.19 (CH), 129.37 (C), 31.25 (CH₂), 27.48 (CH₂), 21.39 (CH₂), 13.51 (CH₃). EI-MS (*m/z*, (relative abundance, %)): 208 (M⁺) (43.9), 179.0 (92.5), 175.0 (23.5), 168.0 (10.0), 167.0 (21.1), 166.0 (BP) (100). UV-Vis (DMSO-*d*₆) (λ_{\max} / nm, (ϵ / L mol⁻¹ cm⁻¹)): 285 (29590).

6-(Pentylsulfanyl)-9H-purine (5). Yield: 94 %; m.p. 117 °C (lit. 115.5 °C²³). Anal. Calcd. for C₁₀H₁₄N₄S: C, 54.03; H, 6.35; N, 25.20%. Found: C, 54.10, H, 6.33, N, 25.18 %. ¹H-NMR (400 MHz, DMSO-*d*₆, δ / ppm): 13.51 (1H, *s*, NH imidazole), 8.66 (1H, *s*, CH imidazole), 8.41 (1H, *s*, CH pyrimidine) 3.32 (2H, *t*, *J* = 7.20 Hz, SCH₂), 1.69 (2H, *quin.*, SCH₂CH₂), 1.40 (2H, *quin.*, *J* = 7.20 Hz, SCH₂CH₂CH₂), 1.32 (2H, *sext.*, *J* = 7.20 Hz, CH₂CH₃), 0.863 (3H, *t*, *J* = 7.20 Hz, CH₃). ¹³C-NMR (100 MHz, DMSO-*d*₆, δ / ppm): 157.91 (C), 151.43 (C), 144.46 (CH), 143.18 (CH), 129.31 (C), 30.39 (CH₂), 28.83 (CH₂), 27.74 (CH₂), 21.67 (CH₂), 13.82 (CH₃). EI-MS (*m/z*, (relative abundance, %)): 222.0 (M⁺) 37.2), 189.1 (15.9), 179.0 (62.1), 175.1 (32.1), 168.0 (7.8), 167.0 (15.1), 166.0 (BP) (100). UV-Vis (DMSO-*d*₆) (λ_{\max} / nm, (ϵ / L mol⁻¹ cm⁻¹)): 335 (46880).

6-(Hexylsulfanyl)-9H-purine (6). Yield: 78 %; m.p. 79 °C (lit. 77 °C²⁴). Anal. Calcd. for C₁₁H₁₆N₄S: C, 55.90; H, 6.82; N, 23.71 %. Found: C, 55.82, H, 6.77, N, 23.85 %. ¹H-NMR (400 MHz, DMSO-*d*₆, δ / ppm): 13.45 (1H, *s*, NH imidazole), 8.66 (1H, *s*, CH imidazole), 8.41 (1H, *s*, CH pyrimidine) 3.32 (2H, *t*, *J* = 7.20 Hz, SCH₂), 1.68 (2H, *quin.*, SCH₂CH₂), 1.39 (2H, *quin.*, *J* = 7.20 Hz, SCH₂CH₂CH₂), 1.26 (2H, *quin.*, *J* = 7.20 Hz, CH₂CH₂CH₃), 1.23 (2H, *sext.*, *J* = 7.20 Hz, CH₂CH₃), 0.835 (3H, *t*, *J* = 7.20 Hz, CH₃). ¹³C-NMR (100 MHz, DMSO-*d*₆, δ / ppm): 158.03 (C), 151.42 (C), 150.43 (CH), 143.17 (CH), 129.35 (C), 30.75 (CH₂), 29.10 (CH₂), 27.87 (CH₂), 27.78 (CH₂), 21.97 (CH₂), 13.84 (CH₃). EI-MS (*m/z*, (relative abundance, %)): 236.1 (M⁺) (71.2), 203 (66.6), 189.1 (68.5), 179.0 (75.7), 175.1 (64.9), 167.0 (49.7), 161.0 (49.2), 154.0 (40.9), 152.0 (BP) (100). UV-Vis (DMSO-*d*₆) (λ_{\max} / nm, (ϵ / L mol⁻¹ cm⁻¹)): 280 (34580).

6-(Heptylsulfanyl)-9H-purine (7). Yield: 79 %; m.p. 80 °C (lit. 79–81 °C²⁴). Anal. Calcd. for C₁₂H₁₈N₄S: C, 57.57; H, 7.25; N, 22.38 %. Found: C, 57.56,

H, 7.20, N, 22.36 %. $^1\text{H-NMR}$ (300 MHz, $\text{DMSO-}d_6$, δ / ppm): 13.45 (1H, *s*, NH imidazole), 8.64 (1H, *s*, CH imidazole), 8.39 (1H, *s*, CH pyrimidine) 3.32 (2H, *t*, $J = 7.20$ Hz, SCH_2), 1.69 (2H, *quin.*, SCH_2CH_2), 1.64–1.24 (8H, *m*, 4 CH_2), 0.842 (3H, *t*, $J = 7.20$ Hz, CH_3); $^{13}\text{C-NMR}$ (75 MHz, $\text{DMSO-}d_6$, δ / ppm): 157.91 (C), 151.30 (C), 150.96 (CH), 143.55 (CH), 31.14 (C), 29.17 (CH_2), 28.20 (CH_2), 28.17 (CH_2), 27.80 (CH_2), 22.00 (CH_2), 13.91 (CH_3). EI-MS (*m/z*, (relative abundance, %)): 249.1 (M^+) (86.1), 235.0 (25.1), 231.7 (48.7), 217.3 (29.5), 203.7 (15.3), 179.0 (47.6), 166.0 (82.3), 152.0 (BP) (100). UV-Vis ($\text{DMSO-}d_6$) (λ_{max} / nm, (ϵ / $\text{L mol}^{-1} \text{cm}^{-1}$)): 285 (29240).

6-(Octylsulfanyl)-9H-purine (8). Yield: 94 %; m.p. 84 °C (lit. 78–80 °C²⁴). Anal. Calcd. for $\text{C}_{13}\text{H}_{20}\text{N}_4\text{S}$: C, 59.06; H, 7.62; N, 21.19 %. Found: C, 59.01, H, 7.58,; N, 21.08 %. $^1\text{H-NMR}$ (400 MHz, $\text{DMSO-}d_6$, δ / ppm): 13.46 (1H, *s*, NH imidazole), 8.66 (1H, *s*, CH imidazole), 8.41 (1H, *s*, CH pyrimidine) 3.26 (2H, *t*, $J = 7.20$ Hz, SCH_2), 1.72–1.65 (12H, *m*, 6 CH_2), 0.85 (3H, *t*, $J = 7.20$ Hz, CH_3). $^{13}\text{C-NMR}$ (100 MHz, $\text{DMSO-}d_6$, δ / ppm): 158.02 (C), 151.41 (C), 150.43 (CH), 143.17 (CH), 129.34 (C), 31.18 (CH_2), 29.12 (CH_2), 28.54 (CH_2), 28.48 (CH_2), 28.18 (CH_2), 27.77 (CH_2), 22.04 (CH_2), 13.91 (CH_3). EI-MS (*m/z*, (relative abundance, %)): 264.0 (M^+) (82.2), 231.1 (57.6), 217.0 (27.2), 179.0 (48.1), 166.0 (85.2), 151.9 (100.0). UV-Vis ($\text{DMSO-}d_6$) (λ_{max} / nm, (ϵ / $\text{L mol}^{-1} \text{cm}^{-1}$)): 285 (32410).

6-(Nonylsulfanyl)-9H-purine (9). Yield: 93 %; m.p. 97 °C. Anal. Calcd. for $\text{C}_{14}\text{H}_{22}\text{N}_4\text{S}$: C, 60.40; H, 7.96; N, 20.12 %. Found: C, 60.37, H, 7.89, N, 20.09. $^1\text{H-NMR}$ (400 MHz, $\text{DMSO-}d_6$, δ / ppm): 13.16 (1H, *s*, NH imidazole), 8.64 (1H, *s*, CH imidazole), 8.39 (1H, *s*, CH pyrimidine), 3.23 (2H, *t*, $J = 7.20$ Hz, SCH_2), 1.70–1.22 (14H, *m*, 7 CH_2), 0.83 (3H, *t*, $J = 7.20$ Hz, CH_3). $^{13}\text{C-NMR}$ (100 MHz, $\text{DMSO-}d_6$, δ / ppm): 157.95 (C), 151.27 (C), 150.51 (CH), 143.55 (CH), 129.38 (C), 31.23 (CH_2), 29.14 (CH_2), 28.84 (CH_2), 28.59 (CH_2), 28.53 (CH_2), 28.17 (CH_2), 27.75 (CH_2), 22.05 (CH_2), 13.91 (CH_3). EI-MS (*m/z*, (relative abundance, %)): 278.1 (M^+) (77.3), 245.1 (47.7), 231.1 (75.8), 221.0 (36.7), 207.0 (17.7), 190.0 (19.3), 179.0 (93.9), 166.0 (100.0). UV-Vis ($\text{DMSO-}d_6$) (λ_{max} / nm, (ϵ / $\text{L mol}^{-1} \text{cm}^{-1}$)): 280 (34810).

6-(Decylsulfanyl)-9H-purine (10). Yield: 92 %; m.p. 89 °C (lit. 84–85 °C²⁵). Anal. Calcd. for $\text{C}_{15}\text{H}_{24}\text{N}_4\text{S}$: C, 61.61; H, 8.27; N, 19.16; S, 10.96 %. Found: C, 61.53, H, 8.24, N, 19.15 %. $^1\text{H-NMR}$ (300 MHz, $\text{DMSO-}d_6$, δ / ppm): 13.48 (1H, *s*, NH imidazole), 8.67 (1H, *s*, CH imidazole), 8.42 (1H, *s*, CH pyrimidine), 3.33 (2H, *t*, $J = 7.20$ Hz, SCH_2), 1.72 (2H, *quin.*, $J = 7.20$ Hz, SCH_2CH_2), 1.41–1.23 (14H, *m*, 7 CH_2), 0.84 (3H, *t*, $J = 7.20$ Hz, CH_3). $^{13}\text{C-NMR}$ (75 MHz, $\text{DMSO-}d_6$, δ / ppm): 157.64 (C), 151.39 (C), 150.53 (CH), 143.19 (CH), 129.36 (C), 31.24 (CH_2), 29.09 (CH_2), 28.88 (CH_2), 28.65 (CH_2), 28.59 (CH_2), 28.50 (CH_2), 28.14 (CH_2), 27.73 (CH_2), 22.05 (CH_2), 13.92 (CH_3). EI-MS (*m/z*, (relative abundance, %)): 292.1 (M^+) (77.9), 259.1 (74.1), 245.1 (76.1), 231.1 (62.3), 221.1

(68.2), 179.0 (89.0), 152.0 (100.0). UV-Vis (DMSO-*d*₆) (λ_{max} / nm, (ϵ / L mol⁻¹ cm⁻¹)): 280 (34340).

6-(Benzylsulfanyl)-9H-purine (II). Yield 88 %; m.p. 195 °C (lit. 195 °C²⁵). Anal. Calcd. for C₁₂H₁₀N₄S: C, 59.48; H, 4.16; N, 23.12 %. Found: C, 59.47, H, 4.12, N, 23.14 %. ¹H-NMR (400 MHz, DMSO-*d*₆, δ / ppm): 13.12 (1H, *s*, NH imidazole), 8.72 (1H, *s*, CH imidazole), 8.40 (1H, *s*, CH pyrimidine), 7.45–7.21 (5H, *m*, ArH), 4.61 (2H, *s*, CH₂). ¹³C-NMR (75 MHz, DMSO-*d*₆, δ / ppm): 57.67 (C), 151.38 (C), 150.79 (CH), 143.40 (CH), 137.83 (C), 129.46 (C), 128.94 (CH), 128.44 (CH), 127.12 (CH), 31.59 (CH₂). EI-MS (*m/z*, (relative abundance, %)): 243.0 (M+1) (48.3), 242.0 (M⁺) (100.0), 210.0 (36.3), 209.0 (100.0), 208.0 (32.0). UV-Vis (DMSO-*d*₆) (λ_{max} / nm, (ϵ / L mol⁻¹ cm⁻¹)): 285 (29270).



J. Serb. Chem. Soc. 76 (10) 1365–1378 (2011)
JSCS–4211

Mechanisms of the interaction between Pr(DNR)₃ and herring-sperm DNA

XIAOCAI LIU¹, XINGMING WANG^{1*} and LISHENG DING²

¹*School of Materials Science and Engineering, Southwest University of Science and Technology, Mianyang 62101 and* ²*Chengdu Institute of Biology, Chinese Academy of Sciences, Chengdu 610041, China*

(Received 26 August, revised 8 November 2010)

Abstract: Research on the interaction mechanism of drugs with DNA is essential to understand their pharmacokinetics. The interaction between rare earth complexes Pr(DNR)₃ and herring-sperm DNA was studied in Tris-HCl buffer solution (pH 7.4) by absorption and fluorescence spectroscopy and viscosity measurements. The results showed that the modes of interaction between Pr(DNR)₃ and herring-sperm DNA were electrostatic and intercalation. The binding ratio was $n_{\text{Pr(DNR)}_3}:n_{\text{DNA}} = 5:1$ and the binding constant was $K^\ominus(292\text{ K}) = 4.34 \times 10^3\text{ L mol}^{-1}$. Furthermore, according to the double reciprocal method and the thermodynamic equation, the intercalative interaction was cooperatively driven by an enthalpy effect and an entropy effect.

Keywords: daunorubicin; rare earth complexes; herring-sperm DNA; acridine orange; interaction mechanism.

INTRODUCTION

Drug therapy is currently one of the main means of combating cancer; therefore, the design of anti-cancer drugs is mostly based on DNA as the target. The study of the mechanism of drugs and DNA interaction has important significance in the synthesis of anti-cancer drugs.¹ Drugs binding to DNA have been studied by numerous researchers.^{2,3}

Daunorubicin (DNR) (Fig. 1) is a clinically used antitumor anthracycline antibiotic.^{4–6} Its anticancer activity is due to the formation of intercalative complexes with DNA and inhibition of the duplication of both DNA and RNA. However, its side effects, especially its cardiotoxicity, have greatly restrained its application.⁷ A great deal of research was aimed at reducing the toxicity of DNR by remodeling its structure,^{8–11} and by forming metal ion–DNR complexes to protect the quinone structure from being reduced.^{12–14}

* Corresponding author. E-mail: xmwang_xkd@yahoo.com.cn
doi: 10.2298/JSC100826121L

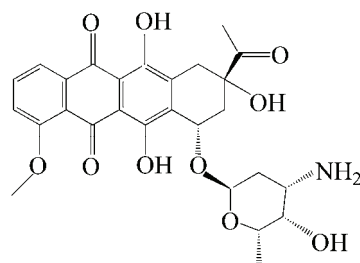


Fig. 1. The structure of DNR.

However, the complexes formed between anthracycline antibiotics and rare earth metals with pharmacological activity have not been researched for anti-cancer applications. In the present study, $\text{Pr}(\text{DNR})_3$ complexes were synthesized and then attention was focused on the mechanism of interaction of $\text{Pr}(\text{DNR})_3$ with DNA. It was expected that the results could be of significance in the fields of the chemistry of rare earth complexes, biological inorganic chemistry and drug inorganic chemistry.^{15,16}

EXPERIMENTAL

Instruments and reagents

Herring-sperm DNA (hs-DNA) and DNA bases were purchased from Sigma Biological Co. and used as received. Acridine orange (AO) was purchased from Shanghai-China Medicine Chemical Plant (A.R.). Pr_2O_3 was purchased from Chengdu-China Kelong Chemical Plant (A.R.). Daunorubicin hydrochloride (DNR) was purchased from JiNan Wedu Industrial Co., Ltd., Tris-HCl buffer (pH 7.40) was used to control the pH of the reaction system. All the samples were dissolved in the Tris-HCl buffer. Other reagents were of at least analytical grade. Solutions in buffer were freshly prepared immediately before use.

The absorption spectra were recorded on an UV-210 spectrophotometer and the fluorescence spectra on a FL-4500 spectrofluorophotometer (Shimadzu, Japan). The infrared absorption spectra were recorded on FT-IR spectrometer (PE Instruments, USA). Elementary analyses were performed on a Vario EL CUBE elementary analyzer (Element Analysis System Inc., Germany). The pH was recorded on a PHS-2C acidometer (Fangzhou Technology Co., China).

Preparation of PrCl_3 solutions

Pr_2O_3 was dissolved in concentrated hydrochloric acid and then the solution was heated to remove the excess water and hydrochloric acid to give PrCl_3 as a white powder. PrCl_3 solutions of different concentrations were prepared in 0.10 mol L^{-1} Tris-HCl buffer solution (pH 7.4).

Synthesis of the $\text{Pr}(\text{DNR})_3$ complex

The complex was prepared from stoichiometric amounts (1:3) of praseodymium chloride and DNR in absolute ethanol. The reaction system was recirculated on a water bath at 343 K for 12 h whereby the color of the solution changed from red to red-brown. The sample was concentrated to 10 mL in an oven for 5 h. During standing for several days, a brownish precipitation of $\text{Pr}(\text{DNR})_3$ formed.

The $\text{Pr}(\text{DNR})_3$ complex was characterized by elemental analysis and IR spectroscopy.

The absorption spectra and fluorescence spectra

A solution of $\text{Pr}(\text{DNR})_3$ ($1.17 \times 10^{-5} \text{ mol L}^{-1}$, 3 mL) in Tris-HCl buffer (pH 7.4) was titrated in a 1 cm pathlength cuvette by adding successively 10 μL of a DNA solution ($1.00 \times 10^{-4} \text{ mol L}^{-1}$). After each addition, the absorption and fluorescence spectra were recorded. Tris-HCl buffer solution served as the reference for the absorption measurements. The excitation wavelength for the fluorescence measurements was 411.7 nm and the excitation and emission slits were both set at 10 nm. The volume effect was so small that it could be ignored. Additionally, AO was used as a fluorescent probe to study the interaction mode between the complex and DNA.

Viscosity measurements

Viscosity measurements were performed using a Ubbelohde viscometer, which was immersed in a thermostat water-bath at room temperature. Different amounts of $\text{Pr}(\text{DNR})_3$ (1.0×10^{-6} – $5.0 \times 10^{-6} \text{ mol L}^{-1}$) were added into the viscometer while keeping the DNA concentration constant at $1.00 \times 10^{-5} \text{ mol L}^{-1}$. The flow time of the samples was repeatedly measured with an accuracy of $\pm 0.20 \text{ s}$ using a digital stopwatch. The flow times were above 250 s and each point represents the average of at least three readings. The data is presented as $(\eta/\eta_0)^{1/3}$ vs. $c_{\text{Pr}(\text{DNR})_3}$, where η and η_0 are the relative viscosities of the DNA solution in the presence and absence of the $\text{Pr}(\text{DNR})_3$ complex, respectively.

RESULTS AND DISCUSSION

Characterization of the $\text{Pr}(\text{DNR})_3$ complex

In contrast to DNR (data in parentheses), the IR spectrum of $\text{Pr}(\text{DNR})_3$ displayed clearly the stretching vibration band of OH at 3428 cm^{-1} ($\nu_{\text{OH}} = 3443 \text{ cm}^{-1}$). The bending vibration of $-\text{CH}_2-$ was at 2931 cm^{-1} ($\nu_{\text{CH}} = 2919 \text{ cm}^{-1}$). The stretching vibration band of the CN and the bending vibration of NH were at 1273 cm^{-1} ($\nu_{\text{CN}} + \delta_{\text{NH}} = 1292 \text{ cm}^{-1}$). The stretching vibration band of CN was at 1115 cm^{-1} ($\nu_{\text{CN}} = 1126 \text{ cm}^{-1}$). These results show that the bands in the IR spectrum of the complex (OH, CN and NH) were shifted to lower frequencies in comparison to the corresponding bands in the spectrum of DNR. This proves the formation of the Pr–DNR complex.

Elemental analysis. C, 51.68; H, 5.29; N, 2.28 % (experimental data). C, 53.17; H, 4.79; N 2.30 % (theoretical value).

From the results of the elemental analysis, the formula of the complex was speculated as $[\text{Pr}(\text{C}_{27}\text{H}_{29}\text{NO}_{10})_3]\text{Cl}_3$.

Determination of the binding ratio of Pr^{3+} and DNR using the mole ratio method

Fluorescence spectra were obtained by titration of a PrCl_3 solution with increasing concentrations of DNR (Fig. 2). With the addition of DNR, the intensity of the fluorescence peak at 593 nm decreased gradually. The experiment results indicated that there was an interaction between Pr^{3+} and DNR, leading eventually to the formation of the Pr–DNR complex.

In order to determine the stoichiometry of the complex, the mole ratio method was employed using the intensity of the fluorescence peak at 593 nm (Fig. 3). The binding ratio¹⁷ of DNR and Pr^{3+} was obtained as $n_{\text{Pr}}:n_{\text{DNR}} = 1:3$.

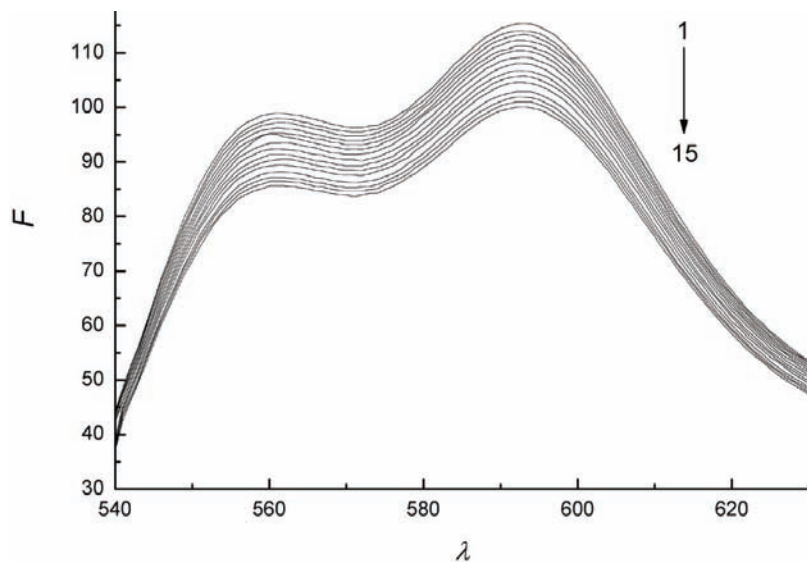


Fig. 2. The emission spectra of DNR in different concentrations of Pr^{3+} ; $c_{\text{DNR}} = 2.00 \times 10^{-5} \text{ mol L}^{-1}$, $c_{\text{Pr}} = 2.68 \times 10^{-4} \text{ mol L}^{-1}$ (10 μL per scan); λ in nm.

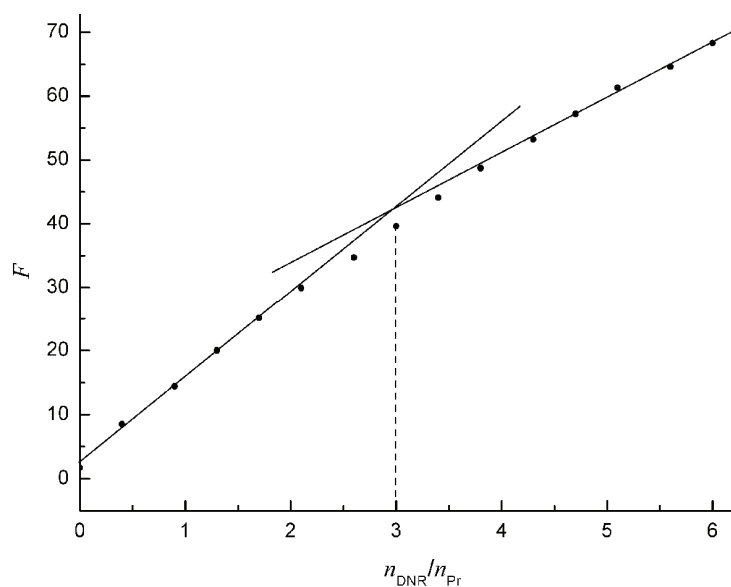


Fig. 3. Mole ratio method. $c_{\text{DNR}} = 2.00 \times 10^{-4} \text{ mol L}^{-1}$ (10 μL per scan), $c_{\text{Pr}} = 1.56 \times 10^{-6} \text{ mol L}^{-1}$.

The fluorescence spectra of Pr(DNR)₃ complex and DNA

With a fixed concentration of Pr(DNR)₃ complex, the concentration of DNA was stepwise increased and after each step, the fluorescence emission spectrum of the system was recorded (Fig. 4). The results show that with increasing DNA concentration, the fluorescence intensity of Pr(DNR)₃ gradually decreased, *i.e.*, the fluorescence of Pr(DNR)₃ was quenched by DNA. This indicates that there was interaction between DNA and Pr(DNR)₃.

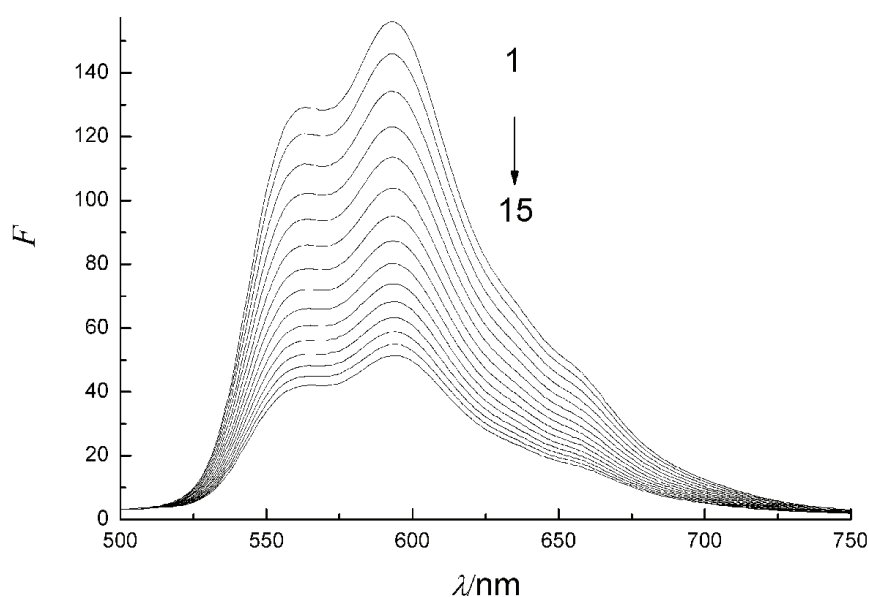


Fig. 4. Fluorescence spectra of the complex in the presence of different concentrations of DNA; $c_{\text{Pr(DNR)}_3} = 1.17 \times 10^{-5} \text{ mol L}^{-1}$, $c_{\text{DNA}} = 1.00 \times 10^{-4} \text{ mol L}^{-1}$ (10 μL per scan).

The electronic absorption spectra of Pr(DNR)₃ complex and DNA

UV–Vis spectroscopy is the most common and convenient way to study interactions between small molecules or rare earth complexes and nucleic acid.

The double helix structure of DNA molecules contains aromatic base and phosphate chromophore groups, therefore, interactions between the small molecules and DNA can be studied according to changes in the absorption spectra before and after reaction.

A red shift (or blue shift), hyperchromic (hypochromic) effect, and the isochromatic point are spectral properties of DNA which are closely related with the double helix structure.¹⁸ Generally, a red shift (or blue shift) and a hypochromic (or hyperchromic) effect¹⁹ are observed in the absorption spectra if small molecules intercalate with DNA. A hypochromic effect will be obvious if the intercalation is strong.²⁰ A red shift and a hypochromic effect are not obvious in the

absorption spectra if the interaction mode of the small molecules with DNA is electrostatic or groove binding.

With a fixed concentration of $\text{Pr}(\text{DNR})_3$ complex, the concentration of DNA was gradually increased and after each step, the UV-Vis spectrum of the system was recorded (Fig. 5). The results show that, with increasing DNA concentration, the absorbance of solution regularly decreased, an isochromatic point appeared at 548 nm and the maximum absorption peak was red shifted (from 479 to 502 nm). These phenomena indicate that $\text{Pr}(\text{DNR})_3$ had interacted with DNA in the intercalation mode.

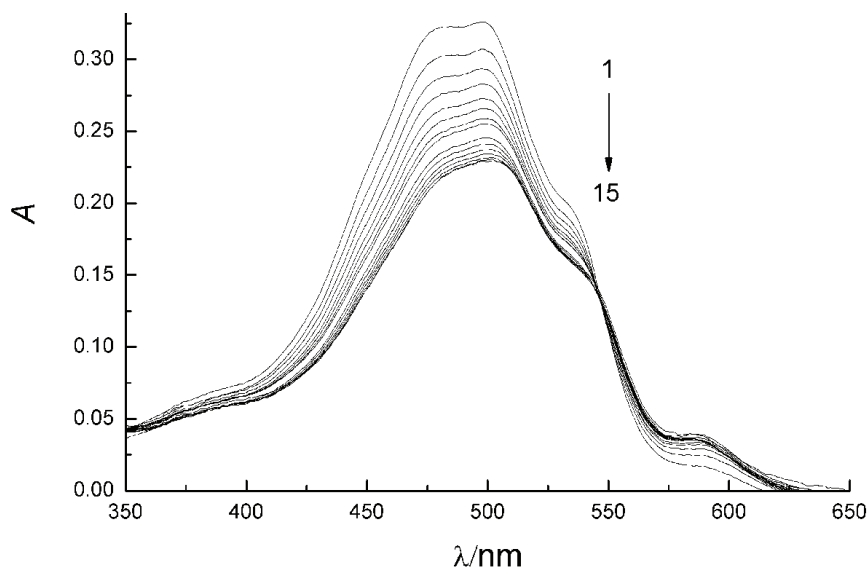


Fig. 5. Electronic absorption spectra of the complex in the presence of different concentrations of DNA; $c_{\text{Pr}(\text{DNR})_3} = 1.17 \times 10^{-5} \text{ mol L}^{-1}$, $c_{\text{DNA}} = 1.00 \times 10^{-4} \text{ mol L}^{-1}$ (10 μL per scan).

Determination of the binding ratio of $\text{Pr}(\text{DNR})_3$ and DNA by the mole ratio method

To a fixed concentration of $\text{Pr}(\text{DNR})_3$ complex in buffer solution (pH 7.40) was added DNA solution in portions. After each addition the fluorescence emission spectrum was recorded. The intensity of the fluorescence peak at 593 nm was used to determine the binding ratio by the mole ratio method (Fig. 6). The binding ratio of $\text{Pr}(\text{DNR})_3$ and DNA of $n_{\text{Pr}(\text{DNR})_3}:n_{\text{DNA}}$ of 5:1 was obtained.

In the same manner, the electronic absorption spectra of the system after successive additions of DNA were recorded (Fig. 7) and the same binding ratio was obtained.

Determination of the binding constants and thermodynamic constants by the double-reciprocal method

In order to further understand the interaction mode of Pr(DNR)₃ with DNA, studies of the thermodynamics were undertaken. For this purpose, absorption spectra were recorded at 292 and 310 K. The following double-reciprocal equation was employed:²¹

$$1/(A_0 - A) = 1/A_0 + 1/(KA_0c_{\text{DNA}}) \quad (1)$$

where A_0 and A are the absorbances of Pr(DNR)₃ in the absence and in the presence of DNA, respectively. K is the binding constants between Pr(DNR)₃ and DNA and c_{DNA} is the concentration of DNA. The double reciprocal plots of $1/(A_0 - A)$ vs. $1/c_{\text{DNA}}$ were linear (at 292 and 310 K) and the binding constants were calculated from the ratio of the intercept/slope (Fig. 8), K (292 K) = $4.34 \times 10^3 \text{ L mol}^{-1}$ and K (310 K) = $3.66 \times 10^3 \text{ L mol}^{-1}$.

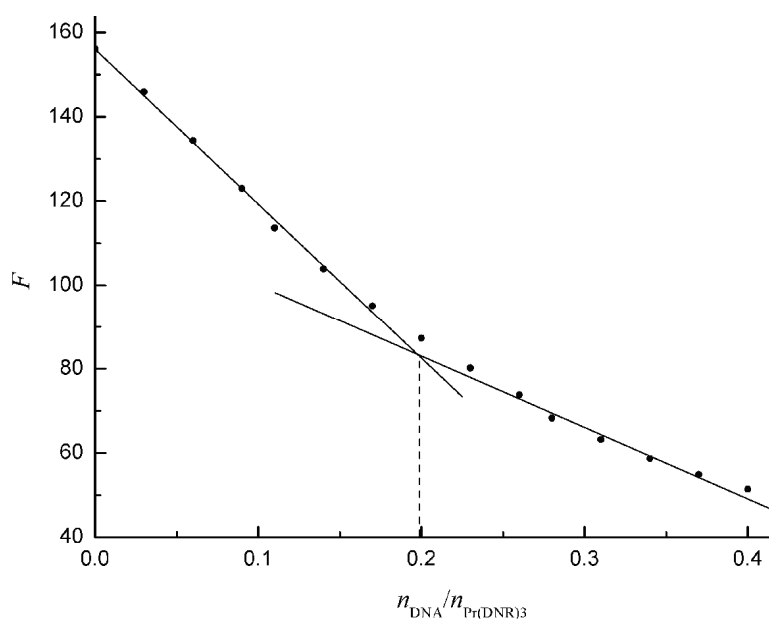


Fig. 6. Mole ratio method; $c_{\text{Pr(DNR)}_3} = 1.17 \times 10^{-5} \text{ mol L}^{-1}$, $c_{\text{DNA}} = 1.00 \times 10^{-4} \text{ mol L}^{-1}$ (10 μL per scan).

The standard molar reaction Gibbs energy ($\Delta_r G_m^\ominus$) and the standard molar reaction entropy ($\Delta_r S_m^\ominus$) were estimated from the following relationships:

$$\log K^\ominus = -\Delta_r H_m^\ominus / (2.303RT) + \Delta_r S_m^\ominus / (2.303R) \quad (2)$$

$$\Delta_r G_m^\ominus = -RT \ln K^\ominus = \Delta_r H_m^\ominus - T\Delta_r S_m^\ominus \quad (3)$$

In the interaction of Pr(DNR)₃ and DNA, the following values were calculated: $\Delta_r H_m^\ominus = -1.35 \times 10^4 \text{ J mol}^{-1}$, $\Delta_r S_m^\ominus = 1.12 \times 10^2 \text{ J mol}^{-1} \text{ K}^{-1}$, $\Delta_r G_m^\ominus$ (292 K) =

$= -2.03 \times 10^4 \text{ J mol}^{-1}$ and $\Delta_r G_m^\ominus(310 \text{ K}) = -2.11 \times 10^4 \text{ J mol}^{-1}$. Therefore, the interaction between Pr(DNR)_3 and DNA could occur spontaneously. As $\Delta_r H_m^\ominus < 0$ and $\Delta_r S_m^\ominus > 0$ according to theory of thermodynamic functions, it is supposed that the intercalative interaction was cooperatively driven by an enthalpy effect and an entropy effect.^{22,23}

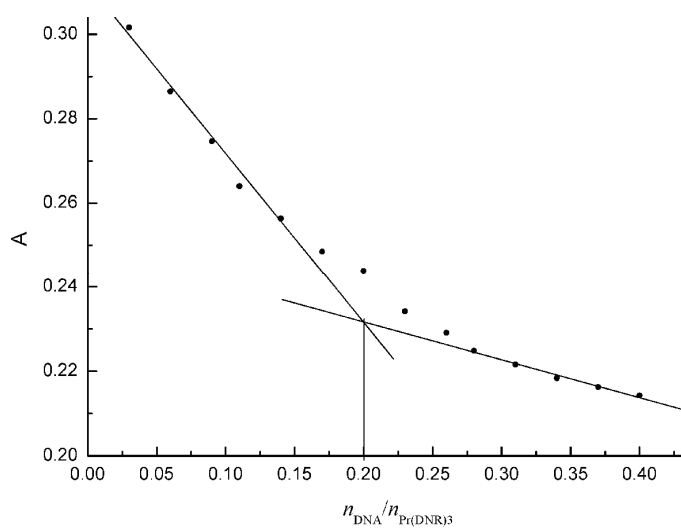


Fig. 7. Mole ratio method; $c_{\text{Pr(DNR)}_3} = 1.17 \times 10^{-5} \text{ mol L}^{-1}$, $c_{\text{DNA}} = 1.00 \times 10^{-4} \text{ mol L}^{-1}$ (10 μL per scan).

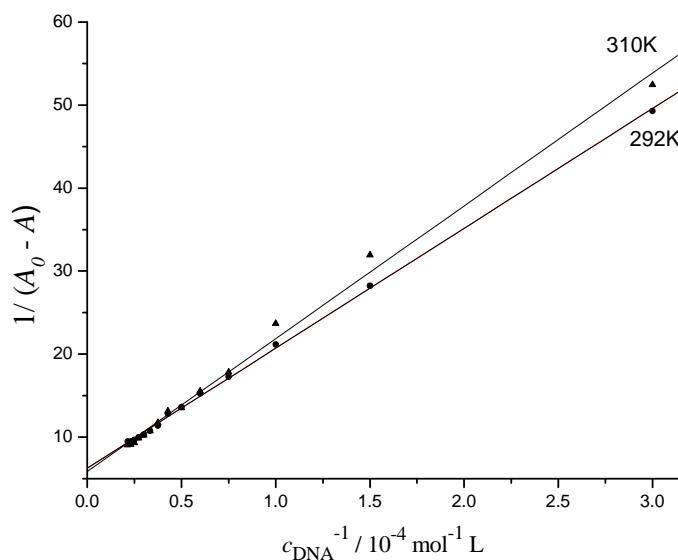


Fig. 8. Double reciprocal plots of Pr(DNR)_3 -DNA; $c_{\text{Pr(DNR)}_3} = 1.17 \times 10^{-5} \text{ mol L}^{-1}$, $c_{\text{DNA}} = 1.00 \times 10^{-4} \text{ mol L}^{-1}$ (10 μL per scan).

Fluorescence measurements using acridine orange as a probe

AO is a type of cationic dye. Due to its planar aromatic chromophore, it can insert between two adjacent base pairs in the DNA helix and significantly enhance the fluorescence. Therefore, AO is often used as a fluorescent probe to study the interaction mode between small molecules and DNA.

Influence of AO on the fluorescence spectra of $\text{Pr}(\text{DNR})_3\text{-DNA}$

The emission spectra of $\text{Pr}(\text{DNR})_3\text{-DNA}$ in the presence of different concentrations of AO are shown in Fig. 9. With increasing concentration of AO, the fluorescence intensity of $\text{Pr}(\text{DNR})_3\text{-DNA}$ gradually increased. This showed that there was competition between AO and $\text{Pr}(\text{DNR})_3$ for interaction with DNA and AO replaced the $\text{Pr}(\text{DNR})_3$ which was inserted into the base pairs of the DNA.

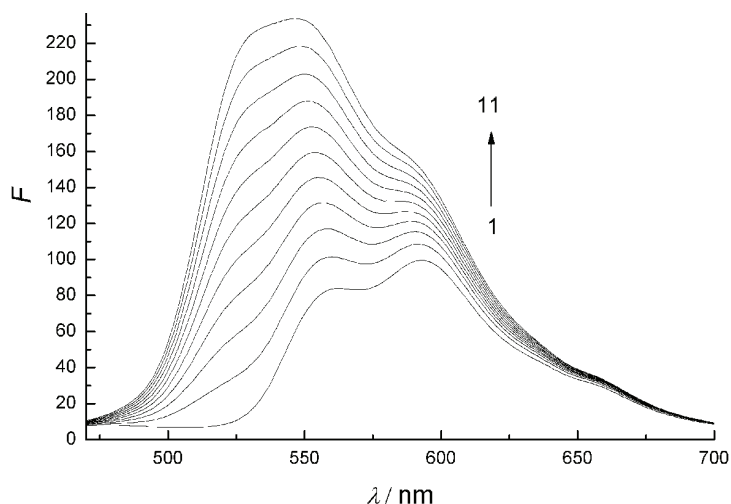


Fig. 9. Influence of AO on the emission spectra of $\text{Pr}(\text{DNR})_3\text{-DNA}$. $c_{\text{Pr}(\text{DNR})_3\text{-DNA}} = 1.00 \times 10^{-5} \text{ mol L}^{-1}$, $c_{\text{AO}} = 3.00 \times 10^{-4} \text{ mol L}^{-1}$ (10 μL per scan).

Influence on fluorescence spectra of $\text{Pr}(\text{DNR})_3$ on AO-DNA

The fluorescence spectra of AO-DNA in the presence of different concentrations of $\text{Pr}(\text{DNR})_3$ are shown in Fig. 10. It can be seen that the characteristic peak intensity of AO-DNA decreased and the equivalent point of the fluorescence intensity near 533 nm. These phenomena proved that AO was replaced by $\text{Pr}(\text{DNR})_3$; hence the characteristic peak of AO-DNA was quenched. The competitive binding experiments indicated the existence of intercalation interaction.

The Scatchard method

The binding mode between small molecules with DNA can be determined using the Scatchard procedure. The binding mode between $\text{Pr}(\text{DNR})_3$ and DNA

was studied by Scatchard analysis of the fluorescence. The situation was studied in the presence and absence of NaCl in the system (Fig. 11). The Scatchard equation expresses the binding of DNA–AO in the presence of Pr(DNR)₃:²⁴

$$r_{\text{AO}}/c_{\text{AO}} = K(n - r_{\text{AO}}) \quad (4)$$

where r_{AO} is the moles of AO bound per mole of DNA, c_{AO} is the molar concentration of free AO, n is the binding site multiplicity per class of binding site and K is the intrinsic binding constant of AO with DNA. Thus $r_{\text{AO}}/c_{\text{AO}}$ vs. r_{AO} describes a linear relation. Relevant data and the calculation process of Scatchard plots are given in Table I (as the first line in Fig. 11 without NaCl, for example).

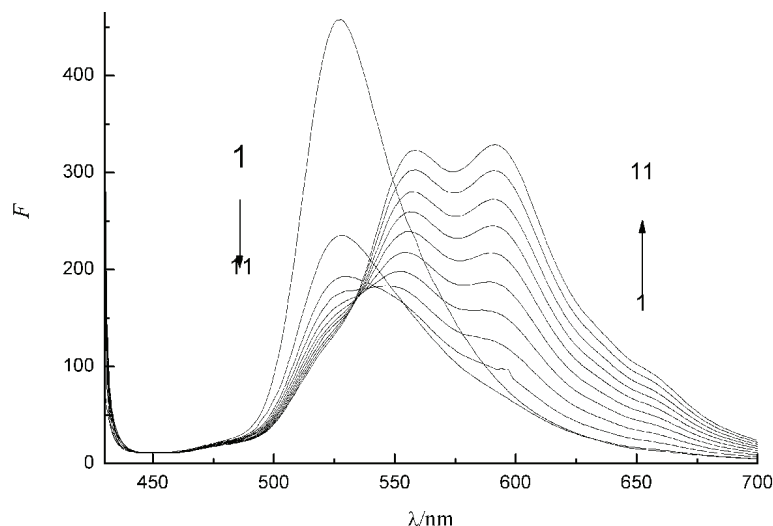


Fig. 10. Influence of Pr(DNR)₃ on the emission spectra of AO–DNA; $c_{\text{Pr(DNR)}_3} = 1.50 \times 10^{-4} \text{ mol L}^{-1}$ (10 μL per scan), $c_{\text{AO-DNA}} = 1.00 \times 10^{-6} \text{ mol L}^{-1}$.

Considering the situation in which NaCl was absent from the system, if Pr(DNR)₃ interacts with DNA *via* the intercalation mode, the value of n remains constant and that of K changes in the Scatchard plot. If Pr(DNR)₃ interacts with DNA through a non-intercalation binding mode involving groove binding or electrostatic interaction, the value of K remains constant while that of n changes in the Scatchard Plot. If Pr(DNR)₃ interacts with DNA by mix modes containing non-intercalation and intercalation modes, the value of K and n change in the Scatchard plot.

The Scatchard Graph (Table II) showed that the values of K and n changed in both high concentration and low concentrations. Thus, the mode of interaction between the complex and DNA was a mix mode that was a mixture of intercalation and non-intercalation modes.

To determine whether electrostatic interaction existed, a comparison was made with the system in the presence of NaCl and it was found that increasing the ionic strength reduced the binding number n . This showed the existence of electrostatic interaction between $\text{Pr}(\text{DNR})_3$ and DNA. The value of n may be due to the Na^+ cationic atmosphere surrounding the DNA interfering with the electrostatic interaction by combining with the negative polyphosphate skeleton of DNA and tightening the DNA-chain, so that it becomes difficult for the complex to intercalate in DNA. The results indicated that the major mode of interaction between the $\text{Pr}(\text{DNR})_3$ complex and DNA was a combination of electrostatic interaction and intercalation.

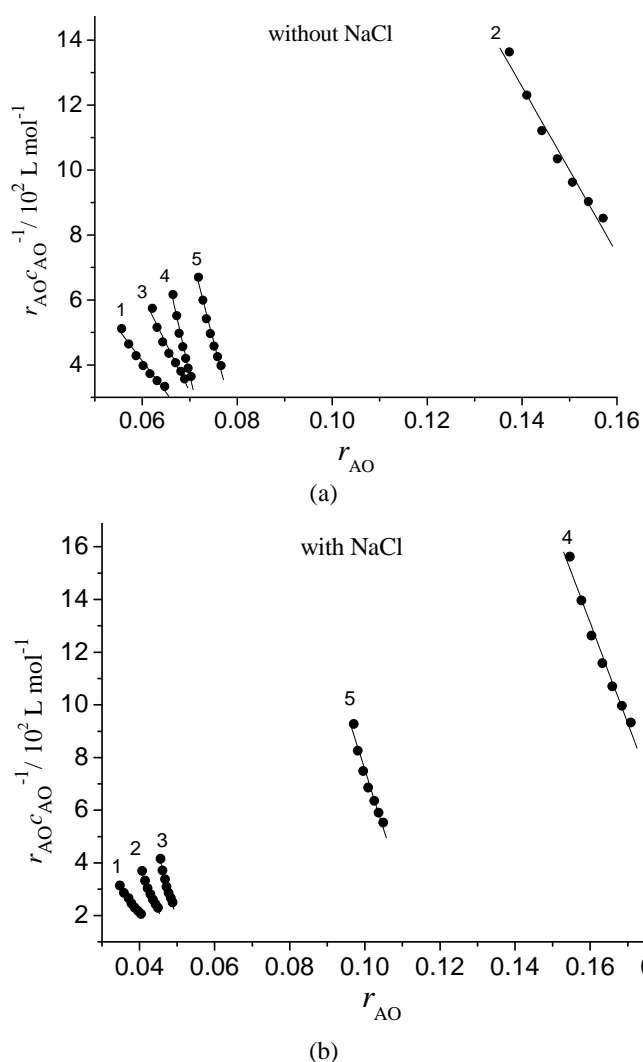


Fig. 11. Scatchard Plots of $\text{Pr}(\text{DNR})_3$ -DNA with (a) and without NaCl (b) in different concentrations of AO; $c_{\text{DNA}} = 1.00 \times 10^{-6} \text{ mol L}^{-1}$; $c_{\text{AO}} = 4.29 \times 10^{-5} \text{ mol L}^{-1}$; $R_t = c_{\text{Pr}(\text{DNR})_3} / c_{\text{DNA}}$: 1, $R_t = 0.00$, 2, $R_t = 0.20$, 3, $R_t = 0.40$, 4, $R_t = 0.60$, 5, $R_t = 0.80$.

Viscosity method

Optical photophysical probes provide necessary but not sufficient clues to support the nature of the binding modes, whereas hydrodynamic measurements, which are sensitive to length change, are regarded as the most critical tests of a binding model in solution.^{25–28} Thus, to further clarify the interaction between Pr(DNR)₃ and DNA, viscosity measurements were performed. A classical intercalation model is known to cause a significant increase in the viscosity of a DNA solution due to an increase in the length of the DNA helix. In contrast, a partial or non-classical intercalation mode could bend (or kink) the DNA helix and reduce its effective length and, concomitantly, its viscosity, while non-intercalation binding causes no obvious increase in the viscosity of a DNA solution.

TABLE I. Relevant data and calculation process of the Scatchard plots (as the first line in Fig. 11 without NaCl, for example); $r_{AO} = (c'_{AO} - c'_{AO}(1-F_0/F))/c_{DNA}$; $c_{AO} = c'_{AO}(1-F_0/F)$; $c_{DNA} = 1.00 \times 10^{-6} \text{ mol L}^{-1}$; a, b, c, d, e, f and g are points on the line; c'_{AO} is the initial molar concentration of AO

Parameter	a	b	c	d	e	f	g
F_0/F	0.04864	0.04441	0.04104	0.03826	0.03591	0.03394	0.03232
$1-F_0/F$	0.95136	0.95559	0.95896	0.96174	0.96409	0.96606	0.96768
$c'_{AO} \times 10^7 / \text{mol L}^{-1}$	11.44	12.87	14.30	15.73	17.16	18.59	20.02
$c_{AO} \times 10^7 / \text{mol L}^{-1}$	10.8835	12.2985	13.7131	15.1281	16.5438	17.9590	19.3730
$(c'_{AO} - c_{AO}) \times 10^7 / \text{mol L}^{-1}$	0.5565	0.5715	0.5869	0.6019	0.6162	0.6310	0.6470
r_{AO}	0.05565	0.05715	0.05869	0.06019	0.06162	0.0631	0.0647
$r_{AO} c_{AO}^{-1} / 10^{-7} \text{ mol L}^{-1}$	0.00511	0.00465	0.00428	0.00398	0.00372	0.00351	0.00334

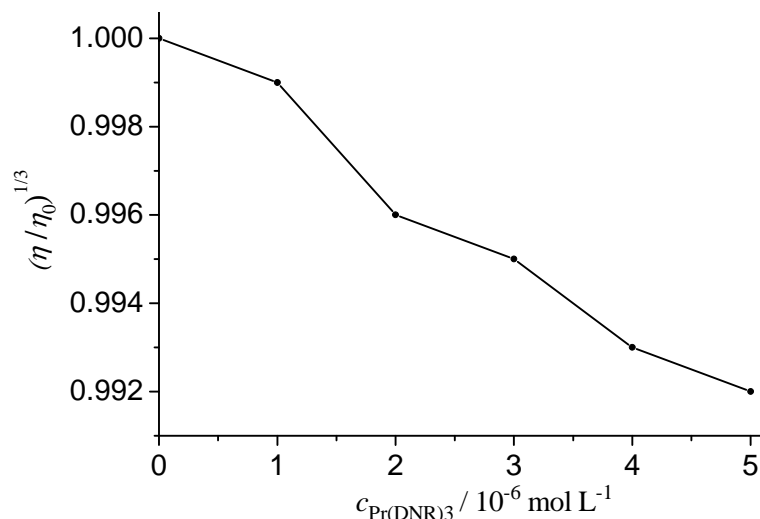


Fig. 12. Effect of increasing amounts of Pr(DNR)₃ on the relative viscosities of DNA at 298 K; $c_{DNA} = 1.00 \times 10^{-5} \text{ mol L}^{-1}$.

The changes in the relative viscosity of the DNA solution with increasing concentration of $\text{Pr}(\text{DNR})_3$ are shown in Fig. 12. The value of relative viscosity decreased with increasing amount of $\text{Pr}(\text{DNR})_3$. Such behavior further suggested that partial or non-classical intercalation binding could be the interaction mode of $\text{Pr}(\text{DNR})_3$ with DNA.

TABLE II. Scatchard equation of the interaction between $\text{Pr}(\text{DNR})_3$ and DNA

Curve	$R_t = c_{\text{Pr}(\text{DNR})_3}/c_{\text{DNA}}$	NaCl content, %	Scatchard Equation	$K / 10^6 \text{ L mol}^{-1}$	n
1	0.00	5.00	$9.72 \times 10^4 - 1.91 \times 10^6 x$	1.91	0.0509
		0	$1.58 \times 10^5 - 1.94 \times 10^6 x$	1.94	0.0814
2	0.20	5.00	$1.69 \times 10^5 - 3.26 \times 10^6 x$	3.26	0.0518
		0	$4.85 \times 10^5 - 1.94 \times 10^6 x$	1.94	0.2500
3	0.40	5.00	$2.74 \times 10^5 - 5.12 \times 10^6 x$	5.12	0.0535
		0	$2.40 \times 10^5 - 2.98 \times 10^6 x$	2.98	0.0805
4	0.60	5.00	$7.41 \times 10^5 - 3.81 \times 10^6 x$	3.81	0.1945
		0	$4.97 \times 10^5 - 6.57 \times 10^6 x$	6.57	0.0756
5	0.80	5.00	$5.28 \times 10^5 - 4.52 \times 10^6 x$	4.52	0.1168
		0	$4.73 \times 10^5 - 5.68 \times 10^6 x$	5.68	0.0833

CONCLUSIONS

The interaction between the $\text{Pr}(\text{DNR})_3$ complex and hs-DNA was investigated using UV-Vis and fluorescence spectroscopy and viscosity measurements. The obtained results indicated that the binding modes of $\text{Pr}(\text{DNR})_3$ to DNA were electrostatic binding and non-classical intercalation binding. The molecular structure of DNR containing an aromatic fused ring plane, which is the internal structure of $\text{Pr}(\text{DNR})_3$ can insert into the DNA molecule. However, because of the large volume of the $\text{Pr}(\text{DNR})_3$ complex, there was the partial or non-classical intercalation. All these strongly support the idea that the research provides an experimental and theoretical reference for new anticancer drugs.

Acknowledgments. This study was supported by National Natural Science Foundation of China (No. 30973634) and Postgraduate Innovation Foundation of Southwest University of Science and Technology, Mianyang, China.

ИЗВОД

МЕХАНИЗАМ ИНТЕРАКЦИЈЕ ИЗМЕЂУ КОМПЛЕКСА $\text{Pr}(\text{DNR})_3$
И ДНК ИЗ СПЕРМЕ ХАРИНГЕXIAOCAI LIU¹, XINGMING WANG¹ и LISHENG DING²¹School of Materials Science and Engineering, Southwest University of Science and Technology, Mianyang 62101 и ²Chengdu Institute of Biology, Chinese Academy of Sciences, Chengdu 610041, China

Испитивање механизма интеракције између лекова и ДНК је важно за разумевање фармакокинетице. У овом раду је анализирана интеракција између комплекса метала ретке земље $\text{Pr}(\text{DNR})_3$ и ДНК из сперме харинге у пуферу Tris-HCl (pH 7,4) одређивањем апсорпције, спектра флуоресценције и вискозитета. Резултати су показали да је интеракција између

Pr(DNR)₃ и ДНК из сперме харинге електростатичког типа и типа интеркалације. Однос везивања је био Pr(DNR)₃:ДНК = 5:1, а константа везивања $K^{\ominus}(292\text{ K}) = 4,34 \times 10^3\text{ L mol}^{-1}$. На основу двоструког реципрочног метода и термодинамичке једначине, може се закључити да је интеракција интеркалације била кооперативно контролисана ефектима енталпије и ентропије.

(Примљено 26. августа, ревидирано 8. новембра 2010)

REFERENCES

1. M. Yang, *J. Beijing Med. Univ.* **28** (1996) 303
2. X. M. Wang, H. B. Li, H. P. Liu, Y. M. Hu, L. S. Ding, S. L. Zhao, *Acta Chim. Sinica* **64** (2006) 2115
3. G. F. Cheng, H. Y. Qu, D. M. Zhang, J. D. Zhang, P. G. He, Y. Z. Fang, *J. Pharm. Biomed. Anal.* **29** (2002) 361
4. G. Murphy, W. J. Lawrence, R. Lenhard, *American Society Textbook of Clinical Oncology*, 2nd ed., American cancer society, Atlanta, GA, USA, 1995
5. P. Wiernik, J. Ductcher, *Leukemia* **6 Suppl. 1** (1992) 670
6. X. Q. Chen, Y. Y. Jin, *The Newly Edited Pharmacology*, 14th ed., People's Medicine Press, Beijing, China, 1997, p. 516
7. S. H. Wei, G. S. Liu, *Foreign Medical Sciences, Fascicle*, **26** (1999) 288
8. T. Masahiko, T.-K. Shozo, I. Masamoto, *J. Coord. Chem.* **18** (1988) 77
9. S. Akihiro, O. Takashi, S. Masakatsu, *Tetrahedron* **58** (2002) 75
10. S. I. Dikalov, G. V. Romyantseva, A. V. Piskunov, L. M. Weiner, *Biochemistry* **31** (1992) 8947
11. P. Zou, *J. Clin. Hematol.* **6** (1993) 78
12. M. Spinelli, J. C. Dabrowiak, *Biochemistry* **21** (1982) 5862
13. S. Mazzini, R. Mondelli, E. Ragg, *J. Chem. Soc., Perkin Trans. 2* (1998) 1983
14. B. Hasinoff, K. T. Tran, *J. Inorg. Biochem.* **77** (1999) 257
15. G. X. Xu, *Rare Earths*, Vol. 2, Metallurgy Industry Press, Beijing, China, 1995, p. 451
16. G. X. Xu, *Rare Earths*, Vol. 3, Metallurgy Industry Press. Beijing, China, 1995, pp. 591–597, 606–609, 614
17. X. M. Wang, H. B. Li, Y. M. Hu, D. M. Yang, D. Fei, *Acta Chim. Sinica* **65** (2007) 140
18. P. Yang, C. Q. Zhou, *Acta Chim. Sinica* **61** (2003) 1455
19. S. A. Ysoe, A. D. Baker, T. C. Streckas, *J. Phys. Chem.* **97** (1993) 1707
20. E. J. Gao, S. M. Zhao, Q. T. Liu, R. Xu, *Acta Chim. Sinica* **62** (2004) 593
21. M. Purcell, J. F. Neault, T. Riahi, *Biochim. Biophys. Acta* **1478** (2000) 61
22. A. A. Ouameur, R. Marty, H. A. Tajmir-Riahi, *Biopolymer* **77** (2005) 129
23. Y. Zhang, X. M. Wang, D. Fei, N. Zhao, T. T. Zhao, H. F. Zhu, L. S. Ding, *Chin. Opt. Lett.* **8** (2010) 236
24. P. D. Ross, S. Subramanian, *Biochemistry* **20** (1981) 3096
25. J. W. Wang, X. P. Zhu, W. Sun, J. G. Xue, Z. X. Wang, M. G. Fu, *Spectrosc. Spectral Anal.* **23** (2003) 899
26. C.A. Mitsopoulou, C. E. Dagas, C. Makedonas, *Inorg. Chim. Acta* **361** (2008) 1973
27. I. H. Bhat, S. Tabassum, *Spectrochim. Acta, A* **72** (2009) 1026
28. C. Y. Chen, K. Chen, Q. Long, M. H. Ma, F. Ding, *Spectroscopy* **23** (2009) 103.



J. Serb. Chem. Soc. 76 (10) 1379–1386 (2011)
JSCS–4212

***In vitro* assessment of the protection from oxidative stress by various fractions of *Artemisia incisa* Pamp.**

AZIZ-UR-REHMAN¹, SEHRISH GULZAR¹, MUHAMMAD A. ABBASI^{1*},
TAYYABA SHAHZADI¹, TAUHEEDA RIAZ¹, SABAHAT Z. SIDDIQUI¹
and MUHAMMAD AJAIB²

¹Department of Chemistry, Government College University, Lahore-54000 and ²Department
of Botany, Government College University, Lahore-54000, Pakistan

(Received 2 January, revised 18 March 2011)

Abstract: The methanolic extract of *Artemisia incisa* Pamp. was dissolved in distilled water and successively partitioned with *n*-hexane, chloroform, ethyl acetate and *n*-butanol. The antioxidant potential of all these fractions and remaining aqueous fraction was evaluated by four methods, *i.e.*, the scavenging activity of the 1,1-diphenyl-2-picrylhydrazyl radical (DPPH), the total antioxidant activity, the ferric reducing antioxidant power (FRAP) assay and the ferric thiocyanate assay. In addition, the total phenolics was determined. The obtained results revealed that among the studied fractions the ethyl acetate soluble fraction showed the most potent DPPH-radical scavenging activity with an IC_{50} value of $5.30 \pm 0.71 \mu\text{g mL}^{-1}$, which is even more effective than the standard antioxidant butylated hydroxytoluene (BHT) (IC_{50} value of $12.10 \pm 0.29 \mu\text{g mL}^{-1}$). The ethyl acetate fraction also showed the highest FRAP value ($3677.13 \pm 0.60 \mu\text{g TE mL}^{-1}$), inhibition of lipid peroxidation ($60.93 \pm 1.15\%$ at $500 \mu\text{g mL}^{-1}$) and total phenolic content ($95.50 \pm 0.58 \mu\text{g GAE g}^{-1}$) as compared to other fractions. However, the remaining aqueous fraction was found to possess the highest antioxidant activity of all the fractions.

Keywords: *Artemisia incisa* Pamp.; DPPH assay; total antioxidant activity; FRAP value; total phenolics; inhibition of lipid peroxidation.

INTRODUCTION

Lipid peroxidation is one of the main reasons for the deterioration of food products during processing and storage. Synthetic antioxidants such as butylated hydroxytoluene (BHT), butylated hydroxyanisole (BHA), propyl gallate (PG) and *tert*-butylhydroquinone (TBHQ) are widely used as food additives to increase the shelf life, especially of lipids and lipid-containing products, by retarding the process of lipid peroxidation. However, BHT and BHA are known to have not only toxic and carcinogenic effects on humans, but also to have abnor-

*Corresponding author. E-mail: atrabbasi@yahoo.com
doi: 10.2298/JSC110102116A

mal effects on enzyme systems. Therefore, the interest in natural antioxidants, especially of plant origin, has greatly increased in recent years.¹ Several reports indicate that the antioxidant potential of medicinal plants may be related to the concentration of their phenolic compounds, which include phenolic acids, flavonoids, anthocyanins and tannins.^{2,3} These compounds are of great value in preventing the onset and/or progression of many human diseases, such as cancer, heart disease, hypertension and stroke.⁴ The health promoting effect of antioxidants from plants is thought to arise from their protective effects by counteracting reactive oxygen species (ROS).³

Artemisia is a quite large genus within the family of Asteraceae (Compositae), with almost 200 individual species known, which are usually found in dry areas, invariably as small fragrant shrubs or herbs and most yield essential oils. Some of these oils have found applications in perfumery and medicine (for example, vermifuges, stimulants, *etc.*), whereas the leaves of some species are used as culinary herbs. The plants themselves are popular among gardeners as cultivated ornamentals. In Pakistan, this genus is represented by almost twenty five species.⁵ The plants of this genus have been used for a wide range of specific ailments including coughs, colds, sore throat, heartburn, haemorrhoids, fever, malaria, asthma, diabetes mellitus, enhancing eyesight, enhancement of the immune system and cardiovascular health, as well as to decrease the risk of atherosclerosis, cancer, arthritis and gastrointestinal disorders. Phytochemical analyses of various species showed that they are rich sources of terpenoids (artemisinin), flavonoids including apigenin, cirsimaritin, and various novel compounds.⁶⁻⁹ but to the best of our knowledge, there is little in the literature on the employment of *Artemisia incisa* Pamp. as a natural antioxidant. Therefore, the present study was undertaken to investigate the *in vitro* antioxidant potential of various fractions of this plant.

EXPERIMENTAL

Plant material

The plant *Artemisia incisa* Pamp. was collected from Kotly, Azad Kashmir in March 2009, and identified by Mr. Muhammad Ajaib (taxonomist), Department of Botany, Government College University, Lahore. A voucher specimen (G.C.Herb.Bot.858) is deposited in the Herbarium of the Botany Department of the same university.

Extraction and fractionation of antioxidants

Shade-dried ground whole plant (6.8 kg) was exhaustively extracted with methanol (4×12 L) at room temperature. The solvent was removed in a rotary evaporator (Laborta 4000-efficient Heidolph) at 40 °C under vacuum to yield the residue (615 g), which was dissolved in distilled water (1.5 L) and successively partitioned with *n*-hexane (4×1 L), chloroform (4×1 L), ethyl acetate (4×1 L) and *n*-butanol (4×1 L) to obtain four organic fractions. The organic fractions as well as the remaining water fraction were all concentrated separately on a rotary evaporator (the *n*-hexane-partitioned fraction at 40 °C, the chloroform-partitioned fraction at 40 °C, the ethyl acetate-partitioned fraction at 43 °C, the *n*-butanol-partitioned fraction at 50

°C and the remaining water fraction at 60 °C under vacuum). The thus obtained residues for each fraction were used to evaluate their *in vitro* antioxidant potential.

Chemicals and standards

1,1-Diphenyl-2-picrylhydrazyl radical (DPPH·), 2,4,6-tripyridyl-*s*-triazine (TPTZ), trolox, gallic acid, Folin–Ciocalteu; BHT was obtained from the Sigma Chemical Company Ltd. (USA) and the organic solvents (*n*-hexane, chloroform, ethyl acetate and *n*-butanol), sulphuric acid, sodium phosphate, ammonium molybdate, ferric chloride and ferrous chloride from Merck (Pvt.) Ltd. (Germany).

DPPH radical scavenging activity

The DPPH radical scavenging activities of the various fractions of the plant were examined by comparison with that of a known antioxidant (BHT) using a reported method.¹⁰ Briefly, various amounts of the samples (1000, 500, 250, 125, 60, 30, 15 and 8 µg mL⁻¹) were mixed with 3 mL of a methanolic solution of DPPH (0.1 mM). The mixture was shaken vigorously and allowed to stand at room temperature for one hour. Then the absorbance was measured at 517 nm against methanol as a blank in a spectrophotometer (CECIL Instruments CE 7200 Cambridge, England). A lower absorbance of the reaction mixture indicated a higher free radical scavenging activity.

The percent of DPPH decolouration of the samples was calculated according to the formula:

$$\text{Antiradical activity (\%)} = 100(A_{\text{control}} - A_{\text{sample}}) / A_{\text{control}}$$

Each sample was assayed in triplicate and mean values were calculated.

Total antioxidant activity by the phosphomolybdenum method

The total antioxidant activities of the various fractions of the plant were evaluated by the phosphomolybdenum complex formation method.¹¹ Briefly, 500 µg mL⁻¹ of each sample was mixed with 4 mL of reagent solution (0.6 M sulphuric acid, 28 mM sodium phosphate and 4 mM ammonium molybdate) in sample vials. The blank solution contained 4 mL of reagent solution. The vials were capped and incubated in a water bath at 95 °C for 90 min. After the samples had cooled to room temperature, the absorbance of the mixture was measured at 695 nm against the blank. The antioxidant activity was expressed relative to that of BHT. All determinations were assayed in triplicate and mean values were calculated.

Ferric reducing antioxidant power (FRAP) assay

The FRAP assay was realised according to Benzie and Strain¹² with some modifications. The stock solutions included 300 mM acetate buffer (pH 3.6), 10 mM TPTZ solution in 40 mM hydrochloric acid and 20 mM ferric chloride hexahydrate solution. The fresh working solution (FRAP solution) was prepared by mixing 25 mL of the acetate buffer, 2.5 mL of the TPTZ solution and 2.5 mL of the ferric chloride hexahydrate solution and then warmed at 37 °C before use. Solutions of the plant samples and that of trolox were prepared in methanol (250 µg mL⁻¹). 10 µL of each of sample solution were taken in separate test tubes and 2990 µL of FRAP solution were added to each to make the total volume 3 mL. The plant samples were allowed to react with the FRAP solution in the dark for 30 min. The absorbance of the coloured product (the ferrous tripyridyltriazine complex) was measured at 593 nm. The *FRAP* values are expressed as µmol of trolox equivalents (*TE*) per mg of the sample using a standard curve constructed for different concentrations of trolox. The results are expressed as *TE* in µg mg⁻¹.

Ferric thiocyanate (FTC) assay

The antioxidant activities of the various fractions of plant on the inhibition of linoleic acid peroxidation were assayed by the thiocyanate method.¹⁴ Samples (0.1 mL, 0.5 mg mL⁻¹) were mixed with 2.5 mL of linoleic acid emulsion (0.02 M, pH 7.0) and 2.0 mL of phosphate buffer (0.02 M, pH 7.0). The linoleic emulsion was prepared by mixing 0.28 g of linoleic acid, 0.28 g of Tween-20 as emulsifier and 50.0 mL of phosphate buffer. The reaction mixture was incubated for 5 days at 40 °C. The mixture without extract was used as the control. The mixture (0.1 mL) was taken and mixed with 5.0 mL of 75 % ethanol, 0.1 mL of 30 % ammonium thiocyanate and 0.1 mL of 20 mM ferrous chloride in 3.5 % hydrochloric acid and allowed to stand at room temperature. Precisely 3 minutes after addition of ferrous chloride to the reaction mixture, absorbance was recorded at 500 nm. The antioxidant activity is expressed as follows:

$$\text{Inhibition of lipid peroxidation (\%)} = 100\{1 - (A_{\text{sample}}) / (A_{\text{control}})\}$$

The antioxidant activity of BHT as a reference standard was assayed for comparison.

Total phenolic content

Total phenolics of the various fractions of plant were determined by a reported method.¹⁴ A 0.1 mL aliquot of the sample solution (0.5 mg mL⁻¹) was combined with 2.8 mL of a 10 % sodium carbonate solution and 0.1 mL of 2 M Folin–Ciocalteu reagent. After 40 min, the absorbance at 725 nm was measured using a UV–Vis spectrophotometer. The total phenolics were determined as milligrams of gallic acid equivalents per gram of sample. These were determined with the help of standard calibration curve, which was constructed for different concentrations of gallic acid. The standard gallic acid curve was linear in the concentration range 50–400 µg mL⁻¹. The results are expressed in µg GAE mL⁻¹.

Statistical analysis

All the measurements were performed in triplicate and the statistical analysis was realised using Microsoft Excel 2003. The results are presented as mean ± SEM.

RESULTS AND DISCUSSION

The scavenging of the stable DPPH radical model is a widely used method to evaluate antioxidant activities in a relatively short time. The addition of the extracts to a DPPH solution caused a rapid decrease in the optical density at 517 nm. The degree of decolouration is an indication of the scavenging capacity of the extracts. Free radicals cause autoxidation of unsaturated lipids in food.¹⁵ The effect of an antioxidant on DPPH radical scavenging is thought to be due to its hydrogen donating ability or radical scavenging activity.¹⁶ Antioxidants cease the free radical reaction by donating a hydrogen from the phenolic hydroxyl groups. Thus, the formation of a stable end-product does not permit further oxidation of the lipid.¹⁷ The decrease in the absorbance of the stable radical DPPH, accompanied with colour changes from violet to yellow, was measured for three concentrations, and the results are given in Table I. According to the obtained results, the ethyl acetate soluble fraction showed the highest DPPH scavenging activity of 87.74±1.75 % at a concentration of 125 µg mL⁻¹, while the *n*-hexane soluble fraction revealed the lowest scavenging value of 68.10±1.70 % at a con-

centration of 1000 $\mu\text{g mL}^{-1}$. For each fraction, the IC_{50} value was calculated and is presented in Table II. The IC_{50} value is the concentration which causes a 50 % inhibition of the DPPH radicals. Different concentrations of the fractions were taken such that some concentrations had an inhibition above 50 % and some below 50 %. The lower the IC_{50} value, the greater is the antioxidant activity. The IC_{50} value of the ethyl acetate soluble fraction was very low ($5.30 \pm 0.71 \mu\text{g mL}^{-1}$) and hence it showed the highest antioxidant activity as compared to the other fractions. The IC_{50} values for other fractions increased in order chloroform soluble fraction < *n*-butanol soluble fraction < remaining aqueous fraction < *n*-hexane soluble fraction (Table II). The total antioxidant capacity of all fractions was measured spectrophotometrically by the phosphomolybdenum method, which is based on the reduction of Mo(VI) to Mo(V) by the sample analyte and the subsequent formation of green phosphate/Mo(V) compounds with a maximum absorption at 695 nm.¹⁸ The aqueous fraction displayed the highest total antioxidant activity value (1.56-fold greater than BHT), followed by the slightly less potent ethyl acetate, chloroform and *n*-hexane soluble fractions (from 1.45 to 1.47-fold greater activity than BHT), while the *n*-butanol soluble fraction had the lowest total antioxidant activity (1.35-fold greater than BHT).

TABLE I. 1,1-Diphenyl-2-picryl hydrazyl radical (DPPH) radical scavenging activity of the various fractions of *Artemisia incisa* Pamp.

Sr. No.	Sample	Concentration in assay, $\mu\text{g ml}^{-1}$	Scavenging of DPPH, $\% \pm SEM^a$
1	<i>n</i> -Hexane soluble fraction	1000	68.10 ± 1.70^b
		500	59.30 ± 1.17^b
		50	36.30 ± 0.61^b
2	Chloroform soluble fraction	125	87.71 ± 1.75
		60	67.43 ± 1.14
		30	40.77 ± 1.14^b
3	Ethyl acetate soluble fraction	125	87.74 ± 1.13
		60	75.90 ± 1.73
		30	58.30 ± 1.76^b
4	<i>n</i> -Butanol soluble fraction	125	87.60 ± 0.99
		60	61.25 ± 1.17^b
		30	44.10 ± 1.17^b
5	Remaining aqueous fraction	250	72.65 ± 1.55^b
		125	61.95 ± 0.68^b
		50	49.8 ± 1.02^b
6	BHT ^c	60	91.17 ± 1.20
		30	72.14 ± 1.14
		15	65.86 ± 2.32

^aAll results are presented as mean \pm standard mean error of three assays; ^b $p < 0.05$ when compared with the negative control, *i.e.*, blank/solvent ($p < 0.05$ is taken as significant); ^cstandard antioxidant. Note: IC_{50} should be calculated by the linear regression method of plots of the percentage of antiradical activity against the concentration of the tested samples. Hence, the concentrations of the fractions were taken in such a way that some concentrations show % inhibition above 50 % and some below 50 %

TABLE II. IC_{50} , total phenolics, total antioxidant activity, *FRAP* values and lipid peroxidation inhibition values of different fractions of *Artemisia incisa* Pamp.; all results are presented as mean \pm standard mean error of three assays

Sr. No.	Sample	IC_{50} $\mu\text{g mL}^{-1}$	Total antioxidant activity	<i>FRAP</i> value $\mu\text{g TE mg}^{-1}$	Inhibition of lipid peroxidation, % ^a	Total phenolics mg GAE g^{-1}
1	<i>n</i> -Hexane soluble fraction	379.10 \pm 9.48	1.45 \pm 0.01 ^b	179.80 \pm 0.46 ^b	47.06 \pm 0.59 ^b	51.20 \pm 0.46 ^b
2	Chloroform Soluble fraction	37.90 \pm 13.59	1.46 \pm 0.01 ^b	1571.30 \pm 0.49 ^b	51.37 \pm 0.56 ^b	54.50 \pm 0.59 ^b
3	Ethyl acetate soluble fraction	5.30 \pm 0.71	1.47 \pm 0.01 ^b	3677.13 \pm 0.60 ^b	60.93 \pm 1.15	95.50 \pm 0.58 ^b
4	<i>n</i> -Butanol soluble fraction	39.80 \pm 12.65	1.35 \pm 0.02 ^b	2136.40 \pm 0.34 ^b	49.60 \pm 0.99 ^b	59.75 \pm 1.17 ^b
5	Remaining aqueous fraction	44.40 \pm 6.60	1.56 \pm 0.01 ^b	620.50 \pm 0.52 ^b	54.20 \pm 0.88 ^b	69.25 \pm 0.59 ^b
6	BHT ^c	12.10 \pm 0.29	1.2186 \pm 0.01	–	62.91 \pm 1.16	–
	Blank ^d	–	–	2.30	–	1.15 ^b

^aTested concentration at 500 $\mu\text{g mL}^{-1}$; ^b $p < 0.05$ when compared with the negative control, *i.e.*, blank/solvent ($p < 0.05$ is taken as significant); ^cexpressed relative to BHT; ^dexpressed relative to blank

The FRAP assay is a simple and inexpensive procedure that measures the total antioxidant levels in a sample. It utilizes the reducing potential of the antioxidants to react with the ferric tripyridyltriazine (Fe(III)-TPTZ) complex and produce the coloured ferrous tripyridyltriazine (Fe(II)-TPTZ) complex.^{19,20} Among all the *Artemisia incisa* fractions, the ethyl acetate soluble fraction showed the highest *FRAP* value (3677.13 \pm 0.60 $\mu\text{g TE mg}^{-1}$) and then the other fractions which followed the order *n*-butanol soluble fraction (2136.40 \pm 0.34 $\mu\text{g TE mg}^{-1}$) > chloroform soluble fraction (1571.30 \pm 0.49 $\mu\text{g TE mg}^{-1}$) > aqueous fraction (620.50 \pm 0.52 $\mu\text{g TE mg}^{-1}$) while the *n*-hexane soluble fraction revealed the lowest *FRAP* value (179.80 \pm 0.46 $\mu\text{g TE mg}^{-1}$).

The ferric thiocyanate method measures the amount of peroxide generated during the initial stage of linoleic acid emulsion during incubation. Here, the peroxide reacted with ferrous chloride to form ferric chloride, which in turn reacted with ammonium thiocyanate to produce ferric thiocyanate, a reddish pigment. The low absorbance values measured *via* the FTC method indicated high antioxidant activity.²¹ The obtained results revealed that the ethyl acetate soluble fraction showed the maximal inhibition of lipid peroxidation (60.93 \pm 1.15 %) and the *n*-hexane soluble fraction the minimal (47.06 \pm 0.59 %) at a concentration of

500 $\mu\text{g mL}^{-1}$; the following order for the different fractions of this plant was observed: ethyl acetate soluble fraction > remaining aqueous fraction > chloroform soluble fraction > *n*-butanol soluble fraction > *n*-hexane soluble fraction. The inhibition of lipid peroxidation by BHT (standard) was 62.91 ± 0.60 % at 500 $\mu\text{g mL}^{-1}$ (Table II). Phenolic compounds are very important plant constituents because of their antioxidant activities.²² It has been revealed that various phenolic antioxidants, such as flavonoids, tannins, coumarins and procyanidins scavenge radicals dose-dependently. Thus, they are viewed as promising therapeutic drugs for free radical pathologies.²³ According to the present results, the ethyl acetate soluble fraction possessed the highest amount of total phenolics, having a value of 95.5 ± 0.58 mg GAE g^{-1} , followed by the remaining aqueous fraction (69.25 ± 0.59 mg GAE g^{-1}), the *n*-butanol soluble fraction (59.75 ± 1.17 mg GAE g^{-1}), the chloroform soluble fraction (54.5 ± 0.59 mg GAE g^{-1}) while the *n*-hexane soluble fraction exhibited the lowest total phenolic content (51.20 ± 0.46 mg GAE g^{-1}) (Table II).

CONCLUSIONS

The results showed that among the studied fractions, the ethyl acetate soluble fraction showed the most potent DPPH-radical scavenging activity with an IC_{50} value of 5.30 ± 0.71 $\mu\text{g mL}^{-1}$ and it was even more effective than the standard antioxidant BHT ($IC_{50} = 12.10 \pm 0.29$ $\mu\text{g mL}^{-1}$). The ethyl acetate fraction also showed the highest FRAP value (3677.13 ± 0.60 $\mu\text{g TE mg}^{-1}$), inhibition of lipid peroxidation (60.93 ± 1.15 % at 500 $\mu\text{g mL}^{-1}$) and total phenolic content (95.50 ± 0.58 $\mu\text{g GAE g}^{-1}$) when compared to the other fractions. However, the remaining aqueous fraction was found to possess the highest total antioxidant activity among all the fractions. Hence, it was concluded that the ethyl acetate soluble fraction of this plant is rich in strong antioxidants but it is also promising to be able to conclude that, except for the *n*-hexane soluble fraction, all the other fractions of this plant are potentially valuable sources of natural antioxidants and might show effectiveness against diseases caused by the over-production of radicals. Thus, further phytochemical studies are required to isolate these potent natural antioxidants.

ИЗВОД

АНТИОКСИДАТИВНА АКТИВНОСТ ЕКСТРАКТА БИЉКЕ *Artemisia incisa* Pamp.

AZIZ-UR-REHMAN¹, SEHRISH GULZAR¹, MUHAMMAD A. ABBASI¹, TAYYABA SHAHZADI¹,
TAUHEEDA RIAZ¹, SABAHAT Z. SIDDIQUI¹ и MUHAMMAD AJAIB²

¹Department of Chemistry, Government College University, Lahore-54000, Pakistan и ²Department of Botany,
Government College University, Lahore-54000, Pakistan

Метанолни екстракт биљке *Artemisia incisa* Pamp. је, након упаравања растварача, растворен у дестилованој води и подвргнут подеоној екстракцији *n*-хексаном, хлороформом, етил-ацетатом и *n*-бутанолом. Антиоксидативна активност фракција је одређивана следећим

методама: а) реакцијом хватања 1,1-дифенил-2-пикрилхидразил радикала (DPPH), б) мерењем укупне антиоксидативне активности, в) тестирањем способности редукције фери јона (FRAP тест) и г) извођењем фери-тиоцијанатног теста. Такође је одређена укупна количина фенолних једињења. Резултати су показали да је етил-ацетатни екстракт показао највећу способност хватања DPPH радикала, његова IC_{50} вредност је била $5,30 \pm 0,71 \mu\text{g mL}^{-1}$ и био је ефикаснији од стандардног антиоксиданса BHT, чија је IC_{50} вредност била $12,10 \pm 0,92 \mu\text{g mL}^{-1}$. Етил-ацетатна фракција је имала и највећу способност редукције фери јона (FRAP вредност је била $3677,13 \pm 27,1 \mu\text{g TE mL}^{-1}$), способност инхибиције липидне пероксидације ($60,93 \pm 0,84$ % при концентрацији $500 \mu\text{g mL}^{-1}$), а и садржај фенолних једињења је био највећи ($95,50 \pm 0,05 \mu\text{g GAE g}^{-1}$). Водена фракција, заостала после екстракције органским растварачима, имала је највећу укупну антиоксидативну активност.

(Примљено 2. јануара, ревидирано 18. марта 2011)

REFERENCES

1. N. G. Baydar, G. Özkan, S. Yaşar, *Food Control* **18** (2007) 1131
2. A. Djeridane, M. Youssfi, B. Nadjemi, P. Boutassouna-Stocker, N. Vidal, *Food Chem.* **97** (2006) 654
3. C. Wong, H. Li, K. Cheng, C. Feng, *Food Chem.* **97** (2006) 705
4. D. Kim, K. Ock, J. Young, M. Hae-Yeon, Y. L. Chang, *J. Agric. Food Chem.* **51** (2003) 6509
5. R. Abid, M. Qaisar, *Pak. J. Bot.* **40** (2008) 1827
6. C.-Z. Liu, Y.-C. Wang, C. Guo, F. Ouyang, H.-C. Ye, G.-F. Li, *Plant Sci.* **135** (1998) 211
7. C. Z. Liu, S. J. Murch, M. El-Demerdash, P. K. Saxena, *J. Biotechnol.* **110** (2004) 63
8. H. A. Arab, S. Rahbari, A. Rassouli, M. H. Moslemi, F. Khosravirad, *Trop. Anim. Health Prod.* **38** (2006) 497
9. J. T. Mukinda, J. A. Syce, *J. Ethnopharmacol.* **112** (2007) 138
10. K. Lee, T. Shibamoto, *Food Chem.* **74** (2001) 443
11. P. Prieto, M. Pineda, M. Aguilar, *Anal. Biochem.* **269** (1999) 337
12. I. F. F. Benzie, J. J. Strain, *Anal. Biochem.* **239** (1996) 70
13. P. Valentao, E. Fernandes, F. Carvalho, P. B. Andrade, R. M. Seabra, M. L. Bastos, *J. Agric. Food Chem.* **50** (2002) 4989
14. H. P. S. Makkar, M. Bluemmel, N. K. Borowy, K. Becker, *J. Sci. Food Agric.* **61** (1993) 161
15. H. Kaur, J. Perkins, in *Free Radicals and Food Additives*, O. I. Aruoma, B. Halliwell, Eds., Taylor and Francis, London, 1991, pp. 17–35
16. J. Baumann, G. Wurm, F. Bruchhausen, *Naunyn-Schmied. Arch. Pharmacol.* **30** (1979) 27
17. E. R. Sherwin, *J. Am. Oil Chem. Soc.* **55** (1978) 809
18. S. Miladi, M. Damak, *J. Soc. Chim. Tunisie* **10** (2008) 101
19. I. F. F. Benzie, J. J. Strain, *Methods Enzymol.* **299** (1999) 15
20. R. L. Prior, G. Cao, *Free Radical Biol. Med.* **27** (1999) 1173
21. J. S. J. Kim, M. J. Kim, *J. Med. Plants Res.* **4** (2010) 674.
22. G. Paganga, N. Miller, C. A. Rice-Evans, *Free Radical Res.* **30** (1999) 153
23. T. J. VanderJagt, R. Ghattas, D. J. VanderJagt, M. Crossey, R. H. Glew, *Life Sci.* **70** (2002) 1035.



J. Serb. Chem. Soc. 76 (10) 1387–1394 (2011)
JSCS–4213

Complexes of some 3d-metals with a Schiff base derived from 5-acetamido-1,3,4-thiadiazole-2-sulphonamide and their biological activity

SUMAN MALIK¹, SUPARNA GHOSH¹ and LIVIU MITU^{2*}

¹Department of Chemistry, Sadhu Vaswani College, Bairagarh, Bhopal – 462030, India and

²Department of Physics and Chemistry, University of Pitesti, Pitesti – 110040, Romania

(Received 11 January, revised 29 March 2011)

Abstract: Using a bidentate ligand, a Schiff base of 5-acetamido-1,3,4-thiadiazole-2-sulphonamide, complexes of transition metals having the general formula ML_2 , where $M = Mn(II), Fe(II), Ni(II)$ and $Cu(II)$, were synthesized. The complexes were characterized by elemental analysis, molar conductivity, magnetic moment, electronic, ESR and IR spectroscopy, and particle size analysis. The conductivity data of the complexes suggests their non-electrolytic nature. The stability constants and free energy change for the complexes were calculated. Spectral studies and magnetic susceptibility measurements revealed an octahedral geometry for all the complexes. The ligand and its complexes were screened for their fungicidal activity against *Aspergillus niger* and *A. flavus*.

Keywords: Schiff base; conductivity; non-electrolytic; stability constant; fungicidal activity.

INTRODUCTION

5-Acetamido-1,3,4-thiadiazole-2-sulphonamide (acetazolamide) is a diuretic drug. Diuretics are described as medicines that help to reduce the amount of water in the body. In the present day scenario, diseases such as high blood pressure, renal failure, diabetes, *etc.* have become very common. Hence, diuretic drugs were chosen for the present study. Schiff base metal complexes played a central role in the development of coordination chemistry. Schiff bases are widely applicable because of their industrial and biological importance and hence were well studied in the past.^{1–4} It was established that the biological activity of a Schiff base is altered many fold on its coordination with suitable metal ions.^{5–7} The introduction of nitrogen atoms into the structure of organic compounds often resulted in important changes in their behaviour towards metal ions. Many investigations

*Corresponding author. E-mail: ktm7ro@yahoo.com
doi: 10.2298/JSC110111118M

were undertaken of the interaction of metal ions with ligands containing oxygen and nitrogen as donor atoms.^{8,9} In the present study, metal complexes of Mn(II), Fe(II), Ni(II) and Cu(II) with a Schiff base derived from 5-acetamido-1,3,4-thiadiazole-2-sulphonamide (acetazolamide) and salicylaldehyde were synthesized and characterized in view of their importance in biological systems.¹⁰⁻¹²

EXPERIMENTAL

All the chemicals used in this work were of analytical reagent grade (anhydrous) and purchased from Merck (USA).

Synthesis of Schiff base

Equimolar (0.01 M) solutions of pure drug (3.26 g) (provided by Shalaks' Pharmaceuticals, Mumbai, India) and salicylaldehyde (1.04 ml) were separately dissolved in a methanol–water mixture (1:1). The mixture was refluxed for four hours and kept for a day. Pale yellow crystals of acetazolamide Schiff base formed in the reaction mixture (Fig. 1), which were filtered and washed thoroughly with 50 % methanol–water mixture, dried under vacuum and weighed. The colour of the solid product was pale yellow (yield 54 %). Melting point of the Schiff base was recorded.

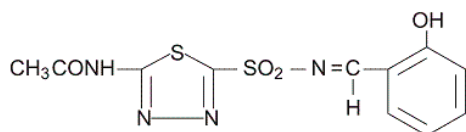


Fig. 1. The structure of the Schiff base.

Synthesis of complexes

For the synthesis of the complexes, 0.02 mol acetazolamide–salicylaldehyde ligand solution (AZM–SA) was prepared in 60 % acetone–water solvent and then the required metal salt (0.01 mol) was added. The resulting solution was refluxed for 4–5 h. The refluxed solutions were kept for some days whereby solid crystalline compounds appeared in the solution, which were filtered, washed with 60 % acetone–water mixture, dried and weighed. The melting points of the complexes were recorded.

Methods and apparatus applied

Elemental analyses were performed on a model 240 Perkin–Elmer elemental analyzer (USA) at CDRI Lucknow, India. The metal contents were determined gravimetrically.¹³ Magnetic susceptibility measurements of the complexes in the solid state were determined on a vibrating sample magnetometer (PAR, model 155, USA) at room temperature. Molar conductance measurements were realized in anhydrous DMF on a Systronics model 305 (India) conductivity bridge. The electronic spectra of the metal complexes in dimethylformamide (DMF) were recorded on a Shimadzu UV-160A UV–Vis (USA) spectrophotometer (5815–32573 cm⁻¹). The infrared spectra were measured on a Nicolet 400 D FT-IR (USA) spectrophotometer in the wave number range 4000–400 cm⁻¹ using KBr pellets. The electron spin resonance (ESR) spectra were recorded on a Bruker DRX-300 (Germany) spectrophotometer and an X-E-4 bands spectrometer (Bruker, Germany) at LNT (liquid nitrogen temperature) and RT (room temperature), respectively. Particle size analysis was performed at Sicart, Gujarat (India) using a laser diffraction particle size analyzer (Cilas, model 1064 L/D, France). The melting points of the ligand and complexes were recorded in open capillaries on a capillary melting point apparatus (EI, model 934, IndiaLine no. 60, India).

Antifungal activity

The antifungal activities of the newly synthesized compounds and ligand were evaluated by the agar growth food poison technique¹⁴ at 500 and 1000 ppm concentrations against *Aspergillus niger* and *A. flavus*. The disc diffusion method was used for the standard drug neta-mycin against *A. niger* and *A. flavus* using Czapek's agar medium. The fungi were grown at 25±1 °C on dextrose agar medium. All the microbial plates were incubated for 48 h at 35 °C. The antifungal activity of all the synthesized compounds was evaluated by percentage zone of growth inhibition. Three replicates were performed for each dilution of the test compounds from the screening results. All the fungal species were procured from the Microbial Type Collection and Gene Bank, Institute of Microbial Technology (IMTECH), Chandigarh, India.

RESULTS AND DISCUSSION

Based on the physicochemical characteristics (Table I), it was found that all the complexes were non-hygroscopic, stable at room temperature and insoluble in water but fairly soluble in dimethyl sulfoxide (DMSO). The magnetic moment data indicated all the complexes to be paramagnetic in nature. The molar conductance values for the complexes were found between 13–17 Ω⁻¹ cm² mol⁻¹ in DMSO, which indicates their non-electrolytic nature.¹⁵ The elemental analysis data, formula weights and melting points are given in Table II.

TABLE I. Synthesis and physico-chemical characteristics of the complexes

Ligand/complex	Ligand– –metal ratio	Colour	Yield %	Stability constant log K L mol ⁻¹	ΔF kJ mol ⁻¹	A _m ^a Ω ⁻¹ cm ² mol ⁻¹	μ _{eff} μ _B
AZM-SA	–	Pale yellow	54	–	–	–	–
[Mn(AZM-SA) ₂ (H ₂ O) ₂]	2:1	Brown	35	11.16	–64.58	15.3	5.38
[Fe(AZM-SA) ₂ (H ₂ O) ₂]	2:1	Black	69	11.15	–64.62	16.4	5.78
[Ni(AZM-SA) ₂ (H ₂ O) ₂]	2:1	Pale green	65	10.84	–65.12	13.0	3.18
[Cu(AZM-SA) ₂ (H ₂ O) ₂]	2:1	Dark green	42	12.08	–71.26	14.6	1.83

^a10⁻³ M solution in DMSO

TABLE II. Analytical data of the ligand and complexes

Ligand/complex	Elemental analysis, found (calcd.), %					M.p., °C
	C	H	N	S	Metal	
C ₁₁ H ₁₀ N ₄ O ₄ S ₂	39.01 (40.46)	4.08 (3.06)	18.21 (17.26)	19.50 (19.61)	–	242
(C ₁₁ H ₉ N ₄ O ₄ S ₂) ₂ Mn·2H ₂ O	38.46 (37.13)	2.63 (2.53)	15.69 (15.75)	18.10 (18.00)	3.38 (3.52)	355
(C ₁₁ H ₉ N ₄ O ₄ S ₂) ₂ Fe·2H ₂ O	37.36 (37.00)	2.53 (2.91)	15.53 (15.67)	18.18 (18.50)	6.88 (7.91)	360

TABLE II. Continued

Ligand/complex	Elemental analysis, found (calcd.), %					M.p., °C
	C	H	N	S	Metal	
(C ₁₁ H ₉ N ₄ O ₄ S ₂) ₂ Ni·2H ₂ O	35.00 (35.45)	2.80 (2.41)	14.93 (15.03)	17.14 (17.18)	7.96 (7.91)	260
(C ₁₁ H ₉ N ₄ O ₄ S ₂) ₂ Cu·2H ₂ O	36.98 (36.00)	2.50 (2.91)	15.69 (16.67)	17.93 (17.50)	8.86 (8.91)	199

Magnetic measurements

The magnetic moment data are presented in Table I. The Mn(II) complex showed a value of 5.38 μ_B , which is slightly lower than the spin only value of 5.92 μ_B for high spin octahedral Mn(II) complexes.¹⁶ The magnetic moment of the Fe(II) complex was 5.78 μ_B , which supports its high spin octahedral geometry.¹⁷ The observed magnetic value of Ni(II) complex was 3.18 μ_B , which is in good agreement with a spin free octahedral geometry.¹⁸ The Cu(II) complex exhibited a value of 1.83 μ_B , which suggests an octahedral geometry¹⁹ around the central metal ion.

Electronic spectra

The electronic spectra of the complexes were recorded in the solution state. The energies of the observed spin allowed bands in all the complexes agreed with the octahedral geometry. The electronic spectrum of Mn(II) complex shows four weak bands at bands at 16000, 19810, 20746 and 26740 cm^{-1} , which can be assigned to ${}^6A_{1g} \rightarrow {}^6T_{1g}$, ${}^6A_{1g} \rightarrow {}^4T_{2g}$, ${}^6A_{1g} \rightarrow {}^4E_g$ and ${}^6A_{1g} \rightarrow {}^4T_{1g}$, respectively, for an Mn(II) ion in an octahedral field.²⁰ The electronic spectrum of the Fe(II) complex showed two bands. The band at 10820 cm^{-1} may be assigned to the ${}^5T_{2g} \rightarrow {}^5E_g$ transition²¹ and the other at 20490 cm^{-1} to charge transfer.²² Similar types of transitions were reported for octahedral Fe(II) complexes.²³ The electronic spectrum of the Ni(II) complex displayed three bands at 12500, 18900 and 26400 cm^{-1} , assigned to ${}^3A_{2g}(F) \rightarrow {}^3T_{2g}(F)$, ${}^3T_{1g}(F)$ and ${}^3T_{1g}(P)$ transitions, respectively, which indicate octahedral geometry²⁴ of the Ni(II) complex. The electronic spectrum of the Cu(II) complex showed two ligand field bands at 13700 and 18000 cm^{-1} , assigned to the transitions ${}^2E_g \rightarrow {}^2T_{2g}$ and charge transfer, respectively. The electronic spectrum of the Cu(II) complex suggests an octahedral geometry.²⁵

Infrared spectra

The IR spectrum of the Schiff base showed a sharp band near 1610 cm^{-1} , which may be due to the azomethine linkage,^{26–28} which was shifted to lower frequencies in the metal complexes, indicating coordination of the metal ions through the azomethine linkage.²⁹ The ligand showed a strong band at 3410 cm^{-1} due to the phenolic –OH group.³⁰ This band was absent in the spectra of all the

metal complexes, indicating involvement of this group in the formation of the complexes.³¹ The bands observed at 1176, 1174, 1178, 1175 and 1173 cm^{-1} are characteristics of $\text{SO}_2\text{-N}$ linkages in the Schiff base and the Mn(II), Fe(II), Ni(II) and Cu(II) complexes, respectively.³² The appearance of the M–N bands at 411, 409, 412 and 415 cm^{-1} and the M–O bands at 505, 508, 511 and 550 cm^{-1} in the complexes indicate that AZM-SA was coordinated through an O and a N atom.^{33,34} The absorption bands at 3410, 3592, 3621 and 3547 cm^{-1} show the presence of coordination water in the complexes.³⁵ The weak bands observed at 1280, 1286, 1282, 1288 and 1290 cm^{-1} are characteristics of $\nu_{\text{C-O}}$ (phenolic)³⁶ in the Schiff base and the metal complexes, respectively. The medium frequencies observed in the region 674 cm^{-1} in the ligand and the respective metal complexes are assigned to $\nu_{\text{C-S}}$.³⁷ The IR spectral data and their tentative assignments are given in Table III.

TABLE III. Infrared spectral data (cm^{-1}) and their tentative assignments (*vs* – very strong, *s* – strong, *m* – medium, *w* – weak)

Ligand/complex	$\nu(\text{HC}=\text{N})$	$\nu(\text{SO}_2\text{N})$	$\nu(\text{N-H})$	$\nu(\text{M-N})$	$\nu(\text{M-O})$	$\nu(\text{H}_2\text{O})$
AZM-SA	1610 <i>vs</i>	1176 <i>vs</i>	3301 <i>s</i>	–	–	–
[Mn(AZM-SA) ₂ (H ₂ O) ₂]	1578 <i>s</i>	1174 <i>vs</i>	3300 <i>s</i>	505 <i>m</i>	411 <i>s</i>	3410 <i>vs</i>
[Fe(AZM-SA) ₂ (H ₂ O) ₂]	1581 <i>s</i>	1178 <i>s</i>	3304 <i>s</i>	508 <i>s</i>	409 <i>w</i>	3592 <i>vs</i>
[Ni(AZM-SA) ₂ (H ₂ O) ₂]	1590 <i>s</i>	1175 <i>vs</i>	3300 <i>s</i>	511 <i>m</i>	412 <i>s</i>	3621 <i>vs</i>
[Cu(AZM-SA) ₂ (H ₂ O) ₂]	1593 <i>s</i>	1173.5 <i>s</i>	3300 <i>s</i>	550 <i>s</i>	415 <i>w</i>	3547 <i>vs</i>

ESR spectra

The ESR spectra of the Fe(II) and Cu(II) complexes were recorded in DMSO at LNT (liquid nitrogen temperature) and RT (room temperature). The spectrum of the Cu complex at RT shows one intense absorption band in the high field. At LNT, the Cu(II) complex shows four well-resolved peaks in the low field region. The g_{\parallel} and g_{\perp} components were calculated respectively from the low and high intensity envelopes. The values obtained for Cu(II) complex were $g_{\parallel} > g_{\perp} > 2$, indicating that the Cu(II) lies predominantly in the $d_{x^2-y^2}$ orbital.³⁸ The observed values of α^2 , β^2 and γ^2 of the Cu(II) complex are less than unity, which indicates that the complex has some covalent character in the ligand environment.³⁹ The ESR spectrum of the Fe(II) complex at both RT and LNT, consisted of a single broad peak of high intensity, explaining its paramagnetic character that is also supported by the value of the magnetic moment (Table I). The values of $g_{\parallel} = g_{\perp}$ and g_{av} were less than two, which predicts the presence of vacant energy shells in Fe(II) ion to accept an electron pair from the ligand.⁴⁰

Particle size analysis

The pure acetazolamide drug (5-acetamido-1,3,4-thiadiazole-2-sulphonamide), its Schiff base and the Mn(II) and Cu(II) complexes derived from the Schiff

base were evaluated for their particle size distribution and average particle diameter using the laser diffraction method. The average particle size of the Mn(II) and Cu(II) complexes were found to be 2.93 and 2.76 μm , respectively, which is smaller than that of the Schiff base (AZM-SA) with an average diameter of 4.01 μm and that of the pure drug with an average diameter of 4.16 μm . The smaller particle size of the complexes results in an enhanced solubility of the drug.⁴¹

Fungicidal activity

Above synthesized compounds and the ligand (Schiff base) were screened against *A. niger* and *A. flavus* by the agar growth food poison technique to assess their potentials as fungicidal agents. The disc diffusion method was used for the standard drug gentamycin against *A. niger* and *A. flavus* using Sabouraud agar medium. The percentage growth by an inhibitor at different dilutions is determined as $100(C - T)/C$ (where C is the diameter of the fungus colony in the control plate and T is the diameter of fungus colony in the test plate). The zone of inhibition based on the size around the disc was measured. The inhibition zone percentages are recorded in Table IV. From the results, it can be observed that the complexes showed greater activity as compared to the Schiff base. The improved activities of some of the metal complexes as compared to the ligand can be explained by the chelation theory. This theory explains that a decrease in the polarizability of the metal could enhance the lipophilicity of the complexes, which leads to a breakdown of the permeability of the cells, resulting in interference with normal cell processes.⁴² This indicates that chelation increases the fungicidal activity.⁴³

TABLE IV. Antifungal activity (inhibition zone, %) of Schiff base and complexes; medium: Czapek's agar; time: 5 days; temperature: 25 ± 1 °C, dose = 500 ppm

Compound	<i>A. niger</i>	<i>A. flavus</i>
AZM-SA	51.23	59.47
(AZM-SA) ₂ Mn	66.38	71.23
(AZM-SA) ₂ Fe	72.25	81.78
(AZM-SA) ₂ Ni	81.46	95.67
(AZM-SA) ₂ Cu	81.45	98.55
Netamycin	55.23	45.53

CONCLUSIONS

Based on elemental analysis, magnetic moment data, conductivity measurements and spectral studies, an octahedral structure for the complexes is proposed (Fig. 2.). All the synthesized metal complexes showed biological activities against the tested pathogenic fungal species by the well agar method. To counter increased fungal disease to their rapid growth in the population, investigation of the fungicidal activities of ligands and their metal complexes would be very use-

ful to control this harmful disease. The present work will be extended to the synthesis of other metal complexes and their biological activities.

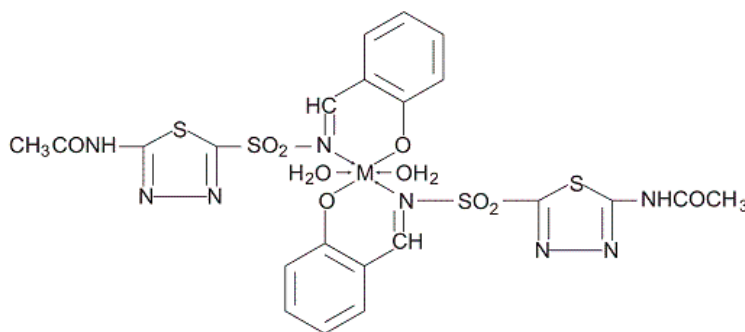


Fig. 2. The proposed structure of the complexes: M = Mn(II), Fe(II), Ni(II), Cu(II).

Acknowledgements. The authors are thankful to the Principal of Sadhu Vaswani College, India, for providing all laboratory facilities. The authors also owe their sincere thanks to UGC for sanctioning a UGC Research Award to Dr Suman Malik, one of the co-authors. The authors are also indebted to CDRI Lucknow, India, for providing the facilities for the elemental analysis, SICART Gujrat, India, for the electronic and ESR spectra and Vikram University Ujjain, India, for recording the IR spectra.

ИЗВОД

КОМПЛЕКСИ НЕКИХ 3d-МЕТАЛА СА ШИФОВИМ БАЗАМА КОЈЕ СУ ДОБИЈЕНЕ ИЗ 5-АЦЕТАМИДО-1,3,4-ТИЈАДИАЗОЛ-2-СУЛФОНАМИДА И ЊИХОВА БИОЛОШКА АКТИВНОСТ

SUMAN MALIK¹, SUPARNA GHOSH¹ и LIVIU MITU²

¹Department of Chemistry, Sadhu Vaswani College, Bairagarh, Bhopal – 462030, India и ²Department of Physics and Chemistry, University of Pitesti, Pitesti – 110040, Romania

Полазећи од бидентатног лиганда, Шифове базе 5-ацетамидо-1,3,4-тијадиазол-2-сулфонамида, синтетизовани су комплекси неких прелазних метала, опште формуле ML_2 (где је $M = Mn(II), Fe(II), Ni(II)$ и $Cu(II)$). За карактеризацију комплекса употребљени су елементална микроанализа, мерења моларне проводљивости и магнетног момента, електронска, ESR и IR спетроскопија, као и метода анализе прахова. На основу мерења моларне проводљивости претпостављено је да су испитивани комплекси електронеутрални. Израчунате су вредности константи стабилности, као и вредности промене слободне енергије. На основу измерених вредности магнетних момената за све испитиване комплексе претпостављена је октаедарска геометрија. Испитивана је антифунгална активност за лиганд и одговарајуће комплексе на сојевима *Aspergillus niger* и *A. flavus*.

(Примљено 11. јануара, ревидирано 29 марта 2011)

REFERENCES

1. N. Fahmi, R. V. Singh, *Transition Met. Chem.* **19** (1994) 453
2. Z. H. Chohan, A. Rauf, C. T. Supuran, *Met. Based Drugs* **8** (2001) 287

3. A. A. Osowale, G. A. Kolawale, O. E. Fagade, *J. Coord. Chem.* **61** (2008) 1946
4. M. Shamsipur, M. Yousefi, M. Hosseini, M. Ganjali, H. Sharghi, H. Naeimi, *Anal. Chem.* **73** (2001) 2869
5. K. D. Rainsford, M. W. Whitehouse, *J. Pharm. Pharmacol.* **28** (1976) 83
6. M. B. Ferrari, S. Capacchi, F. Bisceglie, G. Pelosi, P. Tarasconi, *Inorg. Chim. Acta* **312** (2001) 81
7. L. Singh, G. Mohan, R. K. Prashar, S. P. Tripathi, R. C. Sharma, *Curr. Sci.* **55** (1986) 846
8. L. F. Lindoy, S. E. Livingstone, *Inorg. Chim. Acta* **1** (1967) 365
9. R. Dwivedi, R. Dhakarey, *J. Indian Counc. Chem.* **20** (2003) 56
10. M. Bhattacharya, S. A. Iqbal, S. Malik, *Res. Link* **IV** (2005) 12
11. M. Bhattacharya, S. A. Iqbal, S. Malik, *Orient. J. Chem.* **20** (2004) 643
12. S. Malik, S. Ghosh, B. Jain, *Arch. Appl. Sci. Res.* **2** (2010) 304
13. I. Vogel, *Quantitative Inorganic Analysis*, Longman Green, London, 1959
14. S. Chandra, A. K. Sharma, *Res. Lett. Inorg. Chem.* (2009) 945670
15. B. K. Kumar, V. Ravinder, G. B. Swamy, S. J. Swamy, *Indian J. Chem.* **33A** (1994) 136
16. B. K. Sahu, B. K. Mahapatra, *J. Indian Chem. Soc.* **56** (1979) 825
17. K. M. Patel, N. H. Patel, M. N. Patel, *J. Indian Counc. Chem.* **17** (2000) 19
18. C. L. Sharma, M. S. Islam, *Synth. React. Inorg. Met.-Org. Chem.* **10** (1986) 553
19. L. W. Lane, L. T. Taylor, *J. Coord. Chem.* **2** (1973) 295
20. A. B. P. Lever, *Inorganic Electronic Spectroscopy*, Elsevier, Amsterdam, 1968
21. C. Spinu, M. Pleniceanu, C. Tigae, *J. Serb. Chem. Soc.* **73** (2008) 415
22. A. Ceulemans, L. G. Vanquicken, *J. Am. Chem. Soc.* **103** (1998) 2238
23. A. S. Kuwar, S. R. Shimpi, P. P. Madhulikar, R. S. Bender, *J. Sci. Ind. Res.* **65** (2006) 665
24. B. K. Rai, M. Kumar, *J. Indian Counc. Chem.* **20** (2003) 22
25. N. Raman, J. D. Raja, *Indian J. Chem.* **46A** (2007) 1611
26. C. N. R. Rao, *Chemical Application of IR Spectroscopy*, Academic Press, New York, 1963
27. K. Nakamoto, *IR Spectra of Inorganic and Coordination Compounds*, Wiley, New York, 1956
28. S. Bilge, Z. Kilic, Z. H. Ali, T. Horkelek, S. Safran, *J. Chem. Sci.* **121** (2009) 989
29. A. P. Mishra, K. Kumar, *J. Indian Chem. Soc.* **86** (2009) 1150
30. M. L. H. Nair, L. Sharma, *J. Indian Chem. Soc.* **86** (2009) 133
31. V. Reddy, N. Patil, B. R. Patil, *J. Indian Counc. Chem.* **23** (2003) 1
32. A. Weissberger, *Chemical Application of Spectroscopy*, Inter Science, New York, 1956
33. N. Raman, S. Esthar, C. Thangaraja, *J. Chem. Sci.* **116** (2004) 209
34. C. V. Jose, T. Joy Anto, *Int. J. Chem. Sci.* **6** (2008) 1913
35. T. Arunachalam, R. Bhakayaraj, A. K. Sasi, *E-J. Chem.* **6** (2009) 143
36. M. K. Zaman, M. S. Arayne, N. Sultana, A. Farooq, *Pak. J. Pharm. Sci.* **19** (2006) 114
37. M. Z. A. Rafique, S. Khan, N. Saxena, M. A. Quraishi, *Port. Electrochim. Acta* **25** (2007) 419
38. B. J. Hathaway, D. E. Billing, *Coord. Chem. Rev.* **5** (1963) 143
39. Y. Anjaneyalu, R. P. Pao, *Synth. React. Inorg. Met.-Org. Chem.* **26** (1986) 257
40. N. Jain, S. P. S. Jadon, *Int. J. Chem. Sci.* **5** (2007) 529
41. K. Dua, M. V. Ramana, U. V. Singh, M. Himaja, A. Agarwal, V. Garg, K. Pabreja, *Curr. Drug Delivery* **4** (2007) 21
42. C. H. Collins, P. M. Lyne, *Microbiological Methods*, Butterworth, London, 1976
43. N. Raman, A. Kulandaisam, K. Jeyasubramanian, *Indian J. Chem.* **41A** (2002) 942.



J. Serb. Chem. Soc. 76 (10) 1395–1401 (2011)
JSCS–4214

***Ab initio* study of the mechanism of the formation of a bis-heterocyclic compound containing Si and Ge by reaction of germylene silylene (H₂Ge=Si:) and ethene**

XIUHUI LU*, JUNFENG HAN, ZHENXIA LIAN and YONGQING LI

School of Chemistry and Chemical Engineering, University of Jinan, Jinan, Shandong, 250022, People's Republic of China

(Received 21 September 2010, revised 23 March 2011)

Abstract: The mechanism of the cycloaddition reaction between singlet state germylene silylene (H₂Ge=Si:) and ethene was investigated by the CCSD(T)//MP2/6-31G* method. From the potential energy profile, it can be predicted that the reaction has only one dominant reaction pathway. The presented rule of the dominant reaction pathway is that the [2+2] cycloaddition effect of the two reactants leads to the formation of a four-membered ring silylene with Ge (INT1). Due to sp³ hybridization of the Si atom in four-membered ring silylene with Ge (INT1), INT1 further reacts with ethene to form a bis-heterocyclic compound with Si and Ge (P2).

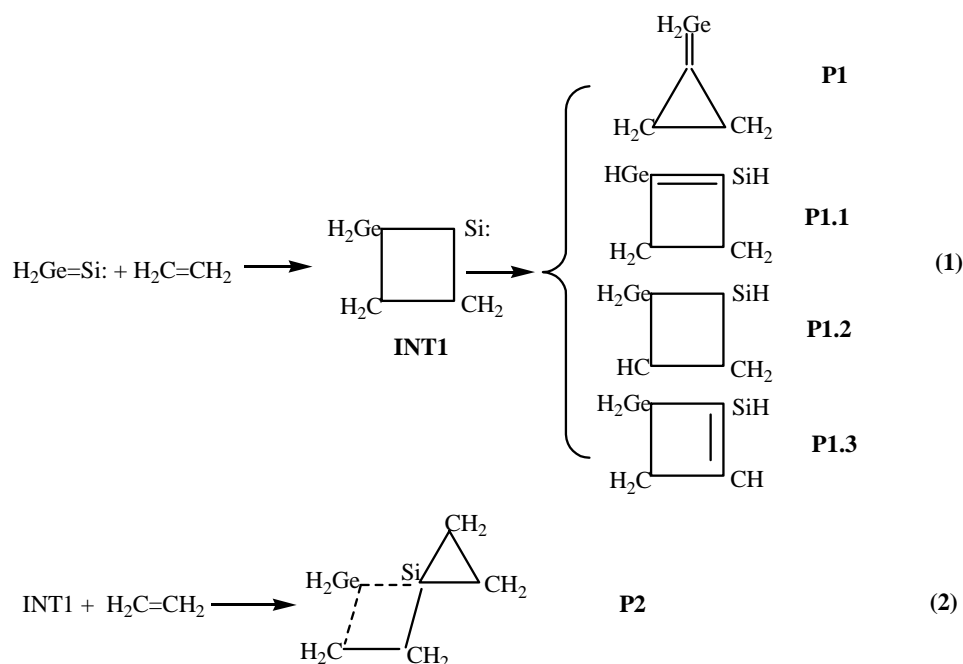
Keywords: germylene silylene; reaction mechanism; potential energy profile.

INTRODUCTION

Unsaturated silylenes are an important type of active intermediates. Their cycloaddition reactions are considered as providing a convenient, short synthesis pathway for the synthesis of tensility cyclotella, silapolycyclic compounds and compounds that are difficult to synthesize by other methods, and are also regarded as an effective method for the syntheses of new bonds and heterocyclic compounds containing Si. H₂C=Si: is the simplest unsaturated silylene, which was first observed experimentally by Leclercq and Dubois in 1979.¹ Srinivas *et al.*² employed neutralization–reionization mass spectrometry to show that H₂C=Si: is a viable molecule in a low-pressure gas phase. A theoretical study indicated that the ground state of H₂C=Si: is a singlet state.³ The energy of H₂C=Si: is 84 kcal mol⁻¹ lower than that of silacetylide; thus, H₂C=Si: is the lowest energy isomer.⁴ Preliminary studies on the cycloaddition reactions of unsaturated silylenes were performed,^{5–9} but these studies were limited to the cycloaddition re-

* Corresponding author. E-mail: lxh@ujn.edu.cn
doi: 10.2298/JSC100921124L

action of methylene silylene and its derivatives ($X_2C=Si:$, $X=H, F, Cl, CH_3$, *etc.*). Hitherto, no reports on the cycloaddition reaction of germylene silylene and its derivatives ($X_2Ge=Si:$, $X=H, F, Cl, CH_3$, *etc.*) exist; it is a new area of research on the cycloaddition reaction of unsaturated silylenes. It is quite difficult to investigate the mechanisms of the cycloaddition reaction directly by experimental methods due to the high activity of germylene silylene, therefore, a theoretical study is more practical. To explore the rules of the cycloaddition reaction between germylene silylene (including its derivatives) and symmetric π -bonded compounds, germylene silylene ($H_2Ge=Si:$) and ethene were selected as model molecules, and the mechanism of the cycloaddition reaction between germylene silylene and ethene was investigated and analyzed theoretically. The results showed that there are two possible pathways for the cycloaddition reaction (considering the H transfer simultaneously) as follows:



CALCULATION METHOD

MP2/6-31G^{*10} implemented in the Gaussian 98 package was employed to locate all the stationary points along the reaction pathways. Full optimization and vibrational analysis were performed for the stationary points on the reaction potential energy profile. Zero point energy and CCSD(T) corrections were included in the energy calculations. In order to explicitly establish the relevant species, the intrinsic reaction coordinates (IRC)^{11,12} were also calculated for all the transition states appearing on the potential energy profile of the cycloaddition.

RESULTS AND DISCUSSION

Reaction (1): The pathways of the formation of a four-membered ring silylene with Ge (INT1), H-transfer products (P1.1, P1.2 and P1.3) and a three-membered ring product (P1)

Theoretical investigations showed that the ground state of germylene silylene ($\text{H}_2\text{Ge}=\text{Si}$) is the singlet state. The geometric parameters of the intermediate (INT1), transition states (TS1, TS1.1, TS1.2 and TS1.3) and products (P1, P1.1, P1.2 and P1.3), which appear in reaction (1) between germylene silylene and ethane, are given in Fig. 1. The energies are listed in Table I, and the potential energy profile for the cycloaddition reaction is shown in Fig. 2. The unique imaginary frequencies of the transition states TS1, TS1.1, TS1.2 and TS1.3 are 196.4 , 600.2 , 1037.0 and 985.6 cm^{-1} , respectively, and, consequently, these transition states can be affirmed as real ones. According to the calculations of the IRC of TS1, TS1.1, TS1.2 and TS1.3, further optimization of the primary IRC results, TS1 connects INT1 with P1, TS1.1 connects INT1 with P1.1, TS1.2 connects INT1 with P1.2 and TS1.3 connects INT1 with P1.3.

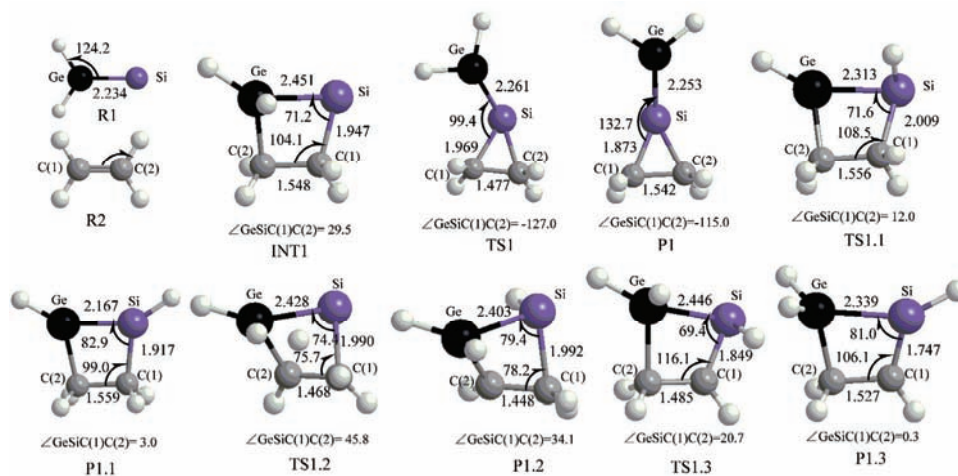


Fig. 1. Optimized MP2/6-31G* geometrical parameters and the atomic numbering for the species in cycloaddition reaction (1). Bond lengths and bond angles are in Å and °, respectively.

According to Fig. 2, it can be seen that reaction (1) consists of five steps: the first step is that the two reactants (R1 and R2) form a four-membered ring silylene (INT1), which is a barrier-free exothermic reaction of 127.9 kJ mol^{-1} ; the second step is that INT1 isomerizes to a three-membered ring product (P1) via the transition state TS1 with an energy barrier of 56.7 kJ mol^{-1} ; the following three steps are that INT1 undergoes H-transfer via transition states TS1.1, TS1.2

and TS1.3 with energy barriers of 42.4, 66.2 and 118.6 kJ mol⁻¹, respectively, resulting in the formation of products P1.1, P1.2 and P1.3. As the energy of P1 is 39.7 kJ mol⁻¹ higher than that of INT1, the reaction INT1→P1 is thermodynamically prohibited at normal temperature and pressure. The energy barriers of TS1.2 and TS1.3 are 14.3 and 23.8 kJ mol⁻¹ higher than that of TS1.1; therefore, INT1→P1.1 is the dominant reaction pathway of the reaction (1).

TABLE 1. Zero point energy (*ZPE* / hartree), total energies (*E_T* / hartree) and relative energies (*E_R* / kJ·mol⁻¹) for the species from various theoretical methods (*E_T* = *E*(Species) + *ZPE*; *E_R* = *E_T* - *E*(R1+R2); *E_R* = *E_T* - *E*(INT1+R2))

Reaction	Species	<i>ZPE</i>	MP2/6-31G*		CCSD(T)/MP2/6-31G*	
			<i>E_T</i>	<i>E_R</i>	<i>E_T</i>	<i>E_R</i>
(1)	R1+R2	0.06544	-2441.59424	0.0	-2441.67589	0.0
	INT1	0.07079	-2441.65402	-157.0	-2441.72461	-127.9
	TS1(INT1-P1)	0.06938	-2441.63161	-98.1	-2441.70301	-71.2
	P1	0.06962	-2441.63776	-114.3	-2441.70947	-88.2
	TS1.1(INT1-P1.1)	0.06935	-2441.63740	-113.3	-2441.70845	-85.5
	P1.1	0.07197	-2441.66161	-176.9	-2441.72835	-137.7
	TS1.2(INT1-P1.2)	0.06714	-2441.63285	-101.4	-2441.69939	-61.7
	P1.2	0.06805	-2441.66461	-184.8	-2441.72831	-137.6
	TS1.3(INT1-P1.3)	0.06492	-2441.60500	-28.3	-2441.67945	-9.3
	P1.3	0.06734	-2441.66052	-174.0	-2441.72664	-133.2
(2)	INT1+R2	0.12283	-2519.88701	0.0	-2519.99449	0.0
	P2	0.12720	-2519.95156	-169.5	-2520.04690	-137.6

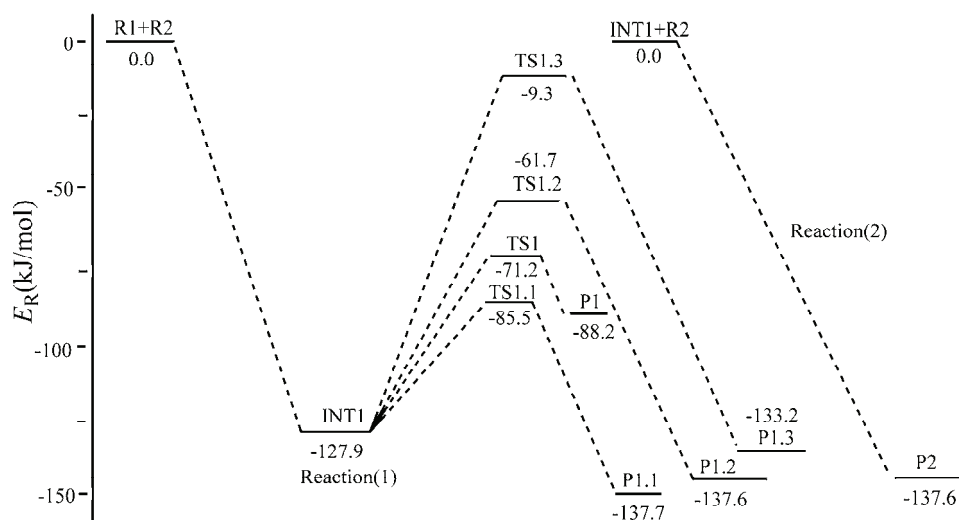


Fig. 2. The potential energy profile for the cycloaddition reactions between H₂Ge=Si: and H₂C=CH₂ with CCSD (T)/MP2/6-31G*.

Reaction (2): The formation pathway of a bis-heterocyclic compound with Si and Ge (P2)

In reaction (2), INT1 further reacts with ethene (R2) to form a bis-heterocyclic compound with Si and Ge (P2). The geometrical parameters of product (P2) which appear in reaction (2) are given in Fig. 3. The energies are listed in Table I, and the potential energy profile for the cycloaddition reaction is shown in Fig. 2. According to Fig. 2, reaction (2) is a barrier-free exothermic reaction of $137.6 \text{ kJ mol}^{-1}$. A careful and detailed study of this reaction, for which no intermediates or transition states exist, was performed. It is believed that due to the large radius of the Si atom before an intermediate or transition state could be formed, sp^3 hybridization of the Si atom in INT1 occurred and INT1 combined with the ethene to form a bis-heterocyclic compound with Si and Ge (P2).

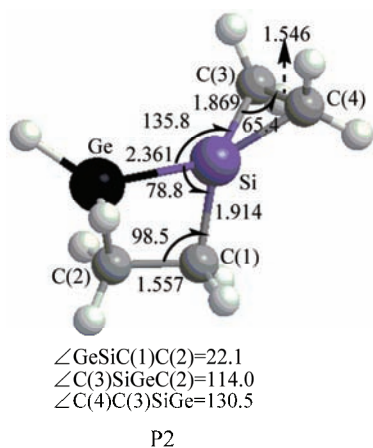


Fig. 3. Optimized MP2/6-31G* geometrical parameters of P2 and the atomic numbering for the species in cycloaddition reaction (2). Bond lengths and bond angles are in Å and °, respectively.

According to Fig. 2, $\text{INT1} \rightarrow \text{P1.1}$ and reaction (2) are two mutually competitive reactions but because $\text{INT1} \rightarrow \text{P1.1}$ requires a barrier of 42.4 kJ mol^{-1} be surmounted, while $\text{INT1} + \text{R2} \rightarrow \text{P2}$ directly reduces the system energy by $137.6 \text{ kJ mol}^{-1}$, reaction (2) should be the main reaction pathway.

Theoretical analysis and explanation of the dominant reaction pathway

According to the above analysis, the dominant reaction pathway of the cycloaddition reaction between singlet state germylene silylene and ethene is as follows:



In this reaction, the frontier molecular orbitals of R1, R2, and INT1 are shown in Fig. 4. According to Fig. 4, the frontier molecular orbitals of R1, R2 and INT1 can be expressed as in the schematic diagram given in Figs.5 and 6. The mechanism of the dominant reaction channel can be explained with the mo-

lecular orbital diagrams (Figs. 5 and 6) and Figs. 1 and 3. According to Figs. 1 and 5, when germylene silylene and ethene approach each other, due to the [2+2] cycloaddition effect of the two π -bonds in germylene silylene and ethene, a four-membered ring silylene with Ge is formed (INT1). As INT1 is an active intermediate, it may further react with ethene to form a bis-heterocyclic compound with Si and Ge (P2). The mechanism of this reaction can be explained with Figs. 3 and 6. As INT1 and ethene approach each other, due to the large radius of the Si atom in INT1, sp^3 hybridization of the Si atom in INT1 occurs before the formation of any intermediate or transition state between INT1 and ethane and then INT1 combines with the ethene to form a bis-heterocyclic compound with Si and Ge (P2).

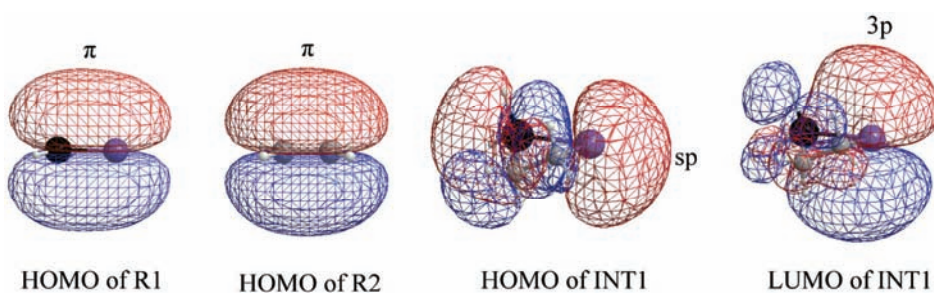


Fig. 4. The frontier molecular orbital of R1, R2 and INT1.

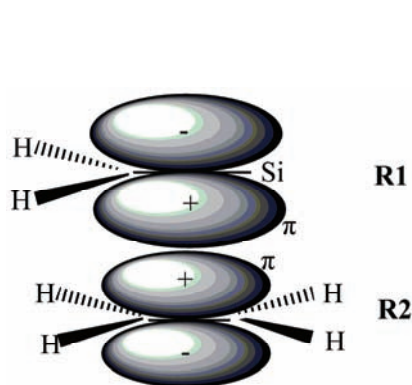


Fig. 5. A schematic interaction diagram for the frontier orbitals of $H_2Ge=Si:$ (R1) and $H_2C=CH_2$ (R2).

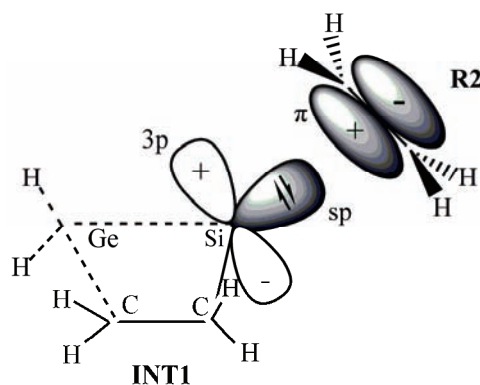


Fig. 6. A schematic interaction diagram for the frontier orbitals of INT1 and $H_2C=CH_2$ (R2).

CONCLUSIONS

From the potential energy profile of the cycloaddition reaction between singlet state germylene silylene and ethene obtained by the CCSD(T)//MP2/6-31G* method, it can be predicted that the reaction has a dominant reaction pathway. The dominant reaction pathway consists of two steps: first the two reactants form

a four-membered ring silylene with Ge (INT1) through a barrier-free exothermic reaction of $127.9 \text{ kJ mol}^{-1}$ and then INT1 further reacts with ethene (R2) to form a bis-heterocyclic compound with Si and Ge (P2), which is also a barrier-free exothermic reaction of $137.6 \text{ kJ mol}^{-1}$.

ИЗВОД

AB INITIO ИСПИТИВАЊЕ МЕХАНИЗМА РЕАКЦИЈЕ ФОРМИРАЊА
БИС-ХЕТЕРОЦИКЛИЧНИХ ЈЕДИЊЕЊА СА Si И Ge ИЗМЕЂУ
ГЕРМИЛЕН-СИЛЕНА ($\text{H}_2\text{Ge}=\text{Si}$) И ЕТЕНА

XIUHUI LU, JUNFENG HAN, ZHENXIA LIAN и YONGQING LI

*School of Chemistry and Chemical Engineering, University of Jinan, Jinan,
Shandong, 250022, People's Republic of China*

Механизам цикло-оксидационе реакције између гермилен-силена ($\text{H}_2\text{Ge}=\text{Si}$) у синглетном стању и етена је био испитиван CCSD(T)//MP2/6-31G* методом из профила потенцијалне енергије уз претпоставку да реакција има само један доминантни реакциони пут. Приказано правило о једном реакционом путу је да [2+2] циклоадиција проузрокује да два реактанта доводе до формирања четворочланог прстена силена са Ge (INT1). Због sp^3 хибридизације Si атома у четворочланом прстену силена са Ge (INT1), INT1 надаље реагује са етеном градећи бис-хетероциклично једињење са Si и Ge (P2).

(Примљено 21. септембра 2010, ревидирано 23. марта 2011)

REFERENCES

1. H. Leclercq, I. Dubois, *J. Mol. Spectrosc.* **76** (1979) 39
2. R. Srinivas, D. Sulzle, H. Schwarz, *J. Am. Chem. Soc.* **113** (1991) 52
3. W. H. Warren, W. W. Kevin, J. C. Dennis, *J. Chem. Phys.* **107** (1997) 8829
4. R. Damrauer, C. H. DePuy, S. E. Barlow, S. Gronert, *J. Am. Chem. Soc.* **110** (1988) 2005
5. X. H. Lu, H. B. Yu, W. R. Wu, *New. J. Chem.* **29** (2005) 332
6. X. H. Lu, H. B. Yu, Y. H. Xu, P. P. Xiang, Y. D. Liu, *J. Mol. Struct. THEOCHEM* **770** (2006) 185
7. X. H. Lu, H. B. Yu, Y. H. Xu, P. P. Xiang, X. Che, *Mol. Phys.* **105** (2007) 1961
8. X. H. Lu, X. Che, H. B. Yu, P. P. Xiang, Y. H. Xu, *J. Mol. Struct. THEOCHEM* **821** (2007) 53
9. X. H. Lu, H. B. Yu, X. Che, P. P. Xiang, *Int. J. Quantum Chem.* **108** (2008) 1114
10. L. A. Curtis, K. Raghavachari, J. A. Pople, *J. Chem. Phys.* **98** (1993) 1293
11. K. Fukui, *J. Phys. Chem.* **74** (1970) 4161
12. K. Ishida, K. Morokuma, A. Komornicki, *J. Chem. Phys.* **66** (1981) 2153.



J. Serb. Chem. Soc. 76 (10) 1403–1410 (2011)
JSCS–4215

Fractal analysis of bentonite modified with heteropoly acid using nitrogen sorption and mercury intrusion porosimetry

SRĐAN P. PETROVIĆ^{1*}, ZORICA M. VUKOVIĆ^{1#}, TATJANA B. NOVAKOVIĆ^{1#},
ZORAN P. NEDIĆ² and LJILJANA S. ROŽIĆ^{1#}

¹*ChTM – Department of Catalysis and Chemical Engineering, University of Belgrade, Njegoševa 12, Belgrade and* ²*Faculty of Physical Chemistry, University of Belgrade, Studentski trg 12–16, Belgrade, Serbia*

(Received 27 October 2010, revised 9 May 2011)

Abstract: Experimental adsorption isotherms were used to evaluate the specific surface area and the surface fractal dimensions of acid-activated bentonite samples modified with a heteropoly acid (HPW). The aim of the investigations was to search for correlations between the specific surface area and the geometric heterogeneity, as characterized by the surface fractal dimension and the content of added acid. In addition, mercury intrusion was employed to evaluate the porous microstructures of these materials. The results from the Frankel–Halsey–Hill method showed that, in the p/p_0 region from 0.75 to 0.96, surface fractal dimension increased with increasing content of heteropoly acid. The results from mercury intrusion porosimetry (MIP) data showed the generation of mesoporous structures with important topographical modifications, indicating an increase in the roughness (fractal geometry) of the surface of the solids as a consequence of the modification with the heteropoly acid. By comparison, MIP is preferable for the characterization because of its wide effective probing range.

Keywords: heteropoly acid; bentonite; fractal geometry; mercury intrusion porosimetry.

INTRODUCTION

Heteropoly acids supported on clay are complex mesoporous systems with an enormous potential for application in adsorption and catalysis processes.^{1–4} It is widely known that the optimum performance of solids in several applications requires an exhaustive control of both the structural and textural characteristics. Hence, the control of porosity and surface area are crucial aspects that largely determine the use of these materials.^{5,6} The fractal dimension is a parameter used to assess quantitatively the fractal geometry and it represents a measure of the irre-

* Corresponding author. E-mail: srlepp@gmail.com

Serbian Chemical Society member.

doi: 10.2298/JSC101027126P

gularities on the surface of a solid. The value for this parameter may vary from 2 to 3, whereby the lowest value (2) corresponds to a perfectly smooth surface, while the upper limit (3) corresponds to a totally irregular or rough surface.⁷ It is known that the irregularities and roughness of a surface are attributed to the existence of distributed pore sizes that contributes to the value of the fractal dimension (D).⁸ The magnitude of the surface fractal dimension of mesoporous materials has a great influence on such important physico-chemical processes as adsorption, surface diffusion and catalysis. Nevertheless, it is still an ambiguous problem to measure the value of D , which may vary according to the method used. One of the simplest relationships employed to determine the fractal dimension of a solid, based on adsorption data, was proposed by Avnir and Jaroniec⁹ from the Frankel–Halsey–Hill (F–H–H) Equation. F–H–H methods¹⁰ are the easiest way to calculate the value of D using nitrogen adsorption data without having to calculate the pore surface area.

In addition, mercury intrusion is a popular method employed to evaluate the microstructures of porous materials. Conventional interpretations of the original mercury intrusion porosimetry data include porosity, density, and pores size distribution, *etc.* Besides these, other structural factors have also been determined based on a calculation model deduced from fractal theories and the Washburn Equation.¹¹

A better description of pore size distribution across a wide range of pore size is not possible using one method. Therefore, the aim of this study was to quantify fractal geometry by employing two methods.

EXPERIMENTAL

Material

The results of previous investigations on the modelling and optimization of bentonite activation *via* the response surface methodology¹² were applied to a modified bentonite, which was also used as the support in the current study. Bentonite obtained under the optimal conditions (AAB) possessed the following chemical composition (mass %): SiO₂, 73.66; Al₂O₃, 12.28; Fe₂O₃, 4.73; CaO, 0.70; MgO, 1.99; Na₂O, 0.60; K₂O, 0.30; TiO₂, 0.57; loss on ignition, 5.17. Polycrystalline H₃PW₁₂O₄₀·6H₂O (HPW) was prepared from commercial phosphotungstic acid (microscopy grade H₃[P(W₃O₁₀)₄]_{aq}, Fluka) by heat treatment at 353 K for 1 h.

12-Tungstophosphoric acid/acid-activated bentonite was prepared according to the method described in the literature.¹³ HPW was dissolved in methanol and the resulting solution was added slowly to 5, 10 or 20 mass % of acid-activated bentonite (HPW5, HPW10 and HPW20). To remove the residual methanol, the wet samples were dried in a water bath and further dried in an oven for 2 h at 100°C. The samples were stored in sealed bottles until use.

Characterisation

The nitrogen sorption experiments were performed at 77 K using a Sorptomatic 1990 Thermo Finning apparatus. The samples were first degassed under vacuum at 453 K until no significant changes in the vacuum were observed (5 nm < t < 10 nm). The adsorbed amount of nitrogen was measured by volume at standard temperature and pressure. The specific sur-

face area of the catalysts was calculated by fitting the adsorption data to the linear range of the BET Equation¹⁴ (relative to p/p_0 (0.05–0.35)).

Mercury porosimetry experiments were performed using Carlo Erba porosimeter 2000. First, physisorbed gases were removed under vacuum from the interior of the sample. The intrusion of mercury volumes were measured at stepwise increasing pressures allowing for equilibration at each pressure step.

Methods

The classical Frenkel–Hill–Halsey (F–H–H) Equation describes the continuous growth of an adsorbate film with thickness z on a flat surface when $x \rightarrow 1$, *i.e.*:¹⁴

$$\ln\left(\frac{1}{x}\right) = \frac{\alpha}{z^m} \tag{1}$$

where α and m depend on the solid–adsorbate interaction. The value of m is determined experimentally by plotting the experimental isotherm:

$$\frac{N}{N_m} \approx \left(\ln\left(\frac{1}{x}\right)\right)^{-\frac{1}{m}} \tag{2}$$

where N is the number of adsorbed moles of nitrogen at a given relative pressure, N_m is the number of adsorbed moles in a monolayer and, in general, $2 \leq m \leq 3$.

Fractal F–H–H type equations were proposed by Avnir *et al.*⁹ and Pfeifer *et al.*¹⁵. In spite of the different adsorption mechanisms of multilayer formation considered by Avnir *et al.*,⁹ they obtained the following isotherm:

$$\frac{N}{N_m} \approx \left(\ln\left(\frac{1}{x}\right)\right)^{-(3-D)} \tag{3}$$

for micropores and mesopores size distributions, where $2 < D < 3$ is the surface fractal dimension.

To calculate D from mercury intrusion porosimetry, the following expression was deduced from fractal theories and the Washburn Equation:¹¹

$$\log\left(\frac{dV}{dR}\right) = \log k_1 + (2 - D)\log R \tag{4}$$

where V is the volume of mercury intruded at a given pressure, R is the pore radius, k_1 an isoproportionality constant and D is the fractal dimension. Hence, D values can be derived from the slop of $\log(dV/dR)$ vs. $\log R$ plots.

RESULTS AND DISCUSSION

Adsorption–desorption isotherms of acid-activated bentonite and bentonite modified with different amounts of HPW are shown in Fig 1. According to the Brunauer, Deming and Teller (BDDT) classification,¹⁶ all isotherms belong to type IV isotherms. A type IV isotherm shape is generally associated with mesoporous adsorbents. The mesopores capacity is the amount adsorbed at the plateau and the mesopore volume is then obtained by assuming the condensate density to be that of liquid nitrogen. Hysteresis loops, which appear in the multilayer range



of physisorption isotherms, are generally associated with the filling and emptying of mesopores. The desorption branch of an isotherm was favoured for mesopore size analysis, but this practice is now considered to be questionable since the desorption path may be dependent on network–percolation effects or variation of the pore diameter along single channels.¹⁷ On the other hand, the persistence of a metastable multilayer is likely to delay the condensation process on the adsorption branch,¹⁸ especially if the pores tend to be slit-shaped.¹⁹

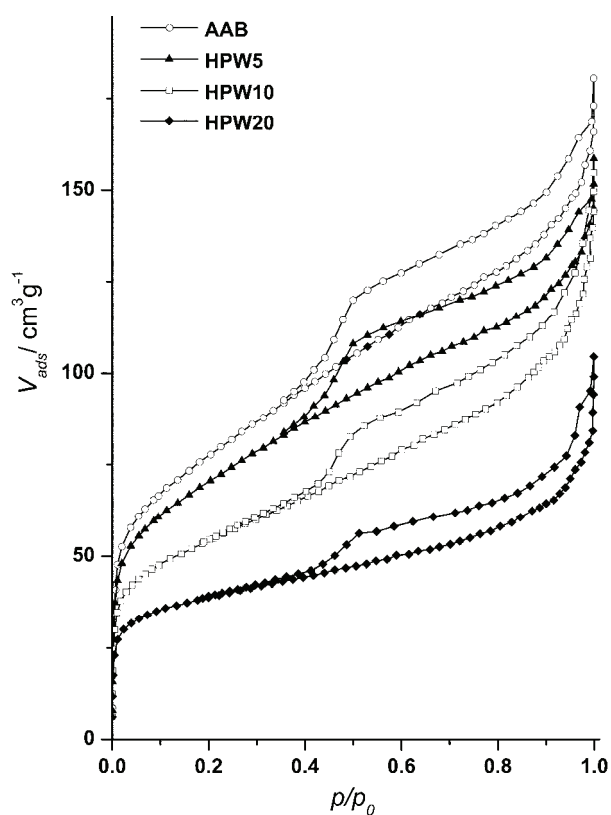


Fig. 1. Adsorption–desorption isotherm of the acid-activated bentonite (AAB) and bentonite modified with different amounts of HPW (HPW5, HPW10 and HPW20).

All isotherms exhibited a hysteresis loop of the H3 type, characteristic for slit-shaped pores. The general shape of the isotherms did not change after impregnation with HPW, showing only a slight decrease in the amount of nitrogen adsorbed.

The dependences of both the fractal dimension obtained from Eq. (1) and the specific surface area on the amount of HPW used to modify the acid-activated bentonite are presented in Table I.

In all cases, there was an excellent linear adjustment for the F–H–H Equation within the range of relative pressures between $0.75 < p/p_0 < 0.96$. The results

showed a slightly decrease in the value of the fractal dimension for the sample with the smallest amount of HPW with respect to the acid-activated bentonite, revealing a decrease in the roughness and the subsequent topographic modification of the surface of the materials as a consequence of the modification process. Addition of HPW to the bentonite reduced the geometric heterogeneity of the sample, probably by closing the existing pores. This was also reflected in a decrease of the specific surface area. These results improve the knowledge to be obtained of the surface characteristic of these solids and, consequently, a better understanding of their catalytic performance. Likewise, it is important to stress how the complexity of the assessed system (acid-activated bentonite modified with HPW) did not interfere with the application and validity of the employed model.

TABLE I. Fractal dimensions of the support and supported samples calculated from the F–H–H equation

Sample	Fractal dimension	R^2	$S_{BET} / m^2 g^{-1}$
AAB	2.907	0.9982	272
HPW5	2.911	0.9986	246
HPW10	2.859	0.9997	188
HPW20	2.858	0.9980	130

On the other hand, the mercury intrusion porosimetry curves of acid-activated bentonite and bentonite modified with HPW are shown in Fig. 2. The raw data from mercury porosimetry experiments on all samples analyzed using the conventional Washburn Equation:¹¹

$$p = \frac{2\gamma_{Hg} \cos \theta}{R} \tag{5}$$

where p is the external pressure (Pa) applied in the vacuum chamber, γ_{Hg} is the surface tension of mercury, θ is the contact angle of mercury and R is the pore radius (nm).

The mercury entered the aggregates of the acid-activated bentonite at the highest pressure, which corresponds to a pore radius of 5 nm. Samples modified with HPW had small particle size that resulted in the smallest pores within aggregates. However, this could also be due to specific orientation of flat bentonite particles. In addition, the small porosity of the acid-activated bentonite (16 %) and samples with HPW loadings of 5, 10 or 20 % (23, 24 and 26 %, respectively) suggested a broad size distribution of the particles or their specific shape and orientation.

The results of the fractal dimension for the bentonite modified with HPW, calculated from mercury intrusion porosimetry, are shown in Fig. 3. In the cases of the HPW modified samples, there was a good linear adjustment for Eq. (4),

but the acid-activated bentonite had very high pore surface fractal dimensions, larger than 3, which is restricted theoretically.

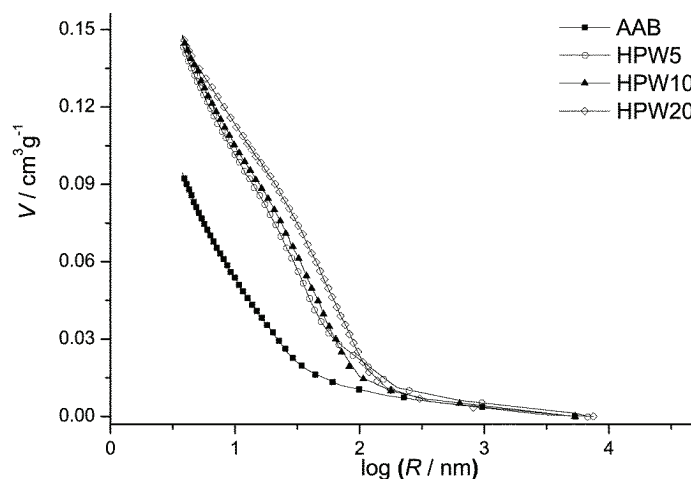


Fig. 2. Mercury intrusion curves for the acid-activated bentonite (AAB) and bentonite modified with different amounts of HPW (HPW5, HPW10 and HPW20).

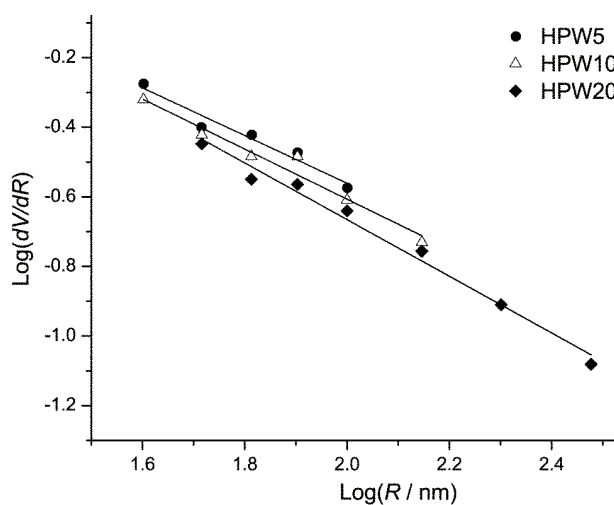


Fig. 3. The dependence of the surface fractal dimension of the modified acid-activated bentonites on the amount of HPW (5, 10 and 20 mass %).

Possibly, pores formed from voids connected by narrower necks started to dominate, due to the removal of the finest particles residing previously in the larger pores. Therefore, a greater pore volume (voids) was attributed to a given pore radius than was formally possible to calculate $D = 3$ in a cylindrical pore model. Thus, dV/dR was also higher, which led to higher D values.

In general, the fractal dimensions of the pore surfaces decreased, indicating a decrease in the complexity of the pore system. The analysis confirmed that fractal dimension calculated from F–H–H method presents the topological complexity of the configuration of the total pores. Similarly, for mercury intrusion porosimetry, the fractal dimension values were different in each pore size range.

CONCLUSIONS

The porous structures of acid-activated bentonite modified with different loadings of HPW were characterized quantitatively by both isothermal N₂ sorption and mercury intrusion porosimetry. The fractal analysis of the nitrogen adsorption isotherms showed a slightly decrease in the value of the fractal dimension for the sample with the smallest amount of HPW with respect to the acid-activated bentonite. Analysis of the mercury intrusion data showed that the small porosity of the acid-activated bentonite (16 %) and the samples with HPW loadings of 5, 10 or 20 % (23, 24 and 26 %, respectively) suggested broad size distributions of the particles or their specific shape and orientation. The results of the two approaches indicate significant differences in porosity, pore size, surface area and pore size distribution.

The analysis of adsorption–desorption and intrusion data always produces several different *D* values, which correlate to the various pores within different size ranges and reflect rough surface morphology and/or complex topology of the pores. By comparison, mercury intrusion porosimetry is preferable for the characterization due to its wide effective probing ranges.

Acknowledgments. This work was supported by the Ministry of Education and Science of the Republic of Serbia (Projects number 172001).

ИЗВОД

ФРАКТАЛНА АНАЛИЗА БЕНТОНИТА МОДИФИКОВАНОГ ХЕТЕРОПОЛИ КИСЕЛИНОМ КОРИШЋЕЊЕМ ПОДАТАКА СОРПЦИОНЕ АНАЛИЗЕ И ЖИВИНЕ ПОРОЗИМЕТРИЈЕ

СРЂАН ПЕТРОВИЋ¹, ЗОРИЦА ВУКОВИЋ¹, ТАТЈАНА НОВАКОВИЋ¹, ЗОРАН НЕДИЋ² и ЉИЉАНА РОЖИЋ¹

¹ИХТМ – Центар за катализу и хемијско инжењерство, Универзитет у Београду, Њевошјева 12, Београд и

²Факултет за физичку хемију, Универзитет у Београду, Студентски тирз 12–16, Београд

Специфична површина и фрактална димензија површине узорака киселински активираниог бентонита модификованог хетерополи киселином (HPW) израчунате су на основу података из адсорпционих изотерми азота. Циљ овог истраживања био је да се нађе корелација између специфичне површине и геометријске хетерогености, као и зависност фракталне димензије површине од садржаја додате хетерополи киселине. Такође, метода живине порозиметрије је коришћена за испитивање порозне микроструктуре синтетисаних узорака. Резултати Frankel–Halsey–Hill методе, примењене у области релативног притиска од 0,75 до 0,96, показују да фрактална димензија површине расте са порастом садржаја хетерополи киселине. Резултати живине порозиметрије су показали да је дошло до значајних топографских промена (пораст храпавости) и развоја мезопорозне структуре узорака, као по-

следица модификације хетерополи киселином. Поређење је показало да је метода живине порозиметрије применљива у ширем опсегу пречника пора.

(Примљено 27. октобра 2010, ревидирано 9. маја 2011)

REFERENCES

1. I. V. Kozhevnikov, *J. Mol. Catal. A* **117** (1997) 151
2. H. Kim, P. Kim, K.-Y. Lee, S. H. Yeom, J. Yi, I. K. Song, *Catal. Today* **111** (2006) 361
3. E. Rafiee, H. Mahdavi, S. Eavani, M. Joshaghani, F. Shiri, *Appl. Catal., A* **352** (2009) 202
4. A. C. Garade, V. S. Kshirsagar, R. B. Mane, A. A. Ghalwadkar, U. D. Joshi, C. V. Rode, *Appl Clay Sci.* **48** (2010) 164
5. G. Yadav, *Catal. Surv. Asia* **9** (2005) 117
6. I. V. Kozhevnikov, *J. Mol. Catal., A* **262** (2007) 86
7. A. B. Jarzebski, J. Lorenc, L. Pajak, *Langmuir* **13** (1997) 1280
8. A. L. Ahmad, N. N. N. Mustafa, *J. Colloid Interface Sci.* **301** (2006) 575
9. D. Avnir, M. Jaroniec, *Langmuir* **5** (1989) 1431
10. M. J. Watt-Smith, K. J. Edler, S. P. Rigby, *Langmuir* **21** (2005) 2281
11. G. Jozefaciuk, C. Slawinski, E. Vrzhashch, *Appl. Clay Sci.* **43** (2009) 63
12. Lj. Rožić, T. Novaković, S. Petrović, *Appl. Clay Sci.* **48** (2010) 154
13. V. V. Bokade, G. D. Yadav, *J. Nat. Gas Chem.* **16** (2007) 186
14. S. H. Gregg, K. S. Sing *Adsorption, Surface Area and Porosity*, Academic Press, New York, 1967
15. P. Pfeifer, M. Olbert, M. W. Cole, *Philos. Trans. R. Soc. London, Ser. A* **423** (1989) 169
16. S. Brunauer, L. S. Deming, E. Teller, *J. Am. Chem. Soc.* **62** (1940) 1723
17. M. Kruk, M. Jaroniec, A. Sayari, *Adsorption* **6** (2000) 47
18. A. V. Neimark, P. I. Ravikovitch, in: *Characterization of Porous Solids V*, K. K. Unger, G. Kreysa, J. P. Baselt, Eds., Elsevier, Amsterdam, 2000, p. 51
19. F. Rouquerol, J. Rouquerol, K. S. W. Sing, *Adsorption by Powders and Porous Solids*, Academic Press, London, 1999.



J. Serb. Chem. Soc. 76 (10) 1411–1425 (2011)
JSCS–4216

A new type of bentonite-based non-woven composite

ALEKSANDRA MILUTINOVIĆ-NIKOLIĆ^{1*#}, JASMINA DOSTANIĆ¹, PREDRAG BANKOVIĆ¹, NATAŠA JOVIĆ-JOVIČIĆ¹, SLAVENKA LUKIĆ², BRANKO ROSIĆ³ and DUŠAN JOVANOVIĆ¹

¹University of Belgrade, Institute of Chemistry, Technology and Metallurgy, Department of Catalysis and Chemical Engineering, Njegoševa 12, Belgrade, ²University of Belgrade, Faculty of Technology and Metallurgy, Karnegijeva 4, Belgrade and ³The Highway Institute, Kumodraška 257, Belgrade, Serbia

(Received 27 July, revised 2 November 2010)

Abstract: Sandwich-like composites based on clays and textiles are extensively applied in various fields, including civil engineering and environmental protection. In this paper, the synthesis of a new type of composite with embedded bentonite particles within a non-woven polyester matrix is presented. The synthesized composite has improved mechanical properties compared to the corresponding non-woven matrix. Although more than two-times thinner, the synthesized composite showed mechanical properties similar to those of a commercial composite chosen for comparison. Sorption test results confirmed that the contribution of the textile component to the sorption of aqueous Cu(II) ions by the composite was negligible. The sorption of aqueous Cu(II) ions on the synthesized composite was best-fitted using the Langmuir model. The presented study confirmed that the loss of bentonite particles from the composite can be eliminated using the suggested synthesis method.

Keywords: composite; bentonite; non-woven; mechanical properties; sorption.

INTRODUCTION

Bentonites are clays rich in smectite but also containing various associated minerals, such as carbonates, feldspars, quartz, *etc.*^{1–3} Due to their high smectite content, bentonites are good sorbents. Numerous investigations were focused on bentonite as a sorbent of inorganic pollutants, particularly of toxic aqueous metal ions.^{4–7} When bentonite is utilized as sorbent, a problem exists of its separation after use. The fineness of the particles and their tendency to swell impede the separation process. This increases the cost of the employment of bentonite as a

* Corresponding author. E-mail: snikolic@nanosys.ihtm.bg.ac.rs

Serbian Chemical Society member.

doi: 10.2298/JSC100702123M

sorbent. One of the possible ways to overcome this is the use of bentonite powder firmly fixed to an inert support.

On the other hand, composites based on clays and textiles are materials that lately have been extensively applied in civil engineering and environmental protection.^{8,9} Commercial composites are most commonly applied as geosynthetic clay barriers. They are produced in a variety of forms. They consist of a clay layer (typically bentonite) bonded to a layer or layers of a geosynthetic material. The geosynthetic materials are either geotextiles or geomembranes. Geotextile-based composites have a sandwich-like structure. They are bonded with an adhesive, needle-punching, stitch-bonding or a combination of these methods. In geomembrane-supported composites, the bentonite is bonded to the geomembrane using an adhesive.^{8,9} The main forms of commercial composites are schematically presented in Fig. 1.

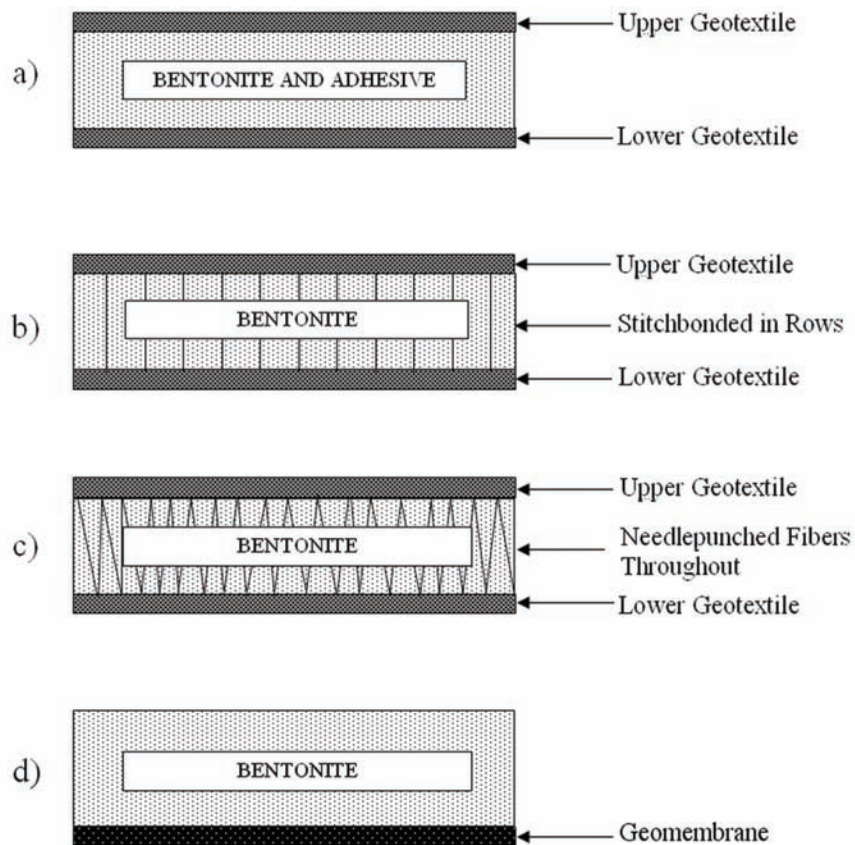


Fig. 1. Forms of bentonite-textile composites: a) adhesive-bonded sandwich structure; b) stitch-bonded sandwich structure; c) needle-punched sandwich structure; d) bentonite adhered to geomembrane (two-layered structure).

Geotextile composites primary differ in the form of the bentonite, type of fiber, type of textile and the bonding methods used to bind the composite. In composite synthesis either the sodium or calcium type of bentonite can be used in powdered or granular form. The type of polymer fiber and their fineness may differ in the composites. Both woven and non-woven textiles are used as geotextiles. Often, the lower geotextile layer is woven, while the upper one is non-woven.^{8,9} Although the overall configuration of the composite affects its performance, the primary factors are clay quality, the amount of clay used per unit area and its uniformity.

One of the drawbacks of composites with a sandwich-like structure is the insufficiently firm fixation of the bentonite layer to the textile. For example, when rolls of these materials are employed, powder is easily displaced, both laterally within the product and through the geotextile. Although bentonite is non-toxic and can even be used as a pharmaceutical,¹⁰ bentonite powder is considered to be a respiratory hazard due to the inhalable crystalline quartz and fine smectite particles.¹¹ Finally, the migration of the powder within the composites with a sandwich-like structure causes localized inconsistencies in the mass per unit area of the product, which in turn creates variability in its hydraulic performance.^{12,13}

In this paper, a new type of composite is presented, synthesized with bentonite particles embedded within a non-woven polyester matrix by applying bentonite in the form of a suspension. The goal was to obtain a composite with a more consolidated structure and avoid losses of the bentonite powder from the composite.

The sorptive properties of textile-bentonite composites have received less attention in the literature¹⁴⁻¹⁶ in comparison to bentonite alone.^{1,4-7,17-20} In the presented investigations more attention was focused on the sorptive properties of the synthesized composite. Removal of aqueous Cu(II) ions was chosen as a model system. Toxic metals, such as lead, copper, cadmium, zinc and nickel, are among the most common pollutants found in industrial effluents.²¹ Of the 71 priority pollutants analyzed, copper, was most frequently detected, along with lead and zinc.²² The increased content of copper in the liver, brain, and other tissues leads to hepatitis, kidney dysfunction, brain disorders, and other problems.^{22,23} According to the Environmental Protection Agency (EPA), the maximum allowed amount for copper in discharged water is 1.3 mg dm^{-3} .²²

The objective of the investigations presented herein was to synthesize a composite with bentonite particles fixed within a non-woven textile structure to prevent bentonite losses. Further investigations presented in this paper were performed in order to prove that the synthesis conditions do not impair the sorptive properties of bentonite and the mechanical properties of non-wovens.

EXPERIMENTAL

The composite was synthesized using bentonite and commercial materials. Needle-punched polyester non-woven fabric (M-PROINTEX, Mladenovac, Serbia) with a nominal mass per unit area $m_A = 300 \text{ g m}^{-2}$ and a thickness of $\delta = 3 \text{ mm}$ was used as the non-woven matrix. A carboxymethyl cellulose-based adhesive (Aero Balkan, Belgrade, Serbia) solution was applied to fix the bentonite particles to the non-woven (NW) material. The mineral constituent was bentonite powder ($< 74 \mu\text{m}$) from the coal and bentonite mine "Bogovina", Serbia. The chemical, physical, morphological and textural properties of bentonite powder were presented previously.^{24,25} The chemical composition of bentonite dried at $110 \text{ }^\circ\text{C}$ (given in mass %) was: SiO_2 , 57.51; Al_2O_3 , 17.13; Fe_2O_3 , 7.67; MgO , 2.35; CaO , 1.81; Na_2O , 0.75; K_2O , 1.18. XRD analysis confirmed smectite as the dominant phase with quartz as the major associated mineral. Small amounts of illite, calcite, feldspar and amorphous material were also detected. The specific surface area of the bentonite powder was calculated according to the Brunauer, Emmett, Teller method from nitrogen adsorption-desorption isotherms and the obtained value was $96 \text{ m}^2 \text{ g}^{-1}$.

The following synthesis procedure was used. First the adhesive was dissolved in distilled water at $35 \text{ }^\circ\text{C}$ and stirred until a homogeneous solution was obtained. Bentonite powder was then dispersed in the aqueous solution of the adhesive. The dispersion was stirred to form a homogeneous suspension.

The viscosity of the bentonite suspension in an adhesive solution was significantly greater than the viscosity of either the adhesive solution or a dispersion of bentonite in pure water. The suspension viscosity of the dispersion affects the ability of the suspension to penetrate the NW material. If the suspension viscosity is higher than optimal, the suspension is unable to pass through the entire NW fabric and a layer of bentonite is formed on the top of it. On the other hand, if the suspension viscosity is lower than optimal, the suspension passes through the NW fabric and the bentonite does not remain within the NW material. A suspension containing 50 g dm^{-3} bentonite dispersed in a solution of adhesive having a concentration of 6.7 g dm^{-3} was found to have the optimal viscosity. The viscosity of this suspension was measured using a Brookfield Eng. Lab. Inc, USA viscometer.

The synthesis of the composite was performed by applying the suspension with the optimal viscosity onto the NW surface. Water from the wet composite was removed by drying to constant mass in an oven at $60 \text{ }^\circ\text{C}$. In the next step, the bentonite suspension was applied once more, but this time on the opposite side of the textile. Drying of composite at $60 \text{ }^\circ\text{C}$ was performed again until a constant mass was reached.

In order to characterize the obtained composite, the standard methods for geosynthetic investigation were used. The British Standard EN 14196 was used for the determination of the mass per unit area²⁶ and the International standard ISO 9863-1 for the measurement of the composite thickness.²⁷

Load per unit length and elongation were determined using a Wykeham Farrance mechanical testing machine (BR-IPGM-KID-03) according to the ISO 10319 test method.²⁸ The experiments were performed on the original NW fabric and the corresponding composite. The materials were examined both in the machine direction (md) and the cross machine direction (cmd).

Scanning electron microscopy (SEM) photos of the synthesized and commercial composite were obtained using an SEM JEOL JSM-6610LV.

There is no standard method to estimate the loss of bentonite powder from a composite. In this study, two different tests, a more and a less severe one, were adopted. Their purpose

was to show firmer incorporation of the bentonite particles within the synthesized composite structure in comparison to a commercial composite with a sandwich-like structure Bentofix BFG 5000.²⁹

The first type of test was performed with a rotating tube attrition tester – the Spence method.³⁰ Samples were loaded into cylindrical tubes placed on a disc-shaped frame. The frame was rotated at a speed of 25 rpm for two hours. For the second test, the samples were placed in an ultrasonic bath (Selecta Ultrasound-H), operating at a frequency of 40 kHz for 30 min. The mass of the samples was measured before and after each test by both methods. The results are presented as mass loss in percents (χ). For each method, 10 samples of the commercial and of the synthesized composite were used. The average values and standard deviation were calculated.

In order to determine the contribution of each constituent of composite to the sorption of aqueous Cu(II) ions, batch experiments were performed separately on: a) NW fabric impregnated with adhesive – the control textile sample; b) bentonite powder and c) the studied composite. The masses of the samples were: 0.25 g for bentonite powder and the control textile, while the composite mass was 0.5 g, containing approx. 0.25 g of NW fabric and 0.25 g of bentonite. The sorption test was performed with 50 cm³ of aqueous solution of Cu(II) nitrate with the initial Cu(II) concentration, c_0 , of 5×10^{-3} mol dm⁻³.

When the contribution of each constituent of the composite to the sorptive properties of the composite had been determined, an isothermal study on the synthesized composite only was performed. All experimental conditions were the same as in the previous test except the initial concentration of aqueous Cu(II) ions was varied within the range 2.5×10^{-3} – 10.0×10^{-3} mol dm⁻³.

In all sorption experiments, the samples were shaken at 20 ± 2 °C in a temperature-controlled water bath shaker (Mettmert WNE 14 and SV 1422). Measurements were performed after predetermined periods (0.25, 0.5, 1, 2, 4, 12 and 24 h). When bentonite was used as the sorbent, the bentonite suspensions were centrifuged at 5000 rpm for 15 min (Hettich EBA-21 to separate the sorbent from the dispersion).

The concentrations of Cu(II) ions before and after the sorption test were analyzed using a Thermo Electron Nicolet Evolution 500 UV–Vis spectrophotometer. The absorption peak at 806 nm, corresponding to Cu(II), was chosen for the estimation of the Cu(II) concentration, since a linear dependence of absorbance on Cu(II) concentration was found to have a correlation coefficient (R) of 0.999.

The Cu(II) uptake (p) given in percents was calculated as follows:

$$p = 100 \frac{c_0 - c_t}{c_0} \quad (1)$$

where c_0 is the initial Cu(II) concentration (mg dm⁻³) and c_t is the Cu(II) concentration in solution after time t .

The amount of the aqueous Cu(II) ions sorbed by the sorbent (composite) at the equilibrium q_e (mg g⁻¹) was calculated by the following mass-balance relationship:

$$q_e = \frac{V(c_0 - c_e)}{W} \quad (2)$$

where c_e is the equilibrium Cu(II) concentration, V is the volume of the solution (dm³) and W is the mass of the sorbent (g).

RESULTS AND DISCUSSION

A mass per unit area of the synthesized composite of $m_A = 590 \pm 20 \text{ g m}^{-2}$ and a thickness of $\delta = 2.89 \pm 0.18 \text{ mm}$ were established according to standard methods.^{26,27} The bentonite content in the composite was determined to be 51 ± 2 mass %.

The viscosity of the suspension with the optimal composition was measured using a Brookfield viscometer. The dependence of the viscosity on the shear rate is given in Fig. 2.

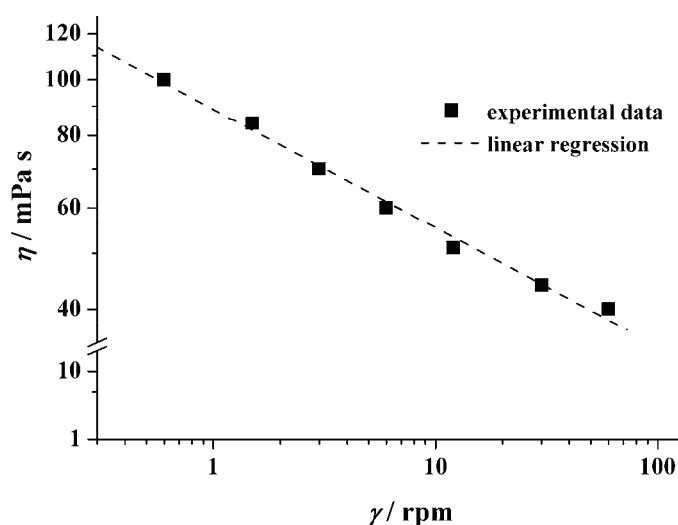


Fig. 2. Dependence of the viscosity of a bentonite/adhesive suspension on shear rate.

The obtained linear regression can be represented by the following equation:

$$\log \eta = 1.948 - 0.205 \gamma \quad (3)$$

where: η – viscosity, $\gamma = dv/dx$ – shear rate, with $R = 0.9959$.

As expected, the viscosity of the bentonite/adhesive suspension obeyed a “power law” and exhibited a behavior characteristic for pseudoplastic fluids.³¹

Since the synthesis of the new type of composite presented in this paper can be performed using bentonites and adhesives of different origin, it is useful to have a synthesis condition figure of merit independent of the origin of the applied raw materials. The use of suspension with a viscosity given in Eq. (3) enables the given synthesis process to be extended to a variety of raw materials.

The SEM microphotographs of the synthesized composite and the commercial Bentofix BFG 5000 with a sandwich-like structure²⁹ are presented in Fig. 3. Bentonite particles firmly embedded within the NW structure of the synthesized composite are clearly visible in Figs. 3a–3b. The particles completely surround the textile fibers and remain connected even in the cases of severe bending and

cutting of the composite during the sample preparation for electron microscopy. On the other hand, the integrity of structure was destroyed during an identical preparation of a commercial sample for SEM. In Fig. 3c only textile fibers relatively loosely in contact with the surrounding bentonite powder are visible.

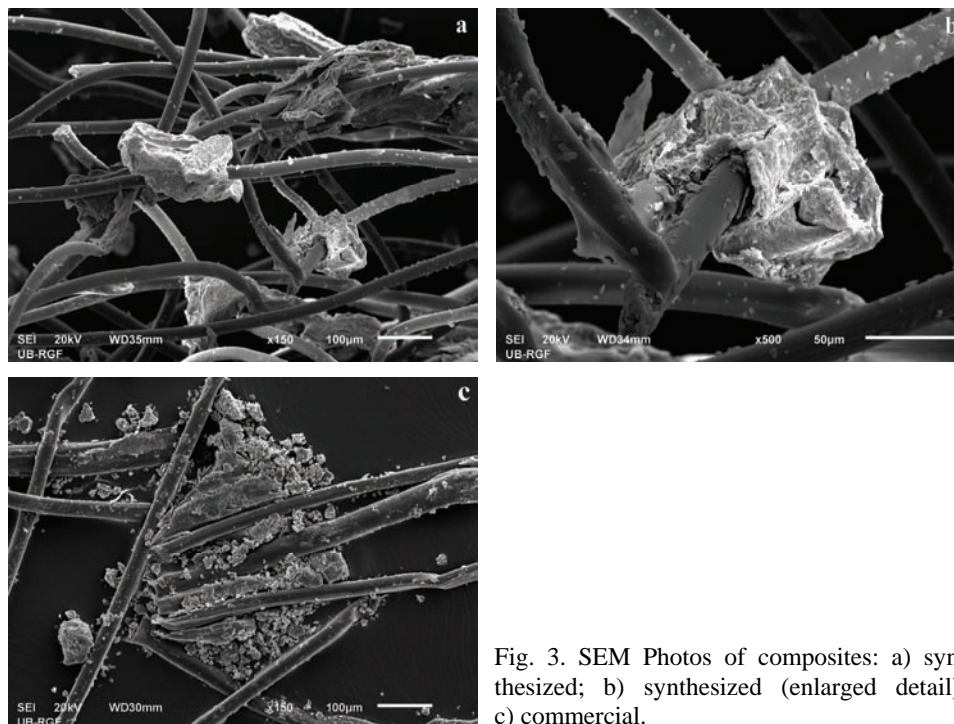


Fig. 3. SEM Photos of composites: a) synthesized; b) synthesized (enlarged detail); c) commercial.

The recorded load per unit length (σ) vs. relative elongation (ε) curves are presented in Fig. 4 for both the NW fabric and the synthesized composite. The obtained mechanical properties are given in Table I.

From the results presented in Fig. 4 and Table I, it can be concluded that the load per unit length at break (σ_{\max}) was higher, while the relative elongation at break (ε_b) was lower in the machine direction than in the cross machine direction for both the NW fabric and the corresponding composite. The composite formation improved the load per unit length and lowered the elongation of the starting non-woven fabric in both directions by approx. 20 %. In addition, it was also necessary to apply 8, 16 and 28 times greater force to the composite than to the corresponding NW in order to achieve elongations of 10, 5 and 2 %, respectively. These data show to what extent the mechanical properties of the composite are improved compared to the corresponding non-woven fabric, especially at lower loadings.

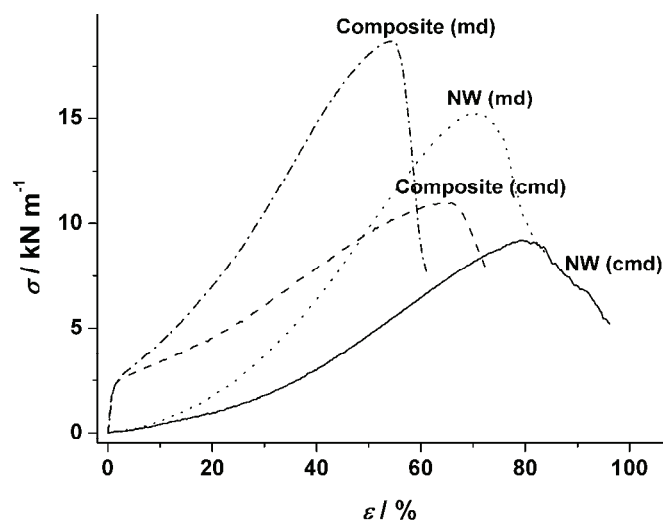


Fig. 4. Load per unit length vs. relative elongation for the NW fabric and the synthesized composite.

TABLE I. Load per unit length and elongation of the composite and the non-woven fabric (σ_{\max} – load per unit length at break, ϵ_x – relative elongation at break, md – machine direction, cmd – cross machine direction)

Sample	$\sigma_{\max} / \text{kN m}^{-1}$	$\epsilon_x / \%$	$\sigma / \text{kN m}^{-1}$ at $\epsilon = 2 \%$	$\sigma / \text{kN m}^{-1}$ at $\epsilon = 5 \%$	$\sigma / \text{kN m}^{-1}$ at $\epsilon = 10 \%$
NW(md)	15	71	0.089	0.222	0.566
Composite (md)	19	55	2.510	3.201	4.309
NW(cmd)	9	79	0.086	0.163	0.412
Composite (cmd)	11	66	2.440	2.830	3.367

Photographs of fractures of the composites after the mechanical tests are presented in Fig. 5 for comparison.

It can be observed that upon rupture, the bentonite phase remains firmly fixed within the synthesized composite, while there is a significant release of the clay from the commercial one.

The results for the mass loss obtained using both the rotating tube attrition tester and ultrasound test are given in Table II for the synthesized composite and for one of the most common commercial composites with a sandwich structure, Bentofix BFG 5000.²⁹ In addition to the data for bentonite loss, Table II contains some physical and mechanical properties of the synthesized and commercial composites.

The loads per unit length required for the rupture of both composites were very similar. The test samples were of equal length and width but the commercial composite was more than two-times thicker than the synthesized one. This implies better mechanical properties of the synthesized material.

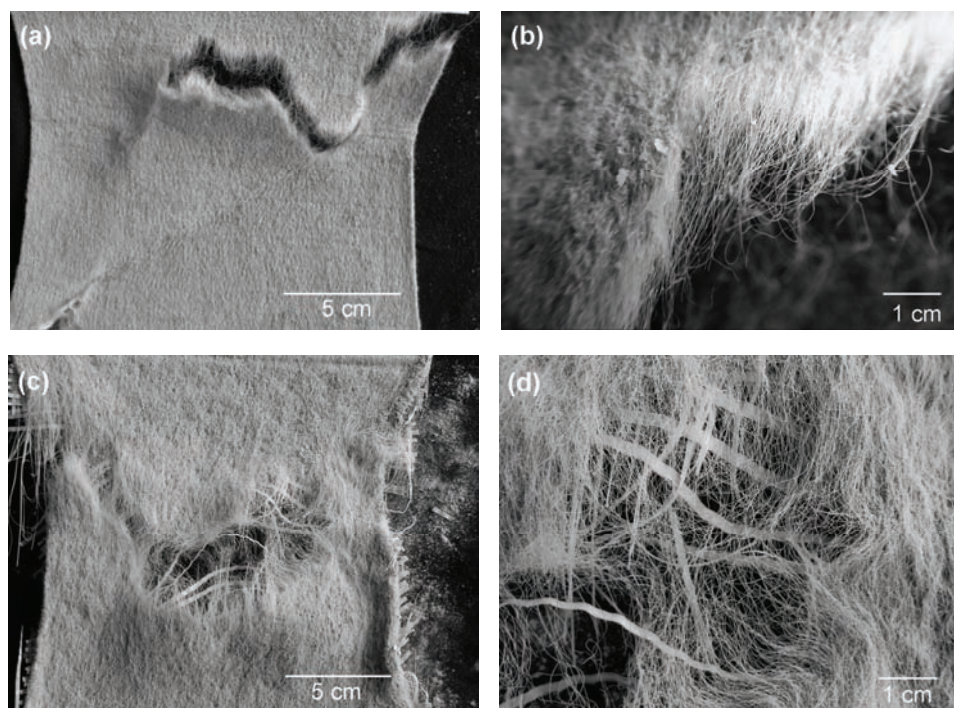


Fig. 5. Photographs of samples after mechanical tests: a) synthesized, b) synthesized (enlarged detail), c) commercial and d) commercial (enlarged detail).

TABLE II. Comparison of the properties of the synthesized and the commercial composite (δ – thickness, m_A – nominal mass per unit area, σ_{\max} – load per unit length at break, ε_x – relative elongation at break, md – machine direction, cmd – cross machine direction, χ – mass loss)

Sample	δ / mm	m_A / g m ⁻²	σ_{\max} / kN m ⁻¹		ε_x / %		Rotating test tube		Ultrasound bath test	
			md	cmd	md	cmd	χ / %	Std.	χ / %	Std.
Commercial	7	5500	20	11	10	5	70	3	4.34	1.1
Synthesized	3	600	19	11	55	66	5	2	0.73	0.1

Table II shows that the mass loss after the performed rotating test tube experiment was 14 times greater for the commercial than for the synthesized composite. In the ultrasonic test, the mass loss was less expressed; however, it was still 6 times greater for the commercial composite than for the synthesized one. Therefore, the most important advantage of the synthesized composite is its compact structure that simultaneously enables a firm fixation of bentonite within the composite matrix.

The sorption data for the relative uptake of aqueous Cu(II) ions on the bentonite, non-woven fabric impregnated with adhesive (control textile sample) and the composite vs. contact time are presented in Fig. 6.

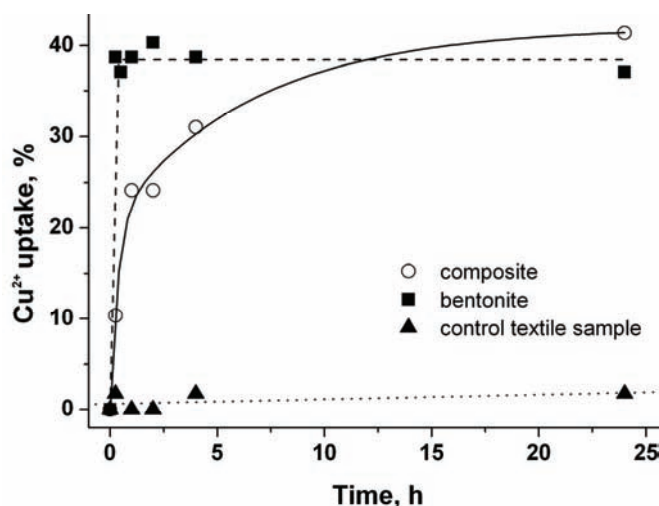


Fig. 6. Kinetics of Cu(II) uptake by the investigated samples; $c_0 = 5.0 \times 10^{-3} \text{ mol dm}^{-3}$.

The data presented in Fig. 6 show that the sorption of aqueous Cu(II) ions by the NW fabric was negligible in comparison to that of bentonite and the composite and that the entire sorption capacity of the composite can be attributed to bentonite. The uptake of aqueous Cu(II) ions by bentonite was faster than by the composite, since in the latter, the bentonite particles were incorporated in the NW fabric and it was more difficult for the aqueous Cu(II) ions to reach the bentonite. For longer sorption times, the composite reached the sorption capacity of pure bentonite. The presence of adhesive did not impair the sorptive properties of bentonite in the composite, *i.e.*, the bentonite did not lose its sorptive properties during composite synthesis.

The sorption data for the uptake of aqueous Cu(II) ions by the composite *vs.* contact time at different initial concentrations are presented in Fig. 7. The pH of the solution after sorption was 6, which is a pH value where no precipitation of Cu(II) occurs and therefore the decrease of the Cu(II) concentration can be ascribed solely to the sorption process.

The percentile uptake of aqueous Cu(II) ions by the composite decreased with increasing initial Cu(II) concentration, but the amount of sorbed ions increased. More useful data can be obtained by analyzing the equilibrium conditions. The equilibrium contact time was estimated to be 12 h, since further sorption was negligible after this time. The equilibrium data, commonly known as sorption isotherms, are the basic requirement for the design of sorption systems. These data provide information on the capacity of the sorbent or the amount required for the removal of a unit mass of sorbate under the system conditions.

The sorption isotherms obtained for different initial Cu(II) concentrations were applied to fit the models of Freundlich³² and Langmuir.³³

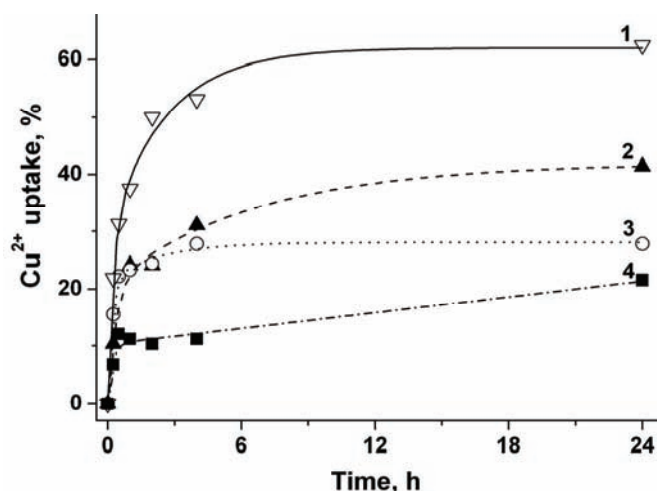


Fig. 7. Influence of contact time and initial Cu(II) concentration (c_0) on the uptake of Cu(II) by the composite (1 – $c_0 = 2.5 \times 10^{-3} \text{ mol dm}^{-3}$; 2 – $c_0 = 5.0 \times 10^{-3} \text{ mol dm}^{-3}$; 3 – $c_0 = 7.5 \times 10^{-3} \text{ mol dm}^{-3}$; 4 – $c_0 = 10.0 \times 10^{-3} \text{ mol dm}^{-3}$).

The linear form of the Freundlich isotherm is represented by Eq. (4):

$$\ln q_e = \ln K_F + \frac{1}{n} \ln c_e \quad (4)$$

where K_F ($\text{dm}^3 \text{ g}^{-1}$) and n are the Freundlich adsorption constants characteristic for the system; they describe the adsorption capacity and adsorption intensity, respectively.

A plot of $\ln q_e$ vs. $\ln c_e$ gives a straight line with the slope and intercept equal to $1/n$ and $\ln K_F$, respectively (Fig. 8).

The Langmuir Equation can be expressed as follows:

$$\frac{c_e}{q_e} = \frac{1}{q_{\max} K_L} + \frac{c_e}{q_{\max}} \quad (5)$$

where q_{\max} is the maximum adsorption capacity of the sorbent (mg g^{-1}) and K_L is the adsorption constant ($\text{dm}^3 \text{ g}^{-1}$).

A plot of the specific adsorption (c_e/q_e) vs. the equilibrium concentration (c_e) gives a straight line with slope $1/q_{\max}$ and intercept $1/(q_{\max} K_L)$ (Fig. 9). The constants and correlation coefficients corresponding to both models are given in Table III.

According to the results presented in Table III, both models can be applied to the experimental data, but the correlation coefficient for the Langmuir model was closer to unity, hence this model was more appropriate. The validity of Langmuir model indicated the formation of a monolayer coverage of aqueous Cu(II) ions at the composite surface containing a finite number of homogenous

sorption sites. It also suggests that all adsorption sites were equivalent and there was no interaction between the adsorbed molecules.³⁴

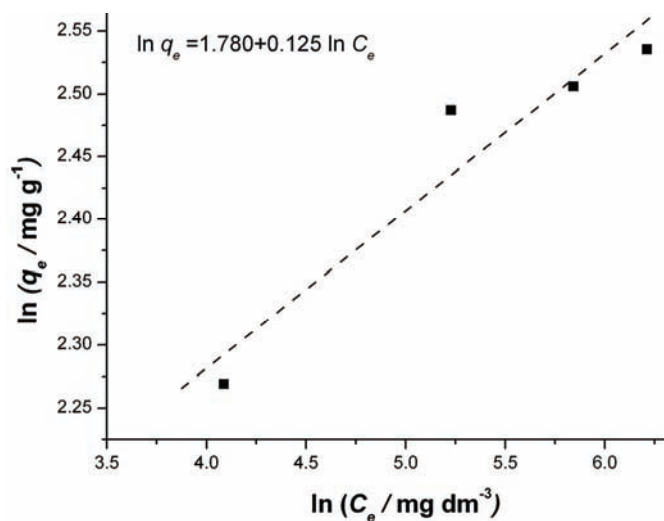


Fig. 8. Freundlich isotherm for Cu(II) sorption onto the composite.

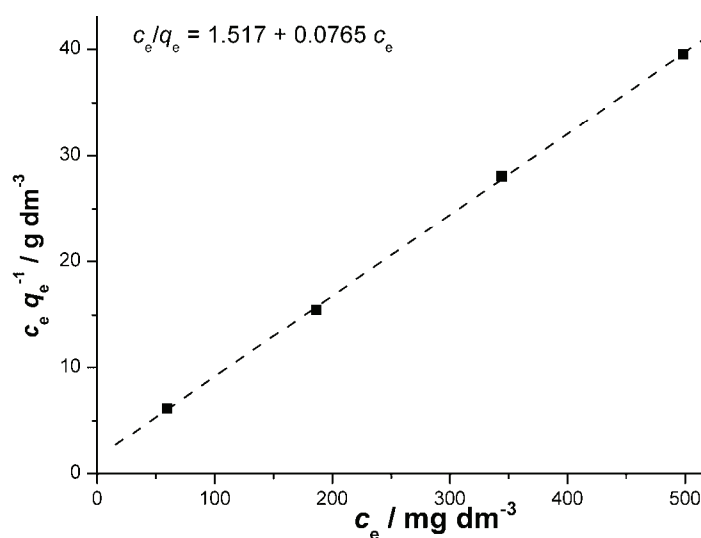


Fig. 9. Langmuir isotherm for Cu(II) sorption onto the composite.

TABLE III. Calculated sorption model constants and correlation coefficients

Freundlich constants			Langmuir constants		
$K_F / \text{dm}^3 \text{g}^{-1}$	n	R	$q_{\text{max}} / \text{mg g}^{-1}$	$K_L / \text{dm}^3 \text{g}^{-1}$	R
5.932	7.982	0.9560	13.09	50.36	0.9999

CONCLUSIONS

A new type of composite with bentonite particles embedded in non-woven textile was synthesized by applying bentonite in the form of suspension onto a non-woven fabric. The optimal viscosity of the bentonite suspension in the adhesive solution that enables appropriate composite formation was established. The composite formation improved the load per unit length and lowered the elongation of the starting non-woven fabric in both the machine and cross-machine direction. Although more than two-times thinner, the synthesized composite showed mechanical resistance similar to that of the commercial composite chosen for comparison.

It was proven that the problem of loss of bentonite particles from the composite structure was greatly reduced with the obtained composite. Both the rotating tube method and the ultrasonic test resulted in much lower mass loss values for the synthesized composite in comparison to the commercial composite.

The sorptive study showed that the contribution of non-woven component to the sorption of aqueous Cu(II) ions by the composite was negligible. The entire sorption capacity of the composite could be attributed to the bentonite. The bentonite did not lose its sorptive properties during the synthesis process. The isothermal data for Cu(II) sorption onto the composite were best fitted using the Langmuir model.

The obtained composite exhibited a compact structure with firm fixation of the bentonite within the composite matrix, as well as good mechanical and sorption properties. It may be regarded as a promising material for various applications in civil engineering and environmental protection, for example as geosynthetic clay barriers and in wastewater purification.

Acknowledgement. This work was supported by the Ministry of Education and Science of the Republic of Serbia (Project III 45001).

ИЗВОД

НОВИ ТИП КОМПОЗИТА НА БАЗИ БЕНТОНИТА И
НЕТКАНОГ ТЕКСТИЛНОГ МАТЕРИЈАЛА

АЛЕКСАНДРА МИЛУТИНОВИЋ-НИКОЛИЋ¹, ЈАСМИНА ДОСТАНИЋ¹, ПРЕДРАГ БАНКОВИЋ¹, НАТАША
ЛОВИЋ-ЛОВИЧИЋ¹, СЛАВЕНКА ЛУКИЋ², БРАНКО РОСИЋ³ и ДУШАН М. ЈОВАНОВИЋ¹

¹Универзитет у Београду, Институт за хемију, технологију и металургију, Центар за катализу и хемијско инжењерство, Њеѓошева 12, Београд, ²Универзитет у Београду, Технолошко-металуршки факултет, Карнегијева 4, Београд и ³Институт за пшине, Кумодрашка 257, Београд

Композити на бази глина и текстила са „сендвич“ структуром имају примену у различитим областима, укључујући грађевинарство и заштиту животне средине. У овом раду синтетисан је нови тип композита са честицама бентонита уграђеним у неткану полиестарску матрицу. Синтетисани композит има побољшана механичка својства у поређењу са одговарајућом нетканом матрицом. Иако два пута тањи од комерцијалног, са којим је упоређиван, синтетисани композит је показао слична механичка својства. Сорпционим

испитивањима потврђено је да текстилна компонента занемарљиво утиче на способност композита да сорбује Cu(II) јоне. Сорпција Cu(II) јона на синтетисаном композиту најбоље се описује Ленгмировим моделом. У овом раду је потврђено да се коришћењем предложене методе синтезе композита елиминише проблем испадања честица бентонита из композита.

(Примљено 27. јула, ревидирано 2. новембра 2010)

REFERENCES

1. F. Bergaya, B. K. G. Theng, G. Lagaly, *Handbook of Clay Science, Developments in Clay Science*, Vol. 1, Elsevier, Amsterdam, 2006, p. 1
2. B. L. Sawhney, *Organic Pollutants in the Environment*, The Clays Mineral Society, Chantilly, VA, USA, 1996, p. 96
3. I. Dananaja, J. Frankovská, I. Janotka, *Appl. Clay Sci.* **28** (2005) 223
4. H. B. Bradl, *J. Colloid Interface Sci.* **277** (2004) 1
5. K. G. Bhattacharyya, S. S. Gupta, *Chem. Eng. J.* **136** (2008) 1
6. R. Naseem, S. S. Tahir, *Water Res.* **35** (2001) 3982
7. G. Bereket, A. Z. Aroguz, M. Z. Ozel, *J. Colloid Interface Sci.* **187** (1997) 338
8. A. Bouazza, *Geotext. Geomembr.* **20** (2002) 3
9. R. K. Rowe, *Geotechnical and Geoenvironmental Engineering Handbook*, Kluwer, Boston, MA, USA, 2001, p. 1
10. C. D. Shackelford, C. H. Benson, T. Katsumi, T. B. Edil, L. Lin, *Geotext. Geomembr.* **18** (2000) 133
11. M. I. Carrerero, *Appl. Clay Sci.* **21** (2002) 155
12. P. J. Fox, E. J. Triplett, R. H. Kim, J. T. Olsta, *Geosynth. Int.* **5** (1998) 491
13. R. M. Koerner, D. J. Narejo, *Int. J. Geotech. Eng.* **121** (1995) 82
14. K. R. Rowe, T. Mukunoki, H. P. Sangam, *J. Geotech. Geoenviron.* **131** (2005) 1211
15. I. Janotka, Š. Kiš, R. Baslik, *Appl. Clay Sci.* **21** (2002) 21
16. A. Baghel, B. Singh, P. Pandey, R. K. Dhaked, A. K. Gupta, K. Ganeshan, K. Sekhar, *J. Hazard. Mater.* **137** (2006) 396
17. M. H. Al-Qunaibit, W. K. Mekhemer, A. A. Zaghoul, *J. Colloid Interface Sci.* **283** (2005) 316
18. Sh. Zhu, H. Hou, Y. Xue, N. Wei, Q. Sun, X. Chen, *J. Colloid Interface Sci.* **315** (2007) 8
19. Ding Shu-li, Sun Yu-zhuang, Yang Cui-na, Xu Bo-hui, *Min. Sci. Technol.* **19** (2009) 489
20. L. Zhi-rong, Z. Shao-qi, *Process Saf. Environ. Prot.* **88** (2010) 62
21. J. Moore, S. Ramamoorthy, *Heavy Metals in Natural Waters: Applied Monitoring and Impact, Assessment*, Springer, New York, 1983, p. 65
22. U.S. Department of health and human services, Public Health Service Agency for Toxic Substances and Disease Registry, *Toxicological profile for copper*, 2004, <http://www.atsdr.cdc.gov/toxprofiles/tp132-p.pdf> (Dec 15th, 2009.)
23. L. Goldman, D. A. Ausiello, W. Arend, J. O. Armitage, D. Clemmons, J. Drazen, R. Griggs, N. LaRusso, J. Newman, E. Foster, *Cecil Medicine*, 23rd ed., Elsevier Health Sciences, Amsterdam, 2007, p. 1613
24. Z. Vuković, A. Milutinović-Nikolić, Lj. Rožić, A. Rosić, Z. Nedić, D. Jovanović, *Clays Clay Miner.* **54** (2006) 697
25. Z. Vuković, A. Milutinović-Nikolić, J. Krstić, A. Abu-Rabi, T. Novaković, D. Jovanović, *Mater. Sci. Forum* **494** (2005) 339

26. *British Standard EN 14196: Geosynthetics-Test methods for measuring mass per unit area of clay geosynthetic barriers* (2003), International standard ISO 9863-1: *Geosynthetics – Determination of thickness at specified pressures – Part 1: Single layers* (2005), International standard ISO 10319: *Geotextiles - Wide-width tensile test method* (1993).
27. Naue GmbH & Co. KG, *Technical documentation of NAUE GmbH & Co. KG*, Espelkamp-Fiestel, Germany, 2005, <http://www.naue.com/content-e/produkte/bentofix.php> (May 26th, 2010)
28. Vinci Technologies, *Technical documentation of Vinci technologies, laboratory and field instruments for Petroleum industry*, Nanterre, France, 2007, <http://www.vinci-technologies.com/images/contenu/documents/VT%20Aval/RDT%20&%20RTT%202010.pdf> (May 26th, 2010)
29. R. H. Perry, D. W. Gree, *Perry's Chemical Engineer's Handbook*, McGraw-Hill, New York, 1999, pp. 6–4
30. H. M. F. Freundlich, *J. Phys. Chem.* **57A** (1906) 385
31. I. Langmuir, *J. Am. Chem. Soc.* **40** (1918) 1361
32. F. Rouquerol, J. Rouquerol, K. Sing, *Adsorption by powder and porous solids*, Academic Press, San Diego, CA, USA, 1999, p. 97.



J. Serb. Chem. Soc. 76 (10) 1427–1436 (2011)
JSCS–4217

Arsenic removal from aqueous solutions by sorption onto zirconium- and titanium-modified sorbents

IVAN ANDJELKOVIĆ^{1*}, DRAGAN D. MANOJLOVIĆ¹, DRAGANA DJORDJEVIĆ²,
BILJANA DOJČINOVIĆ², GORAN ROGLIĆ¹ and LJUBIŠA IGNJATOVIĆ^{3#}

¹Faculty of Chemistry, University of Belgrade, P.O. Box 158, 11001 Belgrade, ²Center of Chemistry, Institute for Chemistry, Technology and Metallurgy, University of Belgrade, Njegoševa 12, 11000 Belgrade and ³Faculty of Physical Chemistry, University of Belgrade, 11001 Belgrade, Serbia

(Received 7 October, 2010)

Abstract: Arsenic reduction in drinking water can include treatment by adsorption, switching to alternative water sources, or blending with water that has a lower arsenic concentration. Commercial sorbents MTM, Greensand and BIRM (Clack Corporation) were modified with zirconium and titanium after activation. The modifications were performed with titanium tetrachloride and zirconium tetrachloride. The modified sorbents were dried at different temperatures. The sorption of arsenate and arsenite dissolved in drinking water (200 µg L⁻¹) onto the sorbents were tested using a batch procedure. After removal of the sorbent, the concentration of arsenic was determined by hydride generation atomic absorption spectrometry (HG-AAS). Zirconium-modified BIRM showed the best performance for the removal of both arsenite and arsenate. Modification of the greensand did not affect arsenic sorption ability. Zirconium-modified BIRM diminished the concentration of total As to below 5 µg L⁻¹.

Keywords: arsenic; sorption; modified sorbent; drinking water.

INTRODUCTION

Arsenic contamination of drinking water resources is a major environmental problem in many countries of the world. As a naturally occurring toxic substance in the Earth's crust, arsenic enters into aquifers and wells through natural processes, and into the water cycle as a result of anthropogenic activities.¹ Arsenic pollution has been reported in the USA, Mexico, Bangladesh, China and Japan.^{2–6} In Serbia, high concentrations of arsenic were found in some regions of the Province Vojvodina.⁷ In January 2001, the United States Environmental Protection

*Corresponding author. E-mail: ivanhem@chem.bg.ac.rs

#Serbian Chemical Society member.

doi: 10.2298/JSC101014125A

Agency (EPA) published a new standard for arsenic in drinking water, requiring public water supplies to reduce arsenic from 50 to 10 ppb by 2006.⁸ Although many different methods, such as precipitation,⁹ ion-exchange¹⁰ and reverse osmosis,^{11,12} have been used for arsenic removal, adsorption from solution has received more attention due to its high concentration efficiency.^{13,14} In this paper, arsenic adsorption onto modified commercial sorbents, BIRM, GS and MTM, is presented. These commercially available sorbents were successfully used for removal iron and manganese compounds from raw water supplies.^{2,15} Previously published results showed the efficiency of zirconium and titanium dioxide in arsenic removal.^{16–22}

The aim of the present study was to examine influence of the modification of commercial sorbents with titanium and zirconium on their sorption characteristics. The influence of the initial pH on the sorption characteristic of the modified sorbents was also investigated.

EXPERIMENTAL

Instrumentation and apparatus

An optical emission spectrometer with inductively coupled plasma iCAP-6500 Duo (Thermo scientific, United Kingdom) was used for the measurements. The system was equipped with an integrated unit for hydride generation. The detector was a RACID86 charge injector device (CID). A SpectrAA 55-Varian (CA, USA) was also used.

Microwave digestion was performed in a pressurized microwave oven (Ethos 1, Advanced Microwave Digestion System, Milestone, Italy) equipped with a rotor holding 10 cuvettes (PTFE).

Sorbent materials

BIRM (Burgess Iron Removal Media) can be used as a replacement media for manganese greensand in an iron and manganese removal filter. This media is manganese dioxide-coated alumina silicate, with the following physical properties: effective size: 0.61 mm and uniformity coefficient: 1.72. When used as an iron removal media, BIRM acts as a catalyst to enhance the reaction between dissolved oxygen (DO) and the iron compounds found in many groundwater supplies.

Manganese greensand (GS) is a zeolite mineral called glauconite processed with manganese sulfide or manganese sulfate and potassium permanganate in alternating steps to produce a black precipitate of manganese dioxide on the granules (effective size: 0.33 mm and uniformity coefficient: <1.60)

MTM is a granular manganese dioxide filtering media used for reducing iron, manganese and hydrogen sulfide from water. Its active surface coating oxidizes and precipitates soluble iron and manganese. MTM consist of a light weight granular core with a coating of manganese dioxide. MTM is an example of contact oxidation where the media itself provides the oxidizing potential (effective size: 0.43 mm and uniformity coefficient: 2.0)

Modification of the sorbents. For the activation of sorbents, 200 g of sorbent was mixed with 800 mL distilled water and 12 mL concentrated HCl in a 1 L glass beaker for 2 h. The sorbent was then filtered and washed with distilled water until a negative reaction for Cl ions was attained. Finally, the sorbent was dried at 105 °C for 2 h.

For the modification of the sorbents with zirconium, $ZrCl_4$ was used. 10.79 g of $ZrCl_4$ was placed in 1 L flask with 800 mL water and 200 g of activated sorbent. The solution was mixed for 24 h. After mixing, the sorbent was filtered and washed with distilled water until a negative reaction for Cl ions was obtained. The sorbents was dried at 105 °C for 2 h and then at 200 °C for 4 h.

For the modification of sorbents with titanium, $TiCl_4$ was used. Into a 250 mL glass containing 100 mL distilled water with ice was added 17.21 g $TiCl_4$ under vigorous stirring. After all the ice had melted, the solution was transferred into a 1 L flask containing 800 mL water and 200 g of activated sorbent. The solution was mixed for 24 h. After mixing, the sorbent was filtered and washed with distilled water until a negative reaction for Cl ions. The sorbent was dried at 105 °C for 2 h and then at 200 °C for 4 h.

The modified sorbents were decomposed in a Pt-crucible. 0.5 g of finely crushed sample was treated with 15 mL hydrofluoric acid (40 %) in a platinum crucible and heated on a water bath (90 °C). The hydrofluoric acid treatment was repeated. To the residue, 8–10 mL of HF (40 %) and 6 mL of 1:1 H_2SO_4 were added followed again by heating in a water bath, initially for 2 h, and then on a hot plate until the fumes of H_2SO_4 ceased to evolve. The H_2SO_4 fuming was repeated in order to completely remove fluoride as HF. The residue was then cooled, 1–2 mL concentrated HNO_3 added and the heating continued. HNO_3 treatment of the residue was repeated two or three times to remove any organic matter present. The residue was then dissolved in 20–30 mL of water on a water bath. The solution was transferred to a 250 mL beaker, and about 200 mL of water was added. The solution was boiled and then filtered. The filtrate was finally transferred to a 250 mL volumetric flask and made up to the mark with distilled water. The amount of Zr, respectively Ti, was determined by AAS. The amounts of Ti and Zr were also determined by ICP-OES after digestion in 5 mL 85 % H_3PO_4 , 4 mL 37 % HCl and 0.5 mL 40 % HF in a pressurized microwave.

Batch sorption tests

All batch experiments were realized in 50 mL plastic flasks with drinking water spiked with 200 $\mu\text{g L}^{-1}$ As(III) or drinking water spiked with 200 $\mu\text{g L}^{-1}$ As(V). The removal of arsenite and arsenate was evaluated for the sorbents BIRM, Greensand (GS) and MTM modified with Zr and Ti and dried at different temperatures. Batch adsorption experiments were conducted by taking 40 mL of 200 $\mu\text{g L}^{-1}$ of As(III) or 40 mL of 200 $\mu\text{g L}^{-1}$ of As(V) into tightly capped 50 mL plastic flasks and adding the sorbent (0.3000 ± 0.0010 g). The plastic flasks were shaken for 1 h at room temperature. Solutions were separated by centrifugation at 3,500 rpm and the As concentrations were determined by HG-AAS.

Adsorption isotherms

Adsorption isotherms were obtained by adding different concentrations of As(III) or As(V) solution to the drinking water in 50 mL plastic flasks with 0.3000 g of MTM-Ti sorbent activated at 200 °C. The concentrations were 0.200, 0.400, 0.600, 0.800, 1.000 and 1.200 mg L^{-1} . The volume of the solution was 40 mL in all experiments. The plastic flasks were shaken for 1 h at room temperature. The solutions were separated by centrifugation at 3500 rpm and the As concentrations were determined by HG-AAS.

Effect of pH on As sorption

For the pH study, 50 mL plastic flasks were filled with 40 mL of 200 $\mu\text{g L}^{-1}$ As(III) or As(V) and 0.3000 g of modified sorbent. The correct amount of acid (HCl) or base (NaOH) solution required to adjust the pH to the target value was added. pH values of approximately 5.0; 5.5; 6.0; 6.5; 7.0 and 8.0 were used. For every pH value, the *Eh* value was measured. The

plastic flasks were shaken for 1 h at room temperature. The solutions were then separated, the pH and *Eh* values were measured and the As concentrations were determined by HG-AAS.

Arsenic analysis

Total arsenic analyses were performed using a SpectrAA 55-Varian instrument (CA, USA) equipped with an integrated unit for hydride generation. The measurements were based on the integrated absorbance using a hollow cathode lamp (Varian) at 193.7 nm.

Arsenic hydride was generated from 0.6 % NaBH₄ (in 0.5 % NaOH) and 6 mol L⁻¹ HCl.¹⁷

RESULTS AND DISCUSSION

After decomposition of modified sorbents and their analysis by AAS and ICP-OES, good agreement between the two methods was obtained. The amounts of Zr and Ti were between 0.25–1.95 % (w/w) after modification of the activated sorbents (Table I).

TABLE I. Content of Zr and Ti (%) after modification of the activated sorbents

Sorbent	Ti	Zr
GS	0.6	0.85
BIRM	1.45	1.95
MTM	0.95	0.25

In the first series of experiments, the adsorption of As(III) and As(V) species on commercial sorbents and modified sorbents was examined. Greensand (GS) showed no capability for As adsorption (Table II). Modification of Greensand did not have a significant influence on the adsorption. Unmodified BIRM also did not adsorb arsenic but after modification with titanium or zirconium, good results were obtained in both cases. MTM adsorbed both species but after modification with titanium, the level of arsenic decreased by up to eight times. After modification with zirconium, inferior results were obtained.

TABLE II. Final arsenic concentrations ($\mu\text{g L}^{-1}$) in solution after treatment with various sorbents dried at 200 °C. Initial As(III) and As(V) concentrations: 200 $\mu\text{g L}^{-1}$

Sorbent	As(III)	As(V)
BIRM	183.8±11.4	192.3±6.1
BIRM-Ti, 200 °C	26.4±1.4	12.2±0.8
BIRM-Zr, 200 °C	24.8±3.3	1.0±0.0
GS	174.2±22.4	191.0±1.2
GS-Ti, 200 °C	133.6±7.8	152.2±7.0
GS-Zr, 200 °C	149.4±10.0	131.4±4.2
MTM	68.8±17.8	41.7±0.7
MTM-Ti, 200 °C	20.4±9.1	9.6±2.0
MTM-Zr, 200 °C	132.7±20.4	137.2±7.8

Batch As(III) and As(V) adsorption tests were performed using activated BIRM modified with Zr and Ti and MTM modified with Ti. The effects of the

temperature employed for drying the sorbents are given in Tables II–V. Sorbents were dried at the defined temperature for 4 h.

From the results presented in Tables II–V, it could be concluded that As(III) and As(V) sorption capabilities were decreased at high drying temperatures. Heating of the sorbents at temperatures higher than 200 °C decreased the As(III) and As(V) sorption. This decrease may be due to dehydration of sorbents. Increasing the drying temperature resulted in a decrease in the number of OH⁻ groups, which were probably the active sorption sites and responsible for the sorption of As. The maximum arsenic sorptions were achieved using sorbents dried at 200 °C.

TABLE III. Final arsenic concentrations ($\mu\text{g L}^{-1}$) in solution after treatment with BIRM–Ti sorbents activated at various temperatures. Initial As(III) and As(V) concentrations: 200 $\mu\text{g L}^{-1}$

$t / ^\circ\text{C}$	As(III)	As(V)
150	3.1±1.0	3.6±1.0
200	4.4±1.8	2.4±1.4
250	15.0±4.6	10.4±2.1
300	16.4±2.4	12.8±0.6
400	38.0±3.6	26.6±2.6

TABLE IV. Final arsenic concentration ($\mu\text{g L}^{-1}$) in solution after treatment with BIRM–Zr sorbents activated at various temperatures. Initial As(III) and As(V) concentrations: 200 $\mu\text{g L}^{-1}$

$t / ^\circ\text{C}$	As(III)	As(V)
150	4.3±1.0	2.4±1.4
200	9.8±3.4	2.6±1.4
250	26.2±4.2	14.6±0.1
300	29.4±10.7	26.5±8.0
400	45.6±2.8	26.8±0.4

TABLE V. Final arsenic concentrations in solution ($\mu\text{g L}^{-1}$) after treatment with MTM–Ti sorbents activated at various temperatures. Initial As(III) and As(V) concentrations: 200 $\mu\text{g L}^{-1}$

$t / ^\circ\text{C}$	As(III)	As(V)
150	4.4±2.4	4.5±1.2
200	3.8±2.8	1.1±0.1
250	12.7±0.2	10.3±0.5
300	15.2±0.6	15.8±4.0
400	43.2±9.7	22.8±9.5

In order to obtain more information on the sorption by the MTM–Ti sorbent activated at 200 °C, another series of batch experiments were performed with different concentrations of As(III) and As(V). These results were used for the calculation of the constants of the Freundlich and Langmuir adsorption isotherms.²³ The linearized form of the Freundlich Equation was used:

$$\log (x/m) = \log K + (1/n)\log c$$

where x is the mass of adsorbed arsenic, m is the mass of sorbent, c is the equilibrium concentration of arsenic in solution after sorption, K is a constant, and n is a constant. The constant K is related primarily to the capacity of the sorbent and n is a function of the strength of the sorption (Figs. 1 and 2).

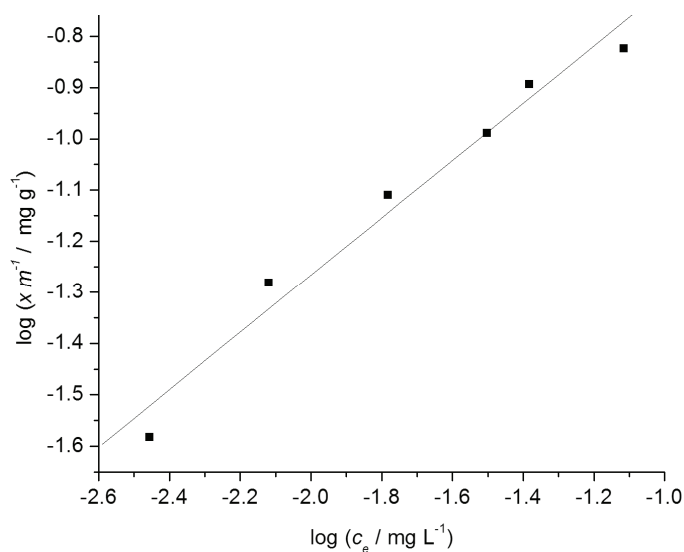


Fig. 1. Freundlich plot for As(III) sorption by MTM-Ti 200 °C.

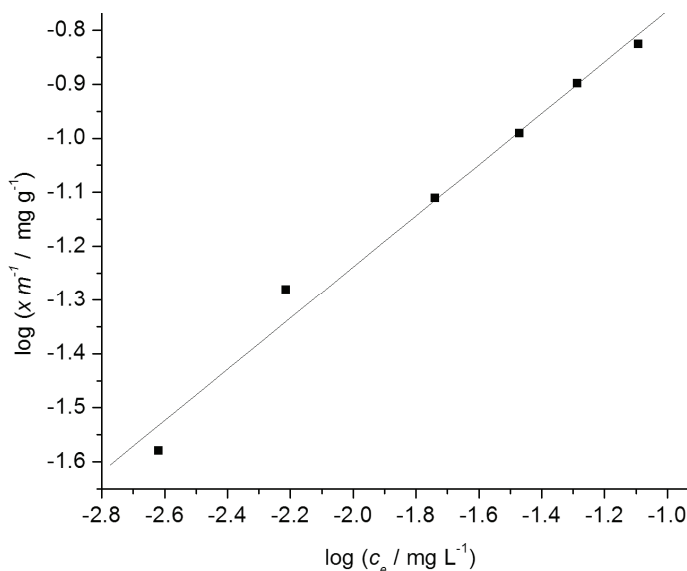


Fig. 2. Freundlich plot for As(V) sorption by MTM-Ti 200 °C.

The values of K and n obtained from adsorption isotherms are summarized in Table VI.

The Langmuir Equation is given by:

$$c_e/Q_e = 1/(bQ^0) + c_e/Q^0$$

where c_e is the equilibrium concentration, Q^0 is a constant that represents the maximum adsorption density corresponding to a monolayer covering of the surface of the adsorbent, b is a constant that represents the adsorption bond energy and Q_e is the mass of arsenate sorbed per unit dry weight of adsorbent. This equation was used to describe the adsorption data presented in Figs. 3 and 4.

TABLE VI. Freundlich and Langmuir constants for the sorption of As(III) and As(V) by the MTM-Ti sorbent activated at 200 °C

Ion	Freundlich			Langmuir	
	$K / \text{mg g}^{-1}$	n	R^2	$Q^0 / \text{mg g}^{-1}$	R^2
As(III)	0.711	1.27	0.9718	0.193	0.9902
As(V)	0.514	2.11	0.9841	0.174	0.9757

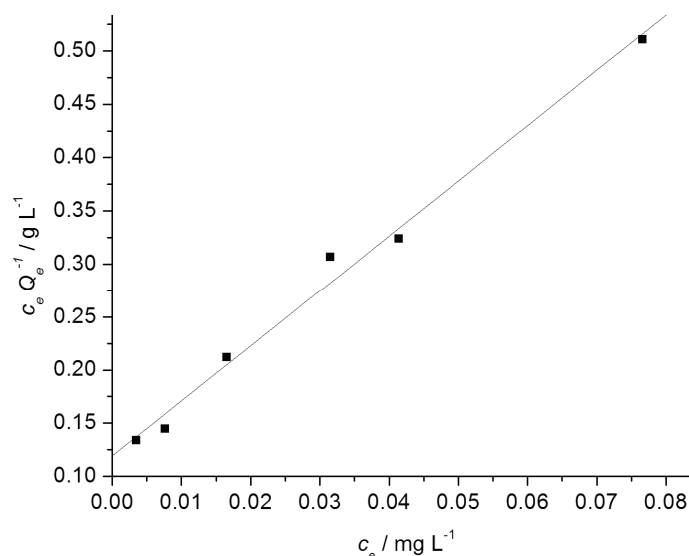


Fig. 3. Langmuir plot for As(III) sorption by MTM-Ti 200 °C.

In the case of As(III), the data fitted the Langmuir model, which assumes reversible mono-layer coverage, was better, while for As(V), a better correlation coefficient was achieved with the Freundlich Equation (Table VI).

As pH is an important parameter in adsorption processes, the effect of the initial pH of the solution on the sorption of As(III) and As(V) was investigated. In the pH range 5 to 8, there was no significant correlation between pH and the

sorption capacity. For an initial arsenic concentration of $200 \mu\text{g L}^{-1}$, the final arsenic concentrations were below the maximum permissible limit ($10 \mu\text{g L}^{-1}$) for all the investigated pH values. The results in Table VII show that the sorbent does not have a significance influence on the pH and Eh of the solution in the pH range and experimental conditions applied in these investigations. This range of pH for adsorption of arsenic should be advantageous under real conditions.

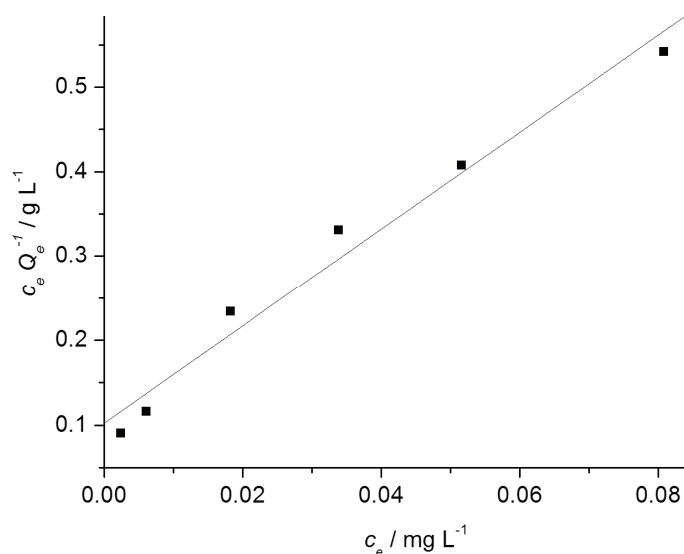


Fig. 4. Langmuir plot for As(V) sorption by MTM-Ti 200 °C.

TABLE VII. Changes in pH and Eh during the adsorption experiments (after 1 h shaking with sorbent MTM-Ti 200 °C)

Initial pH	pH	Initial Eh , mV	Eh / mV
5.00	5.21	404	405
5.52	5.73	385	375
6.04	6.24	361	352
6.49	6.62	346	340
6.95	6.98	336	354
7.56	7.39	293	310
8.01	7.63	280	300

CONCLUSIONS

After activation and modification with Zr and Ti, BIRM had higher sorption capacities. There was no improvement in the sorption capacity of GS after its activation and modification with Zr and Ti. MTM had better sorption capacities after activation and modification with Ti.

The BIRM-Zr, BIRM-Ti and MTM-Ti modified sorbents had high sorption capacities for As(III) and As(V) in the pH range of natural water. These modified

sorbents, dried at 200 °C, removed arsenic from drinking water spiked with 200 µg L⁻¹ of As(III) and As(V) to below the maximum permissible limit. With increasing drying temperature, the sorption capacities decreased. The optimal drying temperature for the modified sorbents was 200 °C.

Changing the pH of the solution in the range from 5 to 8 had no obvious effect on the sorption. In addition, the sorbents had no significant influence on the pH and *Eh* of the solution.

The obtained batch experimental results suggested that these modified sorbents could be used for As(III) and As(V) removal under real conditions.

ИЗВОД

УКЛАЊАЊЕ АРСЕНА ИЗ ВОДЕНИХ РАСТВОРА СОРПЦИЈОМ НА СОРБЕНТИМА МОДИФИКОВАНИМ ЦИРКОНИЈУМОМ И ТИТАНОМ

ИВАН АНЂЕЛКОВИЋ¹, ДРАГАН Д. МАНОЈЛОВИЋ¹, ДРАГАНА ЂОРЂЕВИЋ², БИЉАНА ДОЛЧИНОВИЋ², ГОРАН РОГЛИЋ¹ и ЉУБИША ИГЊАТОВИЋ³

¹Хемијски факултет, Београд, ²Центар за хемију, технологију и металургију, Београд и

³Факултет за физику хемију, Београд

Уклањање арсена из подземних вода може укључивати третман сорпцијом, прелазак на алтернативне изворе воде или мешање са водом која садржи ниске концентрације арсена. Комерцијални сорбенти МТМ, *Greensand* и BIRM су модификовани цирконијумом и титаном после активације. Модификација је урађена титан-тетрахлоридом и цирконијум-тетрахлоридом. Модификовани сорбенти су сушени на различитим температурама. Сорпција арсената и арсенита растворених у пијаћој води је тестирана *batch* поступком. После уклањања сорбента концентрација арсена је одређена HG-AAS методом. BIRM модификован цирконијумом је показао најбоље резултате у уклањању арсенита и арсената. Модификација *Greensand*-а није утицала на повећање сорпционе моћи. BIRM модификован цирконијумом је смањио концентрацију арсена испод 5 µg L⁻¹.

(Примљено 7. октобра 2010)

REFERENCES

1. D. Mohan, C. U. Pittman Jr., *J. Hazard. Mater.* **142** (2007) 1
2. A. Hanson, J. Bates, D. Heil, A. Bristol, *Arsenic removal from water using manganese greensand: Laboratory Scale Batch and Column Studies*, U.S. Department of the Interior, Bureau of Reclamation, Technical Service Center, Water Treatment Engineering and Research Group, Las Cruces, NM, USA, 1999
3. C. J. Wyatt, C. L. Fimbres, R. R. O. M'endez, M. Grijalva, *Environ. Res.* **76** (1998) 114
4. C. F. Harvey, C. H. Swartz, A. B. M. Badruzzaman, N. Keon-Blute, W. Yu, M. A. Ali, J. Jay, R. Beckie, V. Niedan, D. Brabander, P. M. Oates, K. N. Ashfaq, S. Islam, H. F. Hemond, M. F. Ahmed, *Science* **298** (2002) 1602
5. Y. Xia, J. Liu, *Toxicology* **198** (2004) 25
6. H. Kondo, Y. Ishiguro, K. Ohno, M. Nagase, M. Toba, M. Takagi, *Water Res.* **33** (1999) 1967
7. D. Jovanovic, B. Jakovljevic, Z. Rasic-Milutinovic, K. Paunovic, G. Pekovic, T. Knezevic, *Environ. Res.* **111** (2011) 315

8. USEPA, *Federal Register* **66** (2001) 6976
9. M. Borho, P. Wilderer, *Water Sci. Technol.* **34** (1996) 25
10. J. Kim, M. M. Benjamin, *Water Res.* **38** (2004) 2053
11. R. Y. Ning, *Desalination* **143** (2002) 237
12. M. M. Gholami, M. A. Mokhtari, A. Ameri, M. R. Alizadeh Fard, *Desalination* **200** (2006) 725
13. M. Habuda-Stanić, B. Kalajdžić, M. Kuleš, N. Velić, *Desalination* **229** (2008) 1
14. M. Simonić, *J. Serb. Chem. Soc.* **74** (2009) 85
15. V. Zaspalis, A. Pagana, S. Sklari, *Desalination* **217** (2007) 167
16. D. Manojlović, A. Popara, B. P. Dojčinović, A. Nikolić, B. M. Obradović, M. M. Kuraica, J. Purić, *Vacuum* **83** (2009) 142
17. S. Bang, M. Patel, L. Lippincott, X. Meng, *Chemosphere* **60** (2005) 389
18. B. R. Mann, S. C. Bhaf, M. Dasgupta, U. C. Ghosh, *Chem. Environ. Res.* **8** (1999) 51
19. K. Hristovski, A. Baumgardner, P. Westerhoff, *J. Hazard. Mater.* **147** (2007) 265
20. M. E. Pena, G. P. Korfiatis, M. Patel, L. Lippincott, X. Meng, *Water Res.* **39** (2005) 2327
21. Z. Gong, X. Lu, M. Ma, C. Watt, X. Chris Le, *Talanta* **58** (2002) 77
22. P. Westerhoff, *Arsenic removal with agglomerated nanoparticle media*, WERC, Las Cruces, NM, 2006
23. H. Jezequel, K. H. Chu, *Environ. Chem. Lett.* **3** (2005) 132.



Arsenic removal from water using low-cost adsorbents – a comparative study

BRANISLAVA M. JOVANOVIĆ^{1*}, VESNA L. VUKAŠINOVIĆ-PEŠIĆ²,
ĐORĐE N. VELJOVIĆ^{3#} and LJUBINKA V. RAJAKOVIĆ^{3#}

¹Department of Hydraulic and Environmental Engineering, Faculty of Civil Engineering, University of Belgrade, Bulevar kralja Aleksandra 73, 11000 Belgrade, Serbia, ²Faculty of Metallurgy and Technology, University of Montenegro, Cetinjski put bb, 81000 Podgorica, Montenegro and ³Department of Analytical Chemistry, Faculty of Technology and Metallurgy, University of Belgrade, Karnegijeva 4, 11 000 Belgrade, Serbia

(Received 29 October 2010, revised 7 January 2011)

Abstract: Inorganic arsenic removal from water using low-cost adsorbents is presented in this paper. Selective removal of As(III) and As(V) from water was performed with natural materials (zeolite, bentonite, sepiolite, pyrolusite and limonite) and industrial by-products (waste filter sand as a water treatment residual and blast furnace slag from steel production); all inexpensive and locally available. Kinetic and equilibrium studies were realized using batch system techniques under conditions that are likely to occur in real water treatment systems. The natural zeolite and the industrial by-products were found to be good and inexpensive sorbents for arsenic while bentonite and sepiolite clays showed little affinity towards arsenic. The highest maximum sorption capacities were obtained for natural zeolite, 4.07 mg As(V) g⁻¹, and waste iron slag, 4.04 mg As(V) g⁻¹.

Keywords: adsorption; arsenic removal; arsenic remediation; low cost sorbents.

INTRODUCTION

The presence of arsenic in natural waters has become a worldwide problem in the past decades. Arsenic pollution from natural sources was recently reported in China, Taiwan, India, Bangladesh, USA, Canada, Mexico, Chile, Argentina, New Zealand, Poland, Hungary, Croatia, Serbia and Romania.^{1–5}

Arsenic is widely found in the Earth's crust in oxidation states of –3, 0, +3 and +5, often as sulfides or metal arsenides or arsenates.³ In water, it is mostly present as arsenate (+5) but under anaerobic conditions, it is likely to be present as arsenite (+3).⁴ It usually occurs in natural waters at concentrations of less than 1 or 2 µg L⁻¹.² However, in natural groundwater reservoirs where there are

* Corresponding author. E-mail: branaj@grf.bg.ac.rs

Serbian Chemical Society member.

doi: 10.2298/JSC101029122J

sulfide mineral deposits and sedimentary deposits derived from volcanic rocks, the concentrations can be significantly increased (up to 12 mg L^{-1}).²

Increased risks of arsenic related diseases have been reported to be associated with ingestion of drinking-water at concentrations of $<50 \text{ } \mu\text{g L}^{-1}$.^{3,5} However, considering the significant uncertainties surrounding the risk assessment for arsenic carcinogenicity and the practical difficulties in removing arsenic from drinking-water, a provisional guideline value for arsenic was set by the WHO at a limit of 0.01 mg L^{-1} in the 1993 Guidelines. In view of the scientific uncertainties, the guideline value is designated as provisional. A new maximum concentration limit of 0.01 mg L^{-1} for arsenic in drinking water was set by the US EPA in 2001⁶ and EU law⁷ in 2003, requiring public water supply systems to reduce arsenic in drinking water by not later than January 2006. In the Republic of Serbia, the new arsenic concentration limit was set in 1998.⁸

Toxicological review

The most important routes of arsenic exposure are through food and drinking water. Arsenic is found in food, particularly in fish and shellfish, in which it is found mainly in the less toxic organic form.⁹ Arsine is considered the most toxic form, followed by arsenites, then arsenates and organic arsenic compounds.^{4,5}

Environmental exposure to arsenic through drinking-water has been associated with skin cancer.¹⁰ Acute arsenic intoxication associated with the ingestion of water containing a very high concentration of arsenic (21.0 mg L^{-1}) was reported.³ Moreover, it was concluded that long-term exposure to arsenic in drinking water is causally related to increased risks of cancer in the skin, lungs, bladder and kidney, as well as other skin changes, such as hyperkeratosis and pigmentation changes.¹¹ Epidemiological studies^{12,13} in areas with different frequencies of black-foot disease and where drinking water contained $0.35\text{--}1.14 \text{ mg L}^{-1}$ arsenic revealed elevated risks for cancers of the bladder, kidney, skin, lung, liver and colon. Dermal lesions were the most commonly observed symptom occurring after minimum exposure periods of approximately 5 years.^{12,13}

Arsenic removal technologies

It is technically feasible to achieve arsenic concentrations of $10 \text{ } \mu\text{g L}^{-1}$ or lower using any of the following treatment technologies: oxidation/precipitation,^{5,14} coagulation/coprecipitation,¹⁴ sorption^{15,16}, ion-exchange¹⁷ and membrane technologies.¹⁸ Among them, adsorption is considered to be a relatively simple, efficient and low-cost arsenic removal technique, especially convenient for application in rural areas.⁴ A wide range of sorbent materials for aqueous arsenic removal is available nowadays: biological materials, mineral oxides, different soils, activated carbons and polymer resins.¹⁸ Nevertheless, finding inexpensive and effective sorbents for arsenic removal from water is still highly desired.

Natural materials such as clay minerals, zeolites and metal oxides are widespread and abundant in terrestrial environments. Clay minerals and zeolites adsorb cationic, anionic and neutral metal species.¹⁸ As reported in recent papers, certain agricultural and industrial by-products, such as waste tea fungal biomass,¹⁹ rice husks,²⁰ red mud,¹⁸ fly ash,²¹ *etc.*, were found to be good and inexpensive arsenic sorbents. In addition, application of industrial wastes in water treatment follows the reuse-recycle concept.

The aim of this study was to investigate and compare natural materials (zeolite, bentonite, sepiolite, pyrolusite and limonite) and industrial by-products (blast furnace slag and waste filter sand), inexpensive and all locally available, as potential sorbents for arsenic.

EXPERIMENTAL

Reagents and apparatus

An As(V) stock solution (100 mg L⁻¹) was prepared by dissolving 416.5 mg of sodium arsenate (Na₂HAsO₄·7H₂O, Analar analytic reagent) in 1 L of distilled water, which was preserved with 0.5 % HNO₃. An As(III) stock solution (3750 mg L⁻¹) was prepared by dissolving sodium arsenite (0.05 mol NaAsO₂, Riedel-de-Haen (4.946 g As₂O₃ + 1.3 NaOH in 1 L)) in distilled water in a 1 L volumetric flask, which was preserved with 0.5 % HNO₃.

Arsenic was analyzed using the ICP-MS method, according to Standard methods,²² using an Agilent 7500ce spectrometer equipped with octopole reaction system (ORS). Calibration was realized using external standards (2, 4, 20, 40, 80 and 100 µg L⁻¹), which were prepared by appropriate dilution of a 1000 µg L⁻¹ stock standard solution. Working standards, as well as blank solutions, were prepared with high purity HNO₃. The concentrations of the investigated samples were adjusted to the concentration range 5–100 µg L⁻¹. The experimental data measurements were accepted as reasonable data in cases of less than 5 % relative standard deviation (RSD). In order to amplify the consistency of the results, the experiments were performed in triplicate and the mean values considered. The limit of detection was 0.1 µg L⁻¹. A laboratory pH meter (Metrohm 827) was used for pH measurements. The accuracy of the pH meter was ±0.01 pH units.

Materials and characterization techniques

Zeolite (Z), natural clay minerals, bentonite (B) and sepiolite (S), and natural metal oxide minerals, limonite (L) and pyrolusite (P) were selected as the natural materials while waste iron slag (WIS) and waste filter sand (WFS) were selected as the waste materials to be tested within the scope of the presented investigations. The natural materials were obtained from natural deposits located in Serbia and Bosnia. The industrial by-products were obtained from local industrial facilities: blast furnace slag from the steel production plant US Steel Serbia (Smederevo, Serbia) and waste filter from groundwater treatment plant “Bežanija” in Belgrade, Serbia. The physical properties and chemical composition of all materials are presented in the further text.

The microstructure of the analyzed material samples was examined by scanning electron microscopy (SEM) using a Jeol JSM 5800 instrument (operated at 25 kV). The BET specific surface areas were determined by the technique of nitrogen adsorption¹⁷ using a Sorptomatic 1990 Thermo Finning instrument. The chemical composition of the materials was determined by standard silicate analysis.^{23,24}

Kinetic and equilibrium studies

Kinetic batch experiments were performed for As(III) and As(V), with an initial As concentration $c_0 = 0.5 \text{ mg L}^{-1}$. The experiments were performed in different time intervals, up to $\tau = 24 \text{ h}$. During each set of conducted kinetic batch experiments, it was observed that absolute equilibrium was not reached even after 24 h. In each set of experiments, $\tau = 6 \text{ h}$ was found to be the turning point after which the sorption rate was significantly lower and thus changes in sorption efficiency were far less rapid. Moreover, the rapid sorption rate range (0–6 h) was found to be the most interesting for detailed examination in terms of the potential application of waste materials. Finally, the adsorption isotherm experiments were performed under different initial arsenic, As(III) and As(V) concentrations (0.500, 1.00, 5.00, 10.0, 50.0 and 100.0 mg L^{-1}) for a contact time $\tau = 6 \text{ h}$, at pH 7.

RESULTS AND DISCUSSION

Characterization

Chemical composition. The chemical compositions of the selected natural and waste materials are summarized in Table I. The main accessory minerals in the zeolite were quartz, feldspar and carbonate. The clinoptilolite content in the zeolite was 85 %. Bentonite is a clay material consisting mostly of montmorillonite (95 %) with some accessory quartz, calcite, feldspar, muscovite and biotite. Sepiolite is a natural hydrous magnesium silicate. The chemical analyses results indicated that the sepiolite sample consisted of 98 % pure mineral (based on the SiO_2 content). Limonite is a natural ore comprised of hydrated iron(III) oxides, mostly made up of goethite ($\alpha\text{-FeOOH}$). Elemental analysis of the limonite ore indicated that the iron content was 45.5 %. Pyrolusite is a mineral consisting essentially of manganese dioxide (MnO_2) and is important as a manganese ore. The content of manganese in the natural pyrolusite was 51.8 %. The dominant constituent of the waste filter sand was quartz (SiO_2) coated by metal oxide layer

TABLE I. Chemical composition (%) of the studied natural and waste materials (Z – zeolite, B – bentonite, S – sepiolite, L – limonite, P – pyrolusite, WFS – waste filter sand, WIS – waste iron slag)

Material	Deposits location	SiO_2	Fe_2O_3	FeO	Al_2O_3	CaO	MgO	TiO_2	Na_2O	K_2O	Fe	Mn
Z	Vranjska Banja, Serbia	66.57	2.30	–	13.13	3.85	1.27	–	1.27	1.17	–	–
B	Birač, Zvornik, Bosnia	54.97	6.83	–	16.82	2.0	2.6	1.3	0.38	0.15	–	–
S	Antići, Čačak, Serbia	56.68	0.04	–	0.03	0.27	28.6	–	0.15	0.096	–	–
L	Majdanpek, Serbia	2.85	59.19	–	8.12	0.028	2.19	–	–	–	45.5	–
P	Majdanpek, Serbia	3.1	3.9	–	2.5	0.1	0.3	–	–	–	–	51.8
WFS	–	65.16	3.68	0.82	–	1.14	21.23	–	–	–	3.93	15.66
WIS	–	23.82	13.02	15.73	7.70	26.5	11.13	0.08	–	–	21.20	–

consisting of iron (Fe) and manganese (Mn) deposits. The content of Mn was four times higher than that of Fe. The results of the chemical analyses showed that the waste iron slag was a complex heterogeneous material, mainly composed of silica, and iron and calcium oxides.

Physical properties. Clays are natural materials known for their highly developed surface area. The bentonite (B) clay from the Birač deposits exhibited the highest specific surface area of all the investigated materials ($593 \text{ m}^2 \text{ g}^{-1}$) (Table II), two times higher than the sepiolite (S) clay ($286 \text{ m}^2 \text{ g}^{-1}$). The other natural materials exhibited moderate to low specific surface areas. The relatively high surface area obtained for the waste filter sand (WFS) was assigned to the iron and manganese oxides layer which coats the original quartz grain of the sand.²⁵

TABLE II. Physical properties of the studied natural and waste materials

Material	Grain size, mm	BET specific surface area, $\text{m}^2 \text{ g}^{-1}$
Zeolite (Z)	0.4–0.8	45.7
Bentonite (B)	<0.074	593.0
Sepiolite (S)	<0.074	286.0
Limonite (L)	1–2	1.7
Pyrolusite (P)	1–2	1.2
Waste filter sand (WFS)	1.25	94.1
Waste iron slag (WIS)	0.470	2.9

The porous microstructures with pores of different size and shape could be observed from all micrographs (Fig. 1). The limonite microstructure (Fig. 1d) shows that this porous natural material was composed of particles in the size range from approximately a few hundred nanometers to a few microns. The microstructure of the pyrolusite (Fig. 1e) was also porous with particles of different shape and size. Rod-shaped particles were also observed in the pyrolusite microstructure. SEM micrograph in Fig. 1c shows a fibrous texture, typical for the structure of sepiolite. The bentonite microstructure was also porous and shapeless pores a few microns in size can be observed in Fig. 1b.

Batch system investigations

Preliminary investigations. A continuously mixed batch system was employed. The kinetic batch experiments were performed for As(III) and As(V), using initial As concentrations 0.500 and 10.0 mg L^{-1} , respectively, for the time interval $\tau = 2 \text{ h}$. Despite their high specific surface area, the natural mineral clays, bentonite and sepiolite, exhibited low or no affinity towards As(III) and As(V) (Fig. 2). The highest sorption capacity was obtained for sepiolite, $5 \mu\text{g g}^{-1}$ of As(V).

The natural Fe and Mn oxide minerals, limonite and pyrolusite, exhibited low sorption capacities of up to $30 \mu\text{g g}^{-1}$ of As(V) only under high initial arsenic concentrations. At low initial arsenic concentrations, limonite and pyrolusite showed no affinity towards As(III) and As(V).

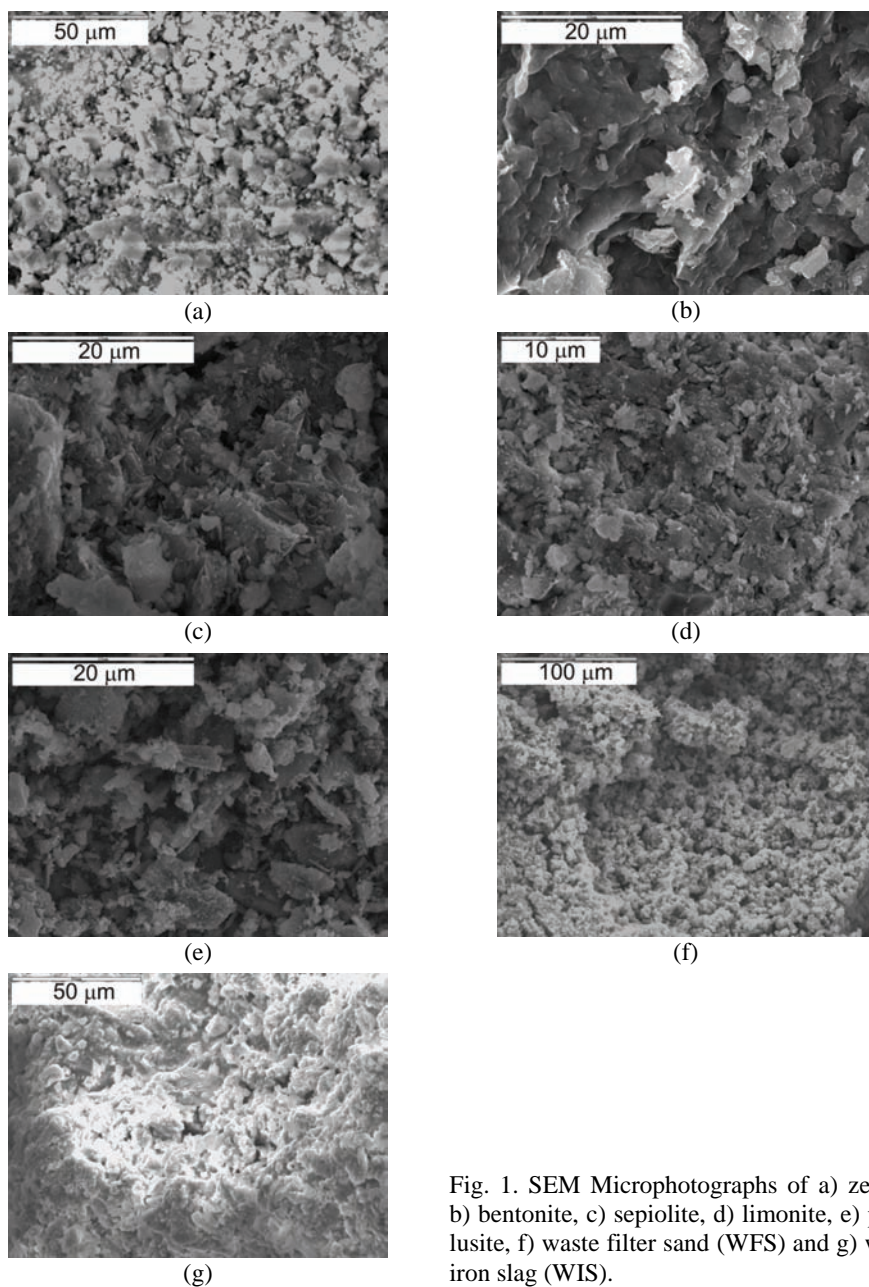


Fig. 1. SEM Microphotographs of a) zeolite, b) bentonite, c) sepiolite, d) limonite, e) pyrolusite, f) waste filter sand (WFS) and g) waste iron slag (WIS).

In the first set of preliminary experiments, only natural the zeolite of all the tested natural materials exhibited certain sorption features, while the waste materials proved to be good arsenic sorbents. Therefore, further detailed examinations were focused on these three materials only.

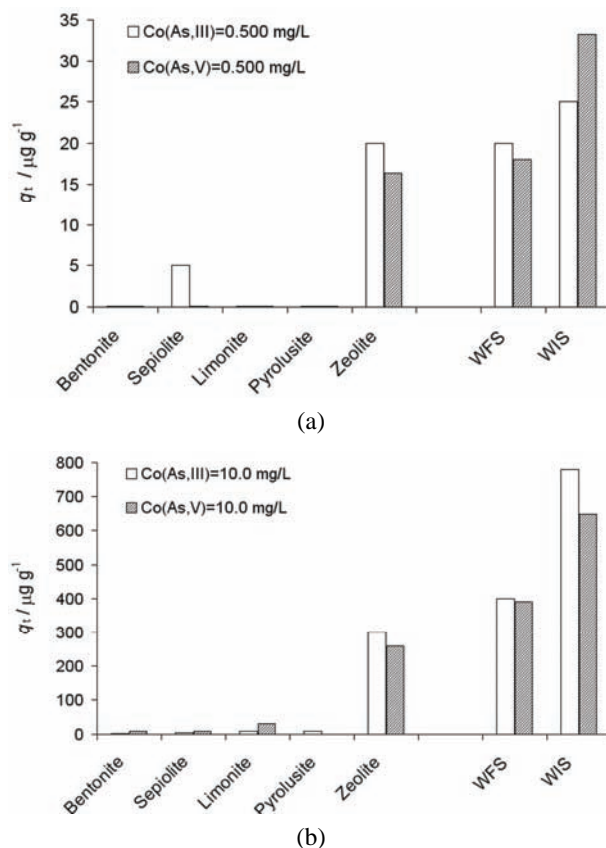
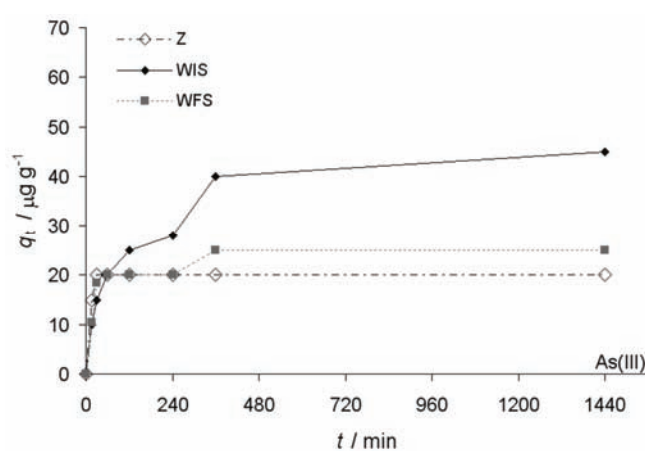


Fig. 2. Preliminary batch experiments for As(III,V) sorption. Conditions: $c_{\text{As(III,V)}} = 0.500$ (a) and 10.0 mg L^{-1} (b), $m = 1.00 \text{ g}$, $t = 20 \text{ }^\circ\text{C}$, $V = 100 \text{ mL}$, $\tau = 2 \text{ h}$.

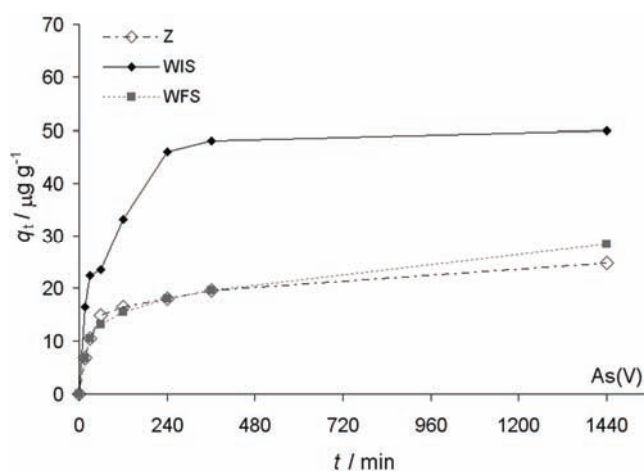
Sorption kinetic studies. The sorption kinetics of As(III) and As(V) onto the natural zeolite and the waste materials are presented in Fig. 3. The waste slag, WIS, exhibited substantial sorption capacities. It was found that the WIS adsorbed $10 \mu\text{g g}^{-1}$ of As(III) and $16.4 \mu\text{g g}^{-1}$ of As(V) in the first 15 min, reaching $45 \mu\text{g g}^{-1}$ for As(III) and $50 \mu\text{g g}^{-1}$ for As(V) after the equilibrium contact time (6 h). The kinetic performance of the natural zeolite was nearly as good as that of the waste filter sand (WFS). In 24 h, the WFS adsorbed $25 \mu\text{g g}^{-1}$ As(III) and $29 \mu\text{g g}^{-1}$ As(V), while in the first 15 min it adsorbed $10.5 \mu\text{g g}^{-1}$ As(III) and $6.8 \mu\text{g g}^{-1}$ As(V).

Several model equations have been established to describe sorption kinetics. The Lagergren First Order and the Pseudo-Second-Order sorption kinetic models are the most frequently used. These models were thoroughly discussed in a recent paper²⁶ and, hence, they are only summarized here (Table III). In Table III, q_t is sorption capacity at time t ($\mu\text{g g}^{-1}$), q_e the equilibrium sorption capacity ($\mu\text{g g}^{-1}$),

k_2 the rate constant of sorption ($\text{g } \mu\text{g}^{-1} \text{ min}^{-1}$), h the initial sorption rate ($\mu\text{g g}^{-1} \text{ min}^{-1}$) and k_L the Lagergren rate constant (min^{-1}). The experimental results were fitted to the pseudo-second-order and the Lagergren First Order model, applying non-linear regression analysis using MS Office 2000 Excel spreadsheets. The correlation coefficients, R , were calculated in order to quantify the applicability of the applied kinetic models. Values of the model parameters obtained from the regression analyses are presented in Table IV.



(a)



(b)

Fig. 3. Sorption kinetics of As(III) (a) and As(V) (b) onto the natural and waste materials. Conditions: $c_{\text{As(III,V)}} = 0.500 \text{ mg L}^{-1}$, $m = 1.00 \text{ g}$, $t = 20 \text{ }^\circ\text{C}$, $V = 100 \text{ mL}$, $\tau = 24 \text{ h}$.

The regression analyses showed that the pseudo-second-order equation is the most appropriate kinetic model for arsenic sorption onto the investigated mate-

rials, which indicates that chemisorption occurs. Although WFS would be presumed to be primarily a weak, physical sorbent, the high correlation coefficient obtained for the pseudo-second-order model, indicating chemisorption, is assumed to result from the presence of iron and manganese oxides on the surface of the sand grains (Table I). Effective arsenic sorption onto the surface of iron oxides has already been reported.²⁷ Depending on the pH, various forms of hydrated iron oxide exist on solid surfaces in contact with water: FeOH₂⁺, FeOH and FeO⁻. At neutral pH, FeOH₂⁺ and FeOH forms are predominant and they are responsible for the selective binding of As(III) and As(V). The sorption process in neutral conditions occurs owing to FeOH sites, which bond molecular forms of As(III) (HAsO₂), and FeOH₂⁺ sites, which bond ionic forms of As(V) (H₂AsO₄⁻ and HAsO₄²⁻).

TABLE III. Adsorption kinetic models and their linear forms

Type	Non-linear form	Linear form	Plot
Pseudo-second-order	$\frac{1}{q_e - q_t} = \frac{1}{q_e} + k_2 t$	$\frac{t}{q_t} = \frac{1}{k_2 q_e^2} + \frac{1}{q_e} t$	$\frac{t}{q_t}$ vs. t
Lagergren	$q_t = q_e (1 - e^{-k_L t})$	$\ln\left(1 - \frac{q_t}{q_e}\right) = -k_L t$	$\ln\left(1 - \frac{q_t}{q_e}\right)$ vs. t

TABLE IV. Kinetic model parameters and correlation coefficients for As(III) and As(V) sorption

Model equation	Parameter	Z		WIS		WFS	
		As(III)	As(V)	As(III)	As(V)	As(III)	As(V)
Pseudo-second order	$q_e / \mu\text{g g}^{-1}$	20.02	25.7	47.6	51.7	25.4	29.8
	$k_2 / \text{g } \mu\text{g}^{-1} \text{ min}^{-1}$	0.0481	0.000593	0.00023	0.00043	0.00157	0.00033
	$h / \mu\text{g g}^{-1} \text{ min}^{-1}$	1.93	0.39	0.53	1.14	1.01	0.29
	R	0.999	0.998	0.997	0.999	0.999	0.995
Lagergren	$k_L / \text{g } \mu\text{g}^{-1} \text{ min}^{-1}$	0.00062	0.00154	0.00204	0.00203	0.00135	0.00169
	R	0.3334	0.934	0.944	0.828	0.721	0.979

The two times higher sorption capacities obtained with the WIS (47.6 $\mu\text{g g}^{-1}$) compared to WFS (25.4 $\mu\text{g g}^{-1}$) contribute to the assumption that chemisorption occurs, since slag material exhibit significantly lower BET specific surface area (Table II), which is a crucial characteristic that enhances the sorption properties of a material. Further insight into the chemical composition of the examined materials (Table I) revealed that the WIS exhibited higher sorption capacities due to the five times higher iron and iron oxides content compared to the WFS, despite its lower BET surface area. The contribution of manganese (15.66 %) in WFS to the sorption mechanism is probable since the low iron content in the metal oxide layer (3.93 %) hinders the WFS from being an efficient sorbent for arsenic. WIS exhibited similar specific arsenic removal efficiencies, $\approx 220 \mu\text{g As g}^{-1} \text{ Fe}$. Ap-

plied to the WFS containing 39.3 mg g^{-1} Fe, the contribution of iron to arsenic removal was expected to be $9 \text{ } \mu\text{g As g}^{-1}$ WFS. The obtained q_e values (25.4 and $29.8 \text{ } \mu\text{g g}^{-1}$ for As(III) and As(V), respectively) suggest that iron was not the only active component in the WFS. Although these results can not be directly correlated (due to the chemical and physical properties), the higher efficiency of the WFS could be assigned to manganese activity. Assuming the difference between the contribution iron to the sorption and the total q_e values is the consequence of manganese activity only, the specific arsenic removal efficiency of manganese was estimated to be $115 \text{ } \mu\text{g As g}^{-1}$ Mn.

The experimental plots of As(III) and As(V) sorption on the waste materials with time initially increase rapidly, which is followed by a very slow increase in the sorption capacity over longer periods (Fig. 3).

The Lagergren First Order model was found to be the less suitable for describing the kinetics of arsenic sorption on the investigated materials. However, the Lagergren rate constants (k_L) were comparable to rate constants of the pseudo-second order model (k_2).

Equilibrium studies. Adsorption isotherms are important for the description of how molecules of a sorbate interact with the sorbent surface and for the prediction of the extent of sorption. The Langmuir isotherm model was derived under the assumption that the sorbate is sorbed in a one molecule layer. The Freundlich isotherm is a consecutive layer model which does not predict any saturation of the sorbent by sorbate. The isotherm model equations and their linear forms are presented in Table V.

TABLE V. Sorption isotherm models and their linear forms

Type	Non-linear form	Linear form	Plot
Langmuir	$q_e = \frac{q_{\max} K_L c_e}{1 + K_L c_e}$	$\frac{1}{q_e} = \frac{1}{q_{\max} K_L} \frac{1}{c_e} + \frac{1}{q_{\max}}$	$\frac{1}{q_e}$ vs. $\frac{1}{c_e}$
Freundlich	$q_e = K_F c_e^{1/n}$	$\ln q_e = \ln K_F + \frac{1}{n} \ln c_e$	$\ln q_e$ vs. $\ln c_e$

In Table V, q_e is the amount of solute sorbed per gram of sorbent (mg g^{-1}), c_e the equilibrium concentration of solute (mg L^{-1}), K_L a constant related to the energy of sorption (L mg^{-1}) (Langmuir model), q_{\max} the maximum amount of solute sorbed per gram of sorbent (mg g^{-1}), K_F the Freundlich constant (mg g^{-1}) and n is a constant related to the sorption intensity of the sorbent.

Values of the isotherm model parameters obtained from regression analyses are presented in Table VI. A dimensionless separation factor constant, R_L , was proposed to estimate the feasibility of the Langmuir isotherm:²⁸

$$R_L = \frac{1}{1 + K_L c_0} \quad (1)$$

Accordingly,²⁸ R_L values in the $0 < R_L < 1$ range indicates favorable sorption. The R_L values for all the tested materials and for the complete c_0 range (0.500–100.0 mg L⁻¹ As) were $0.150 < R_L < 0.973$.

TABLE VI. Langmuir and Freundlich isotherm parameters for the studied natural zeolite and waste materials

Model equation	Parameter	Z		WIS		WFS	
		As(III)	As(V)	As(III)	As(V)	As(III)	As(V)
Langmuir	$q_{\max} / \text{mg g}^{-1}$	0.9691	4.07	0.82	4.04	0.55	0.77
	$K_L / \text{L mg}^{-1}$	0.0565	0.0137	13.22	12.71	0.37	1.18
	R	0.9902	0.9997	0.9666	0.9986	0.7899	0.9738
Freundlich	$K_F / \text{L mg}^{-1}$	50.703	55.106	0.567	3.010	0.110	0.157
	$n^{-1} / \text{L g}^{-1}$	0.884	1.003	0.519	0.591	0.843	0.727
	R	0.9902	0.9989	0.9635	0.8341	0.9618	0.9218

The highest maximum sorption capacities, q_{\max} , were found for natural zeolite, Z: 0.97 and 4.07 mg g⁻¹ for As(III) and As(V), respectively. The Z and WIS exhibited significantly higher q_{\max} values for As(V) compared to As(III), while the WFS attained nearly equal values for both As forms. The differences in the q_{\max} values for As(III) and As(V) might suggest that the arsenic species present under neutral conditions (As(III) in the molecular form while As(V) in the ionic form) influence the sorption efficiency of Z and WIS. The higher sorption capacities of the Z and WIS (4 and 5 times, respectively) for As(V) suggest that molecular arsenic was less efficiently bound to the slag materials than its ionic forms. While iron was the main active component in the slag materials, manganese was dominant in the WFS. The low content of iron in the WFS is presumed responsible for its lower As(V) sorption capacity. The maximum specific As(V) uptake onto the slag materials, derived from the q_{\max} values, was 15.4 mg As(V) g⁻¹ Fe. The calculated difference between the iron responsible (0.62 mg As(V) g⁻¹ WFS) and exhibited q_{\max} value (0.77 mg As(V) g⁻¹ WFS), $\Delta = 0.15$ mg As(V) g⁻¹ WFS, indicates again the presence of a second active substance in the WFS, *i.e.*, manganese. In addition, the same difference of 0.41 mg As(III) g⁻¹ WFS obtained for the trivalent arsenic form suggests that manganese has a greater affinity toward molecular arsenic forms than iron.

The Langmuir constant, K_L , is a function of the sorption strength: the larger the K_L value, the stronger is the sorption bond. The significantly lower K_L values obtained for the WFS and Z (Table VI), indicating weak sorption bonds, confirms the assumption that physical sorption was dominant for these materials. In addition, the relatively strong sorption bonds, indicated by the high K_L value, suggest that chemisorption was dominant for the WIS. However, the complexity of the experimental results requires further examination of the nature of the sorption processes.

Further insight into the nonlinear Langmuir plots (Fig. 4) revealed that the sorption process continued beyond q_{\max} for the industrial waste materials, WIS and WFS, suggesting that the sorption process continued after monolayer saturation. Likewise, applying the subsequent Freundlich Monolayer Model (Fig. 5) also suggests that arsenic uptake continues after the calculated monolayer saturation.

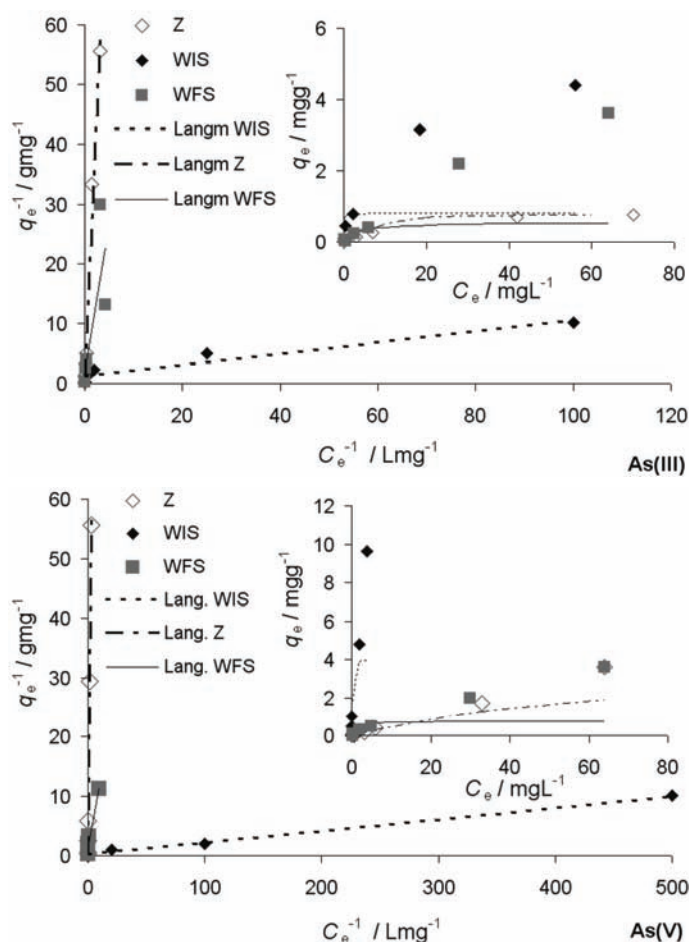


Fig. 4. Langmuir isotherm plots (linear and non-linear) for As(III) and As(V) sorption onto the natural zeolite and the industrial by-products.

These findings might be supported by the complexity of the examined materials in terms of their physico-chemical composition. The presence of active substances, such as iron and manganese (for WFS), and the increased specific surface area contributed to the complex nature of sorption process for all the examined materials.

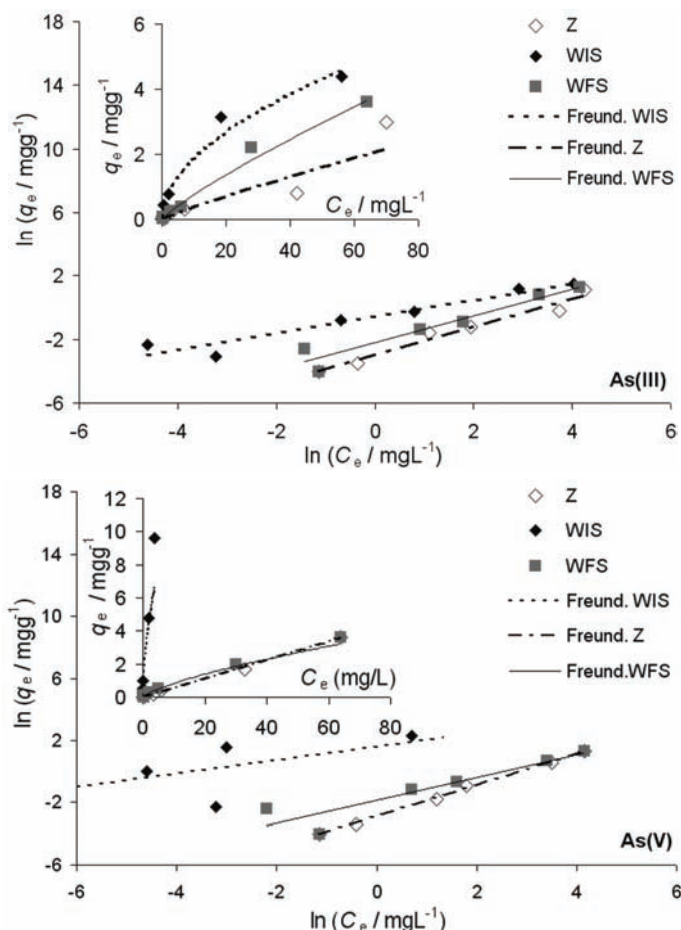


Fig. 5. Freundlich isotherm plots (linear and non-linear) for As(III) and As(V) sorption onto the natural zeolite and the industrial by-products.

The capacities of various low-cost adsorbents reported in recent papers are summarized in Table VII. Although bentonite and sepiolite clays are found to be frequently used for the removal of metal ions from aqueous solution, there was no data available for arsenic removal. Kaolinite clay was reported to be efficient for As(V) removal with 0.23 mg g^{-1} maximum sorption capacity. Zeolite tuffs were reported to exhibit $0.002\text{--}0.0167 \text{ }\mu\text{g As(III) g}^{-1}$ and $0.006\text{--}0.100 \text{ }\mu\text{g As(V) g}^{-1}$ which is significantly lower compared to values obtained for natural zeolite within the scope of this study (0.97 and 4.07 mg g^{-1} for As(III) and As(V), respectively). It is assumed that higher sorption capacities obtained for natural zeolite were due to its higher specific surface area and the higher initial concentration range. A low specific surface area is assumed to contribute to the low sorption capacities obtained for limonite and pyrolusite, although iron (hematite) and

manganese ores are reported to be efficient in As sorption. The lower specific surface area probably contributed to lower sorption efficiencies of WIS for As(III) compared to the values reported in the literature. However, the As(V) sorption capacity obtained by the WIS was 4.07 mg g⁻¹. The WFS obtained the lowest sorption capacities of all tested materials. However, its availability and inexpensiveness makes this waste material an equally valuable alternative for arsenic removal from water.

TABLE VII. Comparative evaluation of various low cost adsorbents for arsenic removal

Adsorbent	pH	Concentration range	Specific surface area m ² g ⁻¹	t / °C	Model used to calculate adsorption capacity	Capacity mg g ⁻¹		Ref.
						As(III)	As(V)	
Natural materials								
Kaolinite	5.5	10–1000 mg L ⁻¹	8.5	25	Langmuir	–	<0.23	18
Zeolitic tuff ZH	4	0.1–4 mg L ⁻¹	–	22	Langmuir.	0.002	0.006	29
Zeolitic tuff ZMS	4	0.1–4 mg L ⁻¹	28	22	Langmuir.	0.0167	0.100	29
Goethite	9.0	0–60 mg L ⁻¹	39	22	–	22	4	18
Mixed rare earth oxide	6.5	50 mg L ⁻¹	6.75	29	Langmuir.	–	2.95	18
Manganese ore	6.3–6.5	–	–	–	Langmuir	0.53	15.38	18
Hematite	4.2	133.5 μmol L ⁻¹	14.4	30	Langmuir	–	0.2	18
Feldspar	4.2	133.5 μmol L ⁻¹	10.25	30	Langmuir	–	0.18	18
Waste materials								
Bauxol	4.5	0.8–32.00 mM	–	23±1	Langmuir	–	1.081	18
Blast furnace slag	7.1	0–1000 mg L ⁻¹	12.56	25	Langmuir	1.4	–	30
Orange juice residue	2–11	–	–	30	Langmuir	70.43	67.43	18
Tea fungal biomass	7.2	0.9–1.3 mg L ⁻¹	–	30	Freundlich	1.11	4.95	18
Human hair	–	0.090–0.360 mg L ⁻¹	–	22	Langmuir	–	0.012	18

CONCLUSIONS

Preliminary investigations showed that natural zeolite and industrial by-products (blast furnace slag and waste filter sand) exhibit substantial arsenic sorption properties. Natural clay minerals (bentonite and sepiolite) and iron and manganese minerals (limonite and pyrolusite) showed very little affinity towards inorganic arsenic species, below 2 μg g⁻¹ in a 2-h contact time, under the conditions that are likely to occur in real water treatment systems. The complex nature of the sorption processes in the selected natural zeolite and industrial by-products, including both chemisorption and physical sorption, was revealed by the equilibrium studies. The sorption capacities for As(V) compared to As(III) were signifi-

cantly higher for the natural zeolite and the blast furnace slag, while the waste filter sand exhibited similar removal efficiencies for both arsenic species. The arsenic sorption process on the natural zeolite followed the monolayer saturation (Langmuir) model, reaching a maximum sorption capacity of 0.97 mg g^{-1} and 4.07 mg g^{-1} for As(III) and As(V), respectively. However, with the waste materials, sorption continued after monolayer saturation (following the Freundlich isotherm model). The blast furnace slag exhibited the highest equilibrium sorption efficiency of 0.05 mg g^{-1} under the conditions that occur in real water treatment systems, while natural zeolite and waste filter sand reached $0.02\text{--}0.03 \text{ mg g}^{-1}$. Comparing to the equilibrium sorption efficiency of 0.05 mg g^{-1} obtained for granular ferric hydroxide, a commercial arsenic sorbent, these results indicate that the application of natural zeolite and the industrial by-products is feasible in real water treatment systems.

Acknowledgements. The authors are grateful to the Ministry of Science and Technological Development of the Republic of Serbia for financial support and the Institute for the Technology of Nuclear and Other Raw Materials (ITNMS) and Belgrade Waterworks Company (JKP BVK) for assistance.

ИЗВОД

ПРЕГЛЕД САВРЕМЕНИХ МЕТОДА ЗА УКЛАЊАЊЕ АРСЕНА ИЗ ВОДЕ

БРАНИСЛАВА М. ЈОВАНОВИЋ¹, ВЕСНА Л. ВУКАШИНОВИЋ-ПЕШИЋ², ЂОРЂЕ Н. ВЕЉОВИЋ³
и ЉУБИНКА В. РАЈАКОВИЋ³

¹Каџедра за хидроџехнику и водно-еколошко инжењерсџиво, Грађевински факулџетџи, Универзитџетџи у Београду, Булевар краља Александра 73, 11 000 Београд, ²Метџалуришко-џихнолошки факулџетџи, Универзитџетџи Црне Горе, Цетџинјски пџуџи бб, 81000 Подђорица, Црна Гора и ³Каџедра за аналџџичку хемџију, Технолошко-метџалуришки факулџетџи, Универзитџетџи у Београду, Карнеђијева 4, 11000 Београд

У овом раду су приказани резултати испитивања ефикасности природних и отпадних материјала за уклањање арсена из воде. Ефикасност уклањања арсена, As(III, V) испитана је у шаржном систему. Као сорбенти коришћени су природни материјали (зеолит, бентонит, сепиолит, пиролузит и лимонит) и отпадни материјали (отпадни филтарски песак са постројења за пречишћавање вода и отпадна шљака из производње челика). Испитивања су показала да отпадни материјали могу ефикасно уклонити и As(III) и As(V) из воде, али да се ефикасност разликује и зависи од валентног стања арсена, почетне концентрације и рН вредности воде. Експерименти на основу којих су добијене криве кинетике сорпције и сорпционе изотерме су рађени у условима какви владају у реалним системима за пречишћавање воде. Природни зеолит о отпадни материјали су се показали као релативно добри материјали за уклањање арсена из воде док су бентонит, сепиолит, лимонит и пиролузит показали слаб афинитет према арсену. Највећи максимални сорпциони капацитет су показали природни зеолит ($4.07 \text{ mgAs(V) g}^{-1}$), и отпадна шљака ($4.04 \text{ mgAs(V) g}^{-1}$).

(Примљено 29. октобра 2010, ревидирано 7. јануара 2011)

REFERENCES

1. D. M. Crnković, N. S. Crnković, A. J. Filipović, Lj. V. Rajaković, A. A. Perić-Grujić, M. Ristić, *J. Environ. Sci. Health.*, A **43** (2008) 1353

2. V. L. Vukašinović-Pešić, Lj. V. Rajaković, *Energy Sources, A* **31** (2009) 1583
3. *Guidelines for Drinking-water Quality*, Third Edition Incorporating The First And Second Addenda, Vol. 1, Recommendations World Health Organization, WHO Press, World Health Organization, Geneva, Switzerland, 2008, p. 306
4. L. Wang, W. E. Condit, A. S. C. Chen, *Technology selection and system design, US EPA Arsenic Removal Technology Demonstration Program Round 1*, EPA/600/R-05/001, Water Supply and Water Resources Division National Risk Management Research Laboratory, Cincinnati, OH, USA, 2004, p. 32
5. Lj. V. Rajaković, *PhD Thesis*, Faculty of Technology and Metallurgy, University of Belgrade, Belgrade, 1986
6. USEPA, *Federal Register* **66** (2001) 6976
7. *Commission Directive 2003/40/EC of 16 May 2003 establishing the list, concentration limits and labelling requirements for the constituents of natural mineral waters and the conditions for using ozone-enriched air for the treatment of natural mineral waters and spring waters*, Official Journal of the European Union, L 126/34 - L 126/39
8. *Drinking Water Quality Standards*, Official Gazette of the SRY No 42/98 (In Serbian)
9. V. L. Vukašinović-Pešić, M. Đikanović, N. Z. Blagojević, Lj. V. Rajaković, *Chem. Ind. Chem. Eng. Q.* **11** (2005) 44
10. R. Zaldivar, L. Prunés, G. L. Arch, *Toxicology* **47** (1981) 145
11. IPCS, *Arsenic and arsenic compounds*, Geneva, World Health Organization, International Programme on Chemical Safety (Environmental Health Criteria 224), 2001, p. 42
12. C. J. Chen, Y. C. Chuang, T. M. Lin, H. Y. Wu, *Cancer Res.* **45** (1985) 5895
13. C. J. Chen, Y. C. Chuang, S. L. You, T. M. Lin, H. Y. Wu, *Br. J. Cancer.* **53** (1986) 399
14. Lj. V. Rajaković, M. Mitrović, S. Stevanović, S. Dimitrijević, *J. Serb. Chem. Soc.* **58** (1993) 131
15. Lj. V. Rajaković, M. Mitrović, *Environ. Pollut.* **75** (1992) 279
16. Lj. V. Rajaković, *Sep. Sci. Technol.* **27** (1992) 1423
17. N. B. Issa, V. N. Rajaković-Ognjanović, B. M. Jovanović, Lj. V. Rajaković, *Anal. Chim. Acta* **673** (2010) 185
18. D. Mohana, C. U. Pittman Jr., *J. Hazard. Mater.* **142** (2007) 1
19. G. S. Murugesan, M. Sathishkumar, K. Swaminathan, *Bioresour. Technol.* **97** (2006) 483
20. D. Ranjan, M. Talat, S. H. Hasan, *J. Hazard. Mater.* **166** (2009) 1050
21. A. F. Bertocchi, M. Ghiani, R. Peretti, A. Zucca, *J. Hazard. Mater.* **134** (2006) 112
22. *Standard Methods for the Examination of Water and Wastewater*, 19th ed., American Public Health Association/American Water Works Association/Water Environment Federation, Washington DC, USA, 1995, p. 3
23. A. I. Vogel, *A Textbook of Quantitative Inorganic Analyses, including Elementary Instrumental Analyses*, Longman, London, 1978, p. 501
24. V. L. Vukašinović-Pešić, N. Z. Blagojević, Lj. V. Rajaković, *Ins. Sci. Technol.* **37** (2009) 482
25. B. M. Jovanović, Lj. V. Rajaković, *J. Environ. Eng-ASCE.* **136** (2010) 1277
26. Y. Jeong, M. Fan, S. Singh, C. L. Chuang, B. Saha, J. H. van Leeuwen, *Chem. Eng. Proc.* **46** (2007) 1030
27. P. L. Smedley, D. G. Kinniburgh, *Appl. Geochem.* **17** (2002) 517
28. G. McKay, H. S. Blair, J. R. Gardener, *J. App. Polym. Sci.* **27** (1982) 3043
29. M. P. Elizalde-González, J. Mattusch, R. Wennrich, P. Morgenstern, *Microporous Mesoporous Mater.* **46** (2001) 277
30. S. R. Kanel, H. Choi, J. Y. Kim, S. Vigneswaran, W. G. Shim, *Water Qual. Res. J. Canada* **41** (2006) 130.

Errata (printed version only)

Issue No. 9 (2011), Vol. 76:

1) Contents, back cover, lines 15 and 16 from below should read:

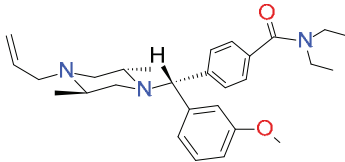
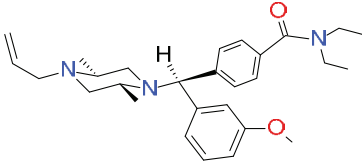
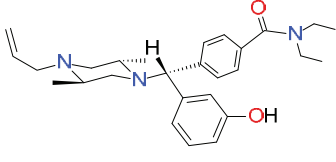
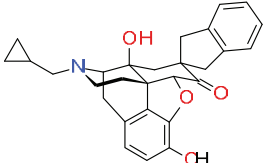
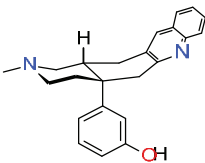
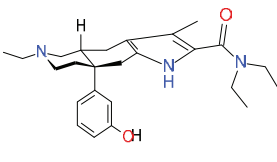
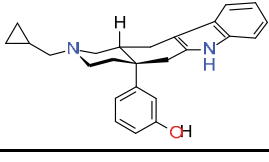
H. A. Zamani, M. R. Ganjali and F. Faridbod: A lutetium PVC membrane sensor based on (2-oxo-1,2-diphenylethylidene)-*N*-phenylhydrazinecarbothioamide 1295

2) Paper JSCS-4201, Tables I and III, pages 1249, 1250 and 1252, respectively, should read:

TABLE I. Compounds **1–11**, ligands of the MOR

Structure	Compound	X	Y
	1	C=O	H
	2	CH ₂ ···OH	H
	3	C=O	OH
	4	CH ₂ ···OH	H
	5	C=O	OH
	6	C=O	H
	7	CH ₂ ···OH	OH
	8	CH ₂ ···OH	OH
	9	C=O	H
	10	CH ₂ ···OH	H
	11	C–OMe	–

TABLE III. Compounds 22–28, ligands of the DOR

Compound name	Structure	Number
SNC80		22
SNC67		23
BW373U86		24
SIOM		25
TAN-67		26
SB219825		27
SB206848		28